MOTION BASED DESIGN METHODOLOGY

FOR BUILDINGS

by

BOUTROS SAMI ABBOUD KLINK
B.E., Civil Engineering
American University of Beirut
(1991)

Submitted to the Department of Civil and Environmental Engineering
in Partial Fulfillment of the Requirements for the Degree of

MASTER OF SCIENCE IN CIVIL AND ENVIRONMENTAL ENGINEERING

at the

MASSACHUSETTS INSTITUTE OF TECHNOLOGY
(June 1993)

Signature of Author _____
Department of Civil and Environmental Engineering
May 7, 1993

Certified by _____
Professor Jerome J. Connor, Jr.
Head, Constructed Facilities Division
Thesis Supervisor

Accepted by _____
Professor Eduardo Kausel
Chairman, Departmental Committee on Graduate Studies

MOTION BASED DESIGN METHODOLOGY FOR BUILDINGS

by

BOUTROS SAMI ABBOUD KLINK

Submitted to the Department of Civil and Environmental Engineering on May 7, 1993
in Partial Fulfillment of the Requirements for the Degree of

MASTER OF SCIENCE IN CIVIL AND ENVIRONMENTAL ENGINEERING

ABSTRACT

The successful design of structures consists of satisfying their functional requirements of strength and serviceability in an effective and integrated manner. The traditional strength based approach, in which structures are designed based on a consideration of strength and are then checked for serviceability constraints, lacks the ability of dealing with drift, acceleration, and damage efficiently. The proposed performance based approach for distributing stiffness, damping, and active control (where needed) provides a more rational design alternative to the strength based approach.

This work is concerned with the development of a methodology for estimating the rigidity distribution in a building such that the response due to seismic excitation is close to the optimal state of uniform maximum inter-story deformation. The method is based on the superposition of modal rigidity contributions derived using various analytical models together with an iterative numerical scheme. Numerical results are presented for a wide range of fundamental periods. They provide an assessment of the variation in behavior with period, the degree of optimality of this type of passive control, and a logical starting point for the incorporation of active control.

Thesis supervisor : Prof. Jerome J. Connor, Jr.
Professor of Civil Engineering
Head, Constructed Facilities Division

dedicated to

Nadia and Sami

with all my love

ACKNOWLEDGMENTS

I would like to express my deepest gratitude to my teacher and supervisor, Prof. Jerome J. Connor whose enthusiasm for this work, his unbounded patience, guidance, and encouragement, as well as his extremely friendly and supportive attitude make my stay at MIT such a wonderful learning experience. Continuing this work together is something I look forward to.

Special thanks to Prof. Eduardo Kausel whose friendly, helpful, and supportive attitude is highly appreciated.

Special thanks to all the teachers I've had who have helped me broaden my horizons and understand the world we live in a little better.

Many thanks to the Hariri Foundation for funding my education, and special thanks to Mr. David Thompson for his help and support.

Thanks to all my friends for their support and love, and for the enjoyable times we've spent together. I look forward to numerous enjoyable moments together in the future. I can't but specifically thank my childhood friend Amal Hechaime whose friendship has shown me how wonderful this world can be.

Finally, I feel the urge of expressing my love and gratitude to the two people who brought me up and directed me into becoming what I am. You've done a great job. Nadia and Sami, you are the best parents one can have. I love you and thank you for everything. God bless you.

Boutros

TABLE OF CONTENTS

1 - INTRODUCTION
- 1 - 1 Introduction 7
- 1 - 2 Design Issues For Buildings 9
- 1 - 3 A Motion Based Approach 12
- 1 - 4 Thesis Outline 15

2 - STRATEGY FOR STATIC LOADING
- 2 - 1 Introduction 17
- 2 - 2 Governing Equations for Deformable Solids 18
  - 2 - 2 - 1 Kinematic Relations 18
  - 2 - 2 - 2 Force - Deformation Relations 26
  - 2 - 2 - 3 Equilibrium Relations 27
- 2 - 3 Strategy For Static Loading 28

3 - GENERAL FORMULATION FOR DYNAMIC LOADING
- 3 - 1 Introduction 31
- 3 - 2 Multi - Modal Based Stiffness Distribution 32

4 - FUNDAMENTAL MODE RESPONSE
- 4 - 1 Introduction 39
- 4 - 2 Fundamental Mode - Uniform Deformation 40
- 4 - 3 Fundamental Mode - Forced Vibration 44
- 4 - 4 Calibration of Fundamental Mode Model 48
- 4 - 5 Examples 50

5 - MULTI - MODAL SHEAR BEAM BASED STIFFNESS
5 - 1 Introduction 62
5 - 2 Free Vibrations of a Cantilever Shear Beam 63
5 - 3 Multi - Modal Based Stiffness Distribution 67
5 - 4 Calibration of Equivalent Shear Beam Model 70
5 - 5 Examples 72

6 - MULTI - MODAL BENDING BEAM BASED STIFFNESS
6 - 1 Introduction 76
6 - 2 Free Vibrations of a Cantilever Bending Beam 77
6 - 3 Multi - Modal Based Stiffness Distribution 82
6 - 4 Calibration of Equivalent Bending Beam Model 86

7 - MULTI - MODAL ITERATIVE SCHEME BASED STIFFNESS
7 - 1 Introduction 89
7 - 2 Step by Step Iteration Procedure 90
7 - 3 Examples 91

8 - CONCLUSION 102

A - EARTHQUAKE RESPONSE SPECTRA ANALYSIS 104

A - 1 Introduction
A - 2 Response Spectra
A - 3 Earthquake Response Analysis: Lumped MDOF Systems
A - 4 Earthquake Response Analysis: Distributed Parameter Systems
A - 5 Superposition of Response Maxima

B - ACCELEROGRAM DATABASE 122

C - DISCRETIZATION 130

D - REFERENCES 131

CHAPTER ONE
INTRODUCTION

1 - 1 INTRODUCTION

It is common knowledge that civil engineering structures must withstand ever-changing dynamic loads over the span of their useful lives. Examples of such loads include earthquake ground motion, tornadoes and high winds, hurricanes, severe sea states and tsunamis, moving vehicles, rotating and reciprocating machines . . . Successful design requires satisfying a structure's functional requirements of strength and serviceability in an effective and integrated manner. However, this design task is made quite challenging by the inherent constraints on the economics, the demand for extreme reliability under highly uncertain loading conditions, the differences in the strength and behavior of the actual structural components as opposed to the design considerations, and the errors that may accompany the analysis, design, and construction stages. Due to the above uncertainties as well as the large number of lives and the extent of

damage involved, the Civil Engineering Community has traditionally adopted the conservative "building the pyramid" design approach: building highly redundant structures relying on their mass and solidity to resist the varying loading conditions, for, mass and solidity have often been equated to safety and reliability. This approach results in larger expenditures than what is actually needed.

Although design means controlling the structure's strength and stiffness, only within the past decade have Civil Engineers started looking at the design problem from the "control" perspective. Structural control involves the regulating of pertinent structural characteristics as to ensure desirable structural response under the effect of disturbances to which the structure may be subjected. Hence, one supplements the basic structure with control force generating mechanisms to obtain the desired response. Structural control can be exerted by using either passive, active, or a combination of these control mechanisms.

Passive control mechanisms operate without using any external energy supply; they use the energy generated by the structure's response to supply the control forces. However, these systems become very costly when satisfying more stringent requirements than those required for optimum design. Active control mechanisms on the other hand, operate by using an external energy supply where the control forces are applied to the structure by means of actuators. They are more efficient than passive systems because they can control the structure for a broader range of loadings provided that it is technically feasible and that one

supplies the required amount of energy. Active control has the advantage of being able to control different loadings differently and provides a clean solution for retrofitting existing structures. This solution may lead to savings although one faces the issues of reliability, maintenance, energy supply . . . By incorporating the advantages of both systems in a rational way, it may be possible to reduce the disadvantages of either solution, leading to the design of very efficient and economical structures.

The ultimate goal of this research is to provide a rational design strategy that optimally integrates passive and active control systems. This particular work establishes a performance based design strategy for passively controlling buildings. It also provides a logical starting point for incorporating active systems in an efficient manner.

1 - 2 DESIGN ISSUES FOR BUILDINGS

The traditional approach for structural design is based on a consideration of strength. Factored loads are used to establish the required strength capacity of the structural components. The appropriate component "sizes" are chosen so as to meet these requirements with an additional safety margin included to allow for material strength variations. Once the structure is fully defined, its performance under service loadings is checked. The displacements corresponding to service loading are usually the primary quantities of interest.

The dominant loading for a structure depends on its function, configuration, and location. Buildings for example, are subjected to two types of loadings, "gravity" and "lateral". Gravity loads consist of the actual weight of the structure and the material, equipment, and people contained in the building. The most frequently occurring lateral loads are the wind and earthquake loads. As the building height increases, the lateral loading becomes more important in comparison to the gravity loading, and eventually becomes the dominant design loading. The relative importance of wind versus earthquake depends on the location, building height, and structural makeup. For steel buildings, the transition from "earthquake dominant" to "wind dominant" loading occurs when the building height reaches approximately 100m. Concrete buildings, because of their larger mass, are controlled by earthquake loading up to at least a height of 250m. In regions where the earthquake action is low (e.g. Chicago in the U.S.A.), the transition occurs at a much lower height and the design is governed primarily by wind loading.

Both wind and earthquake loadings are dynamic in nature and produce time varying response. The critical performance measures are related to the motion of the building and pertain to human (and equipment) comfort and structural damage. For service load conditions, the structural performance measure is expressed as a constraint on inter-story displacement; human comfort is defined by a limiting value for the peak acceleration. For extreme load conditions, inelastic deformation of the structure is the primary design constraint; structural performance is expressed as a "desired" distribution and magnitude of structural damage (i.e. inelastic deformation) throughout the

	FREQUENCY OF OCCURRENCE			
	1/100 IN ONE YEAR		1/10 IN ONE YEAR	
	MAXIMUM ACCELERATION	FRACTION OF CRITICAL DAMPING REQUIRED	MAXIMUM ACCELERATION	FRACTION OF CRITICAL DAMPING REQUIRED
ACROSS-WIND RESPONSE	1.0% g	77.6%	1.0% g	20.7%
	2.0% g	19.4%	2.0% g	5.2%
	3.0% g	8.6%	3.0% g	2.3%
	8.8% g	1.0%	4.5% g	1.0%
ALONG-WIND RESPONSE	1.0% g	32.8%	1.0% g	9.8%
	2.0% g	8.2%	2.0% g	2.4%
	3.0% g	3.6%	3.0% g	1.1%
	5.7% g	1.0%	3.1% g	1.0%

TABLE 1.2.1: WIND DATA FOR TYPICAL BUILDINGS

building height. Structural damage is the key measure for earthquake dominant design; peak acceleration tends to be the controlling criterion for wind-dominant design. Table 1.2.1 shows the variation of peak acceleration with structural damping for a "typical" building with a frequency of 0.17 Hz and different wind conditions. Substantial structural damping is required to meet this constraint.

1 - 3 A MOTION BASED DESIGN APPROACH

The normal design approach generates an initial estimate of the structural components using strength requirements based on factored loads, and then checks for the inter-story displacement and peak acceleration under service loads. Iteration is usually required to satisfy the drift (i.e. inter-story displacement) and acceleration constraints for buildings. Drift under service loads depends mainly on the structural stiffness. The acceleration is governed primarily by the energy dissipation capacity of the structure (i.e. structural damping). Drift under the extreme loading is influenced somewhat by stiffness and damping, but is largely controlled by the inelastic energy absorption capacity of the structure (i.e. damage). A strength based approach to preliminary design lacks the ability to deal with drift, acceleration, and damage in an effective manner. A more rational design approach is needed, especially for building heights in the range where wind and earthquake are of equal importance. Such an approach must support the integration of multiple performance objectives such as drift, acceleration, and damage as well as the more traditional concern of structural integrity (i.e. strength).

A framework for performance based design has been presented by Albano. The methodology combined systems theory with Suh's Principles of Axiomatic Design to synthesize and evaluate design alternatives in a rational manner. The starting point of the approach is the identification of the performance objectives, which are treated as the functional requirements for the product. Design variables are then chosen to satisfy those functional

requirements. Selection of the design variables is the key step. Experience has shown that "good designs" are characterized by a one-to-one correspondence between the functional requirements and the design variables (i.e. each functional requirement is satisfied by a single distinct design variable). Coupling between the functional requirements and the design variables generally makes it more difficult to accommodate changes in the functional requirements and to converge on an acceptable design. Applying the performance based approach to the building design problem leads to the set of functional requirements and their corresponding design variables shown in Table 1.3.1.

	FUNCTIONAL REQUIREMENTS	DESIGN VARIABLES
1	Control the distribution of the inter-story displacement under service load.	Magnitude and distribution of structural stiffness.
2	Control of magnitude of the response (displacement and acceleration) under service load.	Magnitude and distribution of energy dissipation capacity.
3	Control the magnitude of the response under extreme load.	Magnitude and distribution of energy absorption.

TABLE 1.3.1: FUNCTIONAL REQUIREMENTS AND DESIGN VARIABLES FOR THE BUILDING DESIGN PROBLEM

The design strategy is as follows. Firstly, the distribution of stiffness, which involves the choice of material stiffness and cross-sectional properties , is established by enforcing the requirements on the distribution of inter-story deformation corresponding to service loading. The ideal state is "uniform" inter-story deformation throughout the building height. With the stiffness defined, the requirement on the magnitude of the response is met by incorporating energy dissipation mechanisms over the height. One possible choice is viscous damping, distributed in a manner similar to the distribution of the stiffness (i.e. stiffness proportional damping). The last step is to provide the energy absorption over the height through hysteretic damping. Ideally, one would like to have uniform "inelastic" inter-story deformation under the extreme load as well as uniform "elastic" inter-story displacement under service load. Hysteretic damping depends on the yield force level and magnitude of inelastic deformation. In this approach, the yield force level is adjusted throughout the height so as to produce the desired "uniform" inelastic inter-story deformation state. One can then supplement the building with active control devices where needed, or compromise between the passive solution and the active solution if the active solution proves feasible.

The essential difference between this design approach and the conventional "strength-based" approach is that the structural design parameters are determined by deformation rather than strength requirements. Providing sufficient strength capacity is viewed as a constraint. The actual design requirement is "limiting" the deformation to a specified range.

1 - 4 THESIS OUTLINE

This work is concerned with the development of a methodology for estimating the rigidity distribution in a building such that the response due to seismic excitation is close to the optimal state of uniform maximum inter-story deformation. The method is based on the superposition of modal rigidity contributions derived using various analytical models together with an iterative numerical scheme. Numerical results are presented for a wide range of fundamental periods. They provide an assessment of the variation in behavior with period, the degree of optimality of this type of passive control, and a logical starting point for the incorporation of active control.

Chapter Two develops the governing equilibrium, compatibility, and constitutive relations in order to provide the technical foundation for what follows. Those relations are then applied in developing a strategy for handling statically loaded buildings.

Chapters Three through Seven deal with buildings that are dynamically excited. In Chapter, the governing equations are extended to include dynamic effects. Chapter Four discusses the single mode response, applicable to buildings that are excited in their first mode only. Chapter Five, provides a strategy for handling buildings with low fundamental periods that behave as pseudo-shear beams (bending deformation can be neglected). Chapter Six handles the other extreme, where buildings have high fundamental periods and display a pseudo-bending beam behavior (shear deformation can be neglected).

Chapter Seven provides a numerical scheme to handle buildings where both bending deformation and shear deformation are significant.

Chapter Eight draws the conclusions, summarizes the results, and provides directions for future work in this area.

For completeness, Appendix A provides a summary of the Response Spectra Design Method, currently used in designing buildings subjected to seismic excitation. The equations presented therein are extensively used in the presented formulation. Appendix B compiles the Earthquake database used in this research. Appendix C shows the lumping of rigidities and Appendix D lists the references.

CHAPTER TWO

STRATEGY FOR STATIC LOADING

2 - 1 INTRODUCTION

The fundamental relationships (i.e. the displacement-deformation relation, the force-deformation relation, and the equilibrium relations) for static loading are presented first. The approach is applicable when the fundamental period of the building is much smaller than the period of the imposed loading. Extreme wind loads on buildings are usually treated as quasi-static loads, since the wind period is on the order of sixty seconds. An example is provided to illustrate how the stiffness of buildings can be determined to achieve a uniform state of deformation under prescribed static loading conditions.

2 - 2 *GOVERNING EQUATIONS FOR DEFORMABLE SOLIDS*

The formulation of the governing equations for the behavior of a deformable solid involves the following three steps:

2 - 2 - 1 *KINEMATIC (DEFORMATION - DISPLACEMENT) RELATIONS*

This step involves the study of deformation in which one analyzes the change in shape (deformation) of a differential volume element due to the displacement of the body. This leads to a set of equations relating strains (measures of deformations) to displacements at a point. This is a purely geometric problem.

Consider the simple cantilever beam shown in Fig. 2.2.1.1 with u and v representing the longitudinal and transverse displacements respectively. x and y represent the axes along the length of the beam and perpendicular to it respectively. Let β denote the rotation due to bending and γ denote the rotation due to shear also known as the shear deformation. For the limiting case of no shear deformation, the cross sections would remain normal to the elastic axis and v' (the differential of v with respect to x) would be equal to the slope of the elastic axis. Fig. 2.2.1.2 shows the effect of shear deformation. One may relate deformations (strains) to displacements by

$$\varepsilon = u' \qquad (2.2.1.1)$$

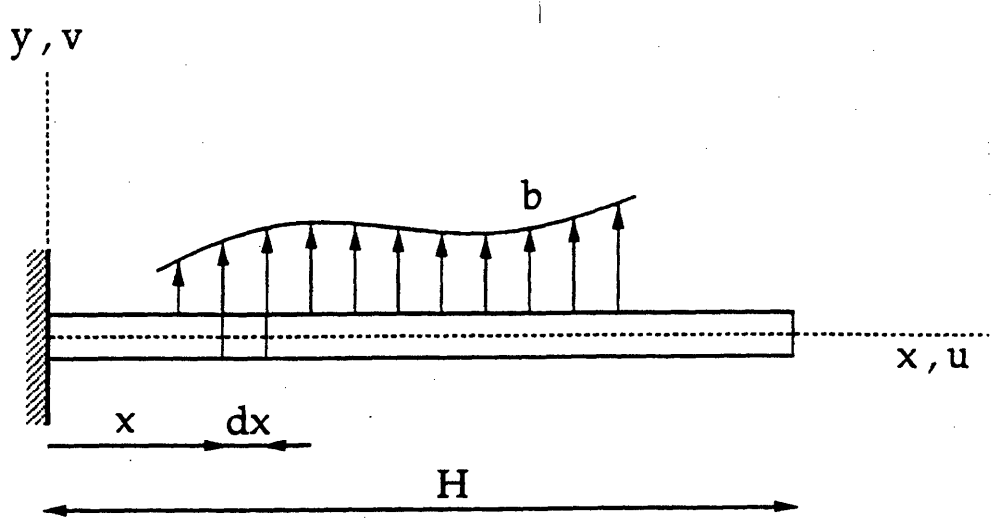

FIGURE 2.2.1.1: SIMPLE CANTILEVER BEAM

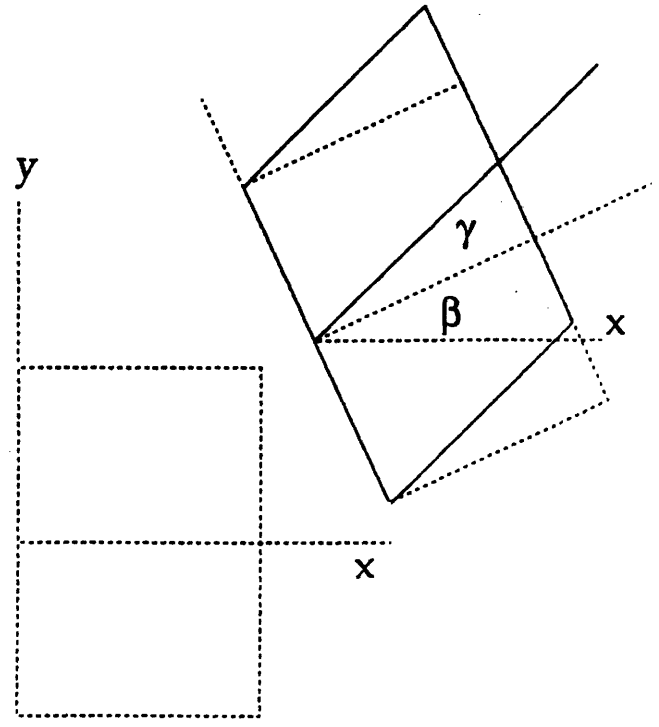

FIGURE 2.2.1.2: EFFECT OF SHEAR DEFORMATION

$$v' = \beta + \gamma \quad \Rightarrow \quad \gamma = v' - \beta \qquad (2.2.1.2)$$

$$k = \beta' \qquad (2.2.1.3)$$

where ε is the axial deformation

γ is the shear deformation

k is the bending deformation (relative rotation due to bending)

In what follows, only shear and bending deformations of the cantilever are considered in modeling the transverse motion of buildings subjected to lateral excitation.

Optimal building design requires uniform shear and bending deformation throughout the building height. Applying the performance based design approach to the building problem, the engineer decides on some target deformation

$$\gamma = \gamma^* \qquad (2.2.1.4)$$

$$k = k^* \qquad (2.2.1.5)$$

and *(2.2.1.3)* and *(2.2.1.2)* become

$$k^* = \beta' \qquad (2.2.1.6)$$

$$\gamma^* = v' - \beta \qquad (2.2.1.7)$$

Typical values of γ^* are around 1/200 in Japan and 1/300 - 1/400 in the U.S.A. for buildings under service loads. Under extreme loads, the Japanese go for 1/100 whereas in the U.S.A. the values are kept around 1/200.

Integrating *(2.2.1.6)* and *(2.2.1.7)* and enforcing fixity conditions at $x = 0$, yields

$$\beta = k^*x \qquad (2.2.1.8)$$

$$v' = \gamma^* + \beta \qquad (2.2.1.9)$$

$$v = \gamma^*x + \frac{1}{2}k^*x^2 \qquad (2.2.1.10)$$

The deflection at the tip of the beam can be obtained by substituting H for x

$$v(H) = \gamma^*H + \frac{1}{2}k^*H^2 \qquad (2.2.1.12)$$

which can be split into the a shear deformation contribution

$$v_s = \gamma^*H \qquad (2.2.1.13)$$

and a bending deformation contribution

$$v_b = \frac{1}{2}k^*H^2 \qquad (2.2.1.14)$$

The relative importance of the transverse shear deformation versus the bending deformation depends on the ratio of γ^* to k^*. Buildings with very small aspect ratios display pseudo-shear beam behavior and $k^* \rightarrow 0$. On the other hand, buildings with very large aspect ratios display pseudo-bending beam behavior and $\gamma^* \rightarrow 0$.

The approach which is followed is based on approximating the deflected shape in terms of a set of functions which characterize the spatial variation. If one defines $\mathbf{\Phi}$ as a matrix containing spatial variation functions related to the shear deformation, and $\boldsymbol{\psi}$ as a matrix containing functions related to the bending deformation (bold letters are used to denote vectors and matrices), then v can be expressed as

$$v(x) = \mathbf{\Phi}(x)\mathbf{Q}_s + \boldsymbol{\psi}(x)\mathbf{Q}_b \qquad (2.2.1.14)$$

$$\beta(x) = \boldsymbol{\psi}'(x)\mathbf{Q}_b \qquad (2.2.1.15)$$

where $\mathbf{Q}_s$ and $\mathbf{Q}_b$ are vectors containing the corresponding function participation factors. Substituting *(2.2.1.14)* and *(2.2.1.15)* in *(2.2.1.2)* and *(2.2.1.3)*, results in

$$\gamma = v' - \beta = \mathbf{\Phi}'\mathbf{Q}_s + \boldsymbol{\psi}'\mathbf{Q}_b - \boldsymbol{\psi}'\mathbf{Q}_b = \mathbf{\Phi}'\mathbf{Q}_s \qquad (2.2.1.16)$$

$$k = \beta' = \boldsymbol{\psi}'\mathbf{Q}_b \qquad (2.2.1.17)$$

The single mode constant deformation case corresponds to taking

$$\Phi = \bar{x} \qquad (2.2.1.18)$$

$$\psi = \frac{\bar{x}^2}{2} \qquad (2.2.1.19)$$

$$\bar{x} = \frac{x}{H} \qquad (2.2.1.20)$$

$$Q_s = \gamma^* H \qquad (2.2.1.21)$$

$$Q_b = k^* H^2 \qquad (2.2.1.22)$$

Normally, one considers Q_s and Q_b to be independent variables which depend on the loading and rigidity distributions. Ideally, one would like to control the magnitude and distribution of strain over the cross section as well as along the axis of the beam. The following simple example illustrates the concept.

Consider the section of a truss shown in Fig. 2.2.1.3 consisting of a pair of columns with diagonal bracings making an angle α with the columns. This can be considered as a section of a building megastructure. The extensional deformation measures for the columns ε_c and for the diagonals ε_d are related to γ and k by

$$\varepsilon_c = \frac{\Delta_c}{H} = \frac{\beta}{2}\frac{B}{H} \qquad (2.2.1.23)$$

but

$$\frac{\beta}{H} = k \qquad (2.2.1.24)$$

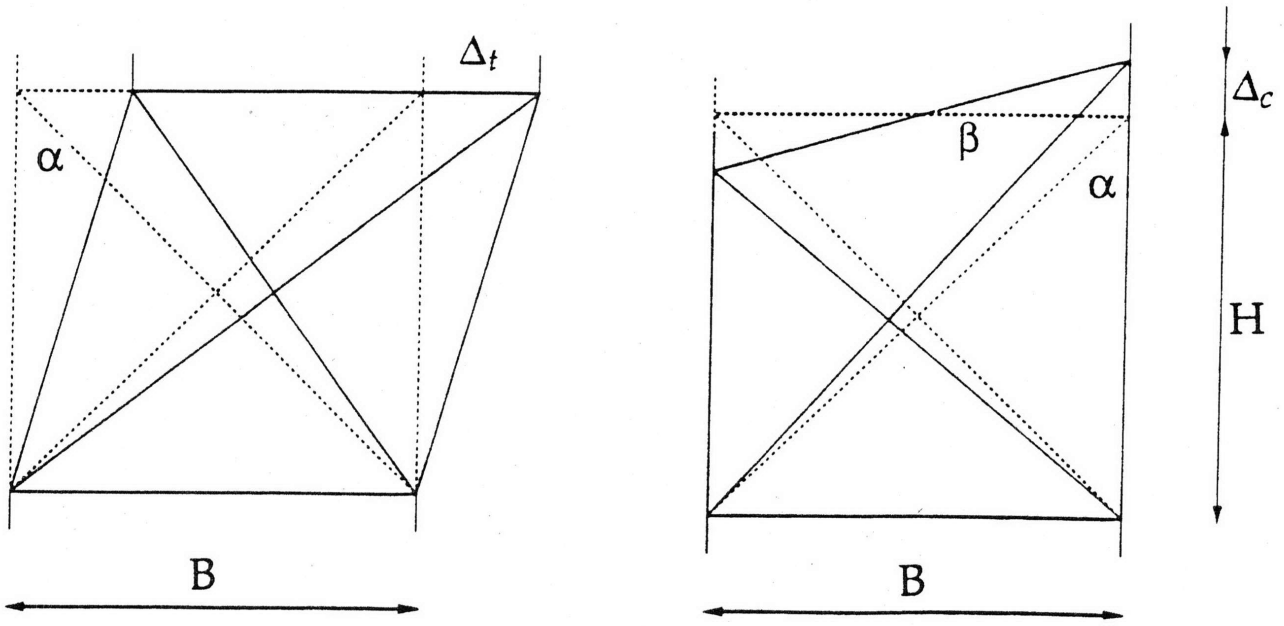

FIGURE 2.2.1.3: TRUSS SECTION

thus $$\varepsilon_c = \frac{B}{2} k \qquad (2.2.1.25)$$

Similarly $$\varepsilon_d = \Delta_t \sin\alpha \frac{\cos\alpha}{H} \qquad (2.2.1.26)$$

and $$\frac{\Delta_t}{H} = \gamma \qquad (2.2.1.27)$$

leading to $$\varepsilon_d = \gamma \sin\alpha \cos\alpha = \gamma \frac{\sin 2\alpha}{2} \qquad (2.2.1.28)$$

For the case where $\alpha = 45°$, *(2.2.1.28)* becomes

$$\varepsilon_d = \frac{1}{2}\gamma \qquad (2.2.1.29)$$

One should allow for a difference between the column and diagonal extensional strains since the columns also carry the axial loading. One can reasonably write

$$\varepsilon_d = f\,\varepsilon_c \qquad (2.2.1.30)$$

where typical values of f range from about 3 for elastic structures to 6 for inelastic structures. Substituting *(2.2.1.25)* and *(2.2.1.29)* in *(2.2.1.30)* results in a relation between k and γ

$$k = \frac{1}{f\,B}\gamma \qquad (2.2.1.31)$$

Enforcing *(2.2.1.31)* for the single mode case results in

$$k^* = \frac{1}{f\,B}\gamma^* \qquad (2.2.1.32)$$

And from *(2.2.1.21)* and *(2.2.1.22)*

$$Q_b = a\,Q_s \qquad (2.2.1.33)$$

$$a = \frac{H}{f\,B} = \frac{H\,k^*}{\gamma^*} \qquad (2.2.1.34)$$

The displacement terms due to shearing and bending deformation effects reduce to

$$\left|\frac{v_b}{v_s}\right|_{x=H} = \frac{a}{2} \qquad (2.2.1.35)$$

For tall buildings, $(H/B) = 5 \rightarrow 7$, and the contribution will be essentially equal when f is about 3.

2 - 2 - 2 FORCE - DEFORMATION RELATIONS

The force-deformation relations, also known as the constitutive relations depend on the characteristics of the materials which make up the structure. For the static case, assuming the structure is in the linearly elastic range, the expressions relating the shear and bending moment to the shear deformation and bending deformation respectively can be expressed as

$$V(x) = D_T(x)\,\gamma(x) \qquad (2.2.2.1)$$

$$M(x) = D_B(x)\,k(x) \qquad (2.2.2.2)$$

where V is the shear force

M is the bending moment

D_T is the shear rigidity

D_B is the bending rigidity

The above equations have to be modified slightly for the dynamic case as will be seen in the next chapter.

2 - 2 - 3 *EQUILIBRIUM EQUATIONS*

Consider Figure 2.2.3.1 which defines the sign convention used in the analysis.

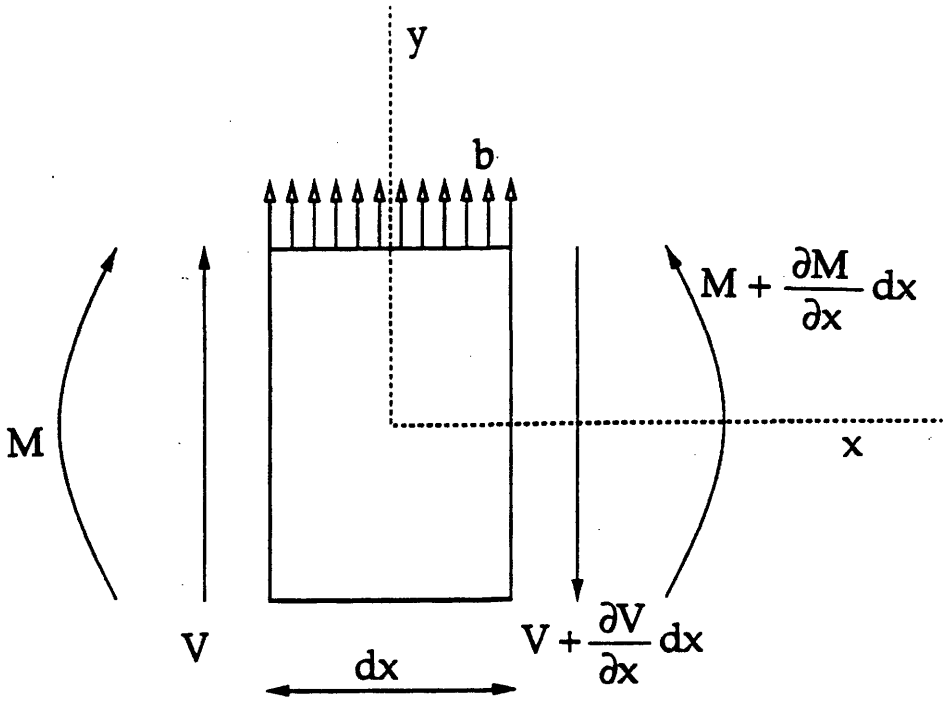

FIGURE 2.2.3.1: FORCES ACTING ON A DIFFERENTIAL ELEMENT

Summing up the vertical forces gives

$$V + \frac{\partial V}{\partial x} dx - V - b\,dx = 0 \qquad (2.2.3.1)$$

which for the cantilever beam results in

$$V = \int_x^H b\, dx \qquad (2.2.3.2)$$

Similarly summing up moments gives

$$M + \frac{\partial M}{\partial x} dx - M - V\, dx - b\, dx \frac{dx}{2} = 0 \qquad (2.2.3.3)$$

Neglecting the higher order term and simplifying gives

$$M = \int_x^H V\, dx \qquad (2.2.3.4)$$

For the static problem, b represents the externally applied loads, however for the dynamic problem, the inertia forces of the moving body as well as the damping forces have to be included in b.

2 - 3 *STRATEGY FOR STATIC LOADING*

The strain based approach for determining the stiffness distribution along the length of the beam is developed in this section for the case where the loads are applied statically. Once the load distribution $b(x)$ and the deformation distributions are specified, the transverse shear force and bending moment

distributions can be determined, and consequently, the required rigidity distributions for the specified deformations can be evaluated. By specializing the equations developed in the previous section for the constant deformation case, one obtains

$$D_T(x) = \frac{V(x)}{\gamma^*} = \frac{1}{\gamma^*}\int_x^H b(x)\,dx \qquad (2.3.1)$$

$$D_B(x) = \frac{M(x)}{k^*} = \frac{1}{k^*}\int_x^H V(x)\,dx \qquad (2.3.2)$$

For example, taking a uniform loading as shown in Figure 2.3.1, which is a reasonable assumption for the wind action on a tall building,

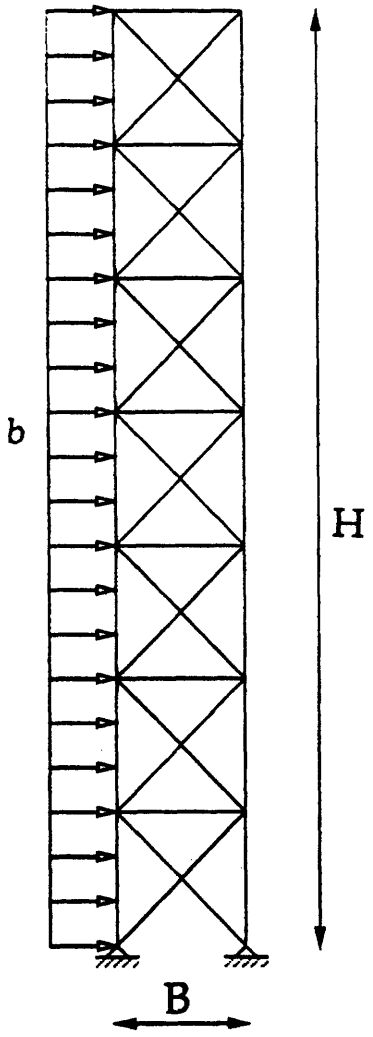

FIGURE 2.3.1: THE MODEL

$$V(x) = b(H - x) \qquad (2.3.3)$$

$$M(x) = \frac{b}{2}(H - x)^2 \qquad (2.3.4)$$

and

$$D_T(x) = \frac{b(H - x)}{\gamma^*} = \frac{bH}{\gamma^*}(1 - \bar{x}) \qquad (2.3.5)$$

$$D_B(x) = \frac{b(H - x)^2}{2k^*} = \frac{bH}{2\gamma^*}(1 - \bar{x})^2\frac{H^2}{a} \qquad (2.3.6)$$

So, one can see that for a cantilever beam subjected to a uniform transverse load, one requires a linear shear rigidity distribution and a quadratic bending rigidity distribution to get a state of uniform deformation. Typical values for γ^* , f , and aspect ratio are

$$\gamma^* = \frac{1}{400} \qquad f = 3 \qquad \frac{B}{H} = \frac{1}{6} \tag{2.3.7}$$

lead to $$a = \frac{H}{f\,B} = 2 \tag{2.3.8}$$

and a tip displacement of

$$v(H) = \gamma^* H + \frac{1}{2} k^* H^2 = \gamma^* H \left(1 + \frac{a}{2}\right) = \frac{H}{200} \tag{2.3.9}$$

which corresponds to service load value. One would use these typical values together with b and H to establish an appropriate value for D_T at $x = 0$. As will be seen later on, the rigidity distributions shall be modified near $x = H$ to avoid excessive deformation under dynamic load.

CHAPTER THREE

GENERAL FORMULATION FOR DYNAMIC LOADING

3 - 1 INTRODUCTION

Chapter Two established a performance based approach for static and quasi-static problems. However, a lot of times, a static analysis is not adequate and a dynamic analysis is required. This kind of analysis is needed when the inertia forces become significant relative to the other forces, leading to significant dynamic amplification. Examples of such excitations are wind gust loading and earthquake loading. The strategy developed for determining stiffness distributions has to be modified to account for inertia and damping. As stated earlier, the goal is a state of uniform maximum deformation throughout the height of the building.

The current chapter formulates the general problem where the

distribution of rigidities is based on combining both shear and bending modes to achieve the desired performance assuming that those modes uncouple. So, one can uncouple the problem, by first solving for the mode shapes of a pure "shear beam" and the pure "bending beam", and then combining the two sets of modes to obtain the desired rigidity distributions.

3 - 2 *GENERAL FORMULATION FOR MULTI-MODAL BASED STIFFNESS DISTRIBUTION*

The basic idea, going back to Chapter Two, is approximating the deflected shape of the structure in terms of a set of functions which characterize the spatial variation. However, for the dynamic case, the time variable has to be incorporated in the formulation. Expressing the displacement as a linear combination of the bending mode shapes and the shear mode shapes assuming that they can be uncoupled leads to

$$v(x,t) = \Phi(x)\, Q_s(t) + \psi(x)\, Q_b(t) \qquad (3.2.1)$$

$$\beta(x,t) = \psi'(x)\, Q_b(t) \qquad (3.2.2)$$

which are analogous to *(2.2.1.14)* and *(2.2.1.15)* but with Q_s and Q_b functions of the time variable t.

Differentiation with respect to time shall be denoted by dots, as will be seen later

on. Equations *(2.2.1.16)* and *(2.2.1.17)* become functions of time as well, and are restated here for completeness

$$\gamma = v' - \beta = \Phi' Q_s + \psi' Q_b - \psi' Q_b = \Phi' Q_s \qquad (3.2.3)$$

$$k = \beta' = \psi'' Q_b \qquad (3.2.4)$$

Applying the Principle of Virtual Displacements (the first-order work done by the external forces acting on the system through a set of compatible arbitrary virtual displacements, is equal to the first-order work done by the resulting internal forces through the corresponding deformations), which for a beam can be written as

$$\int_0^H \left(M\delta k + V\delta\gamma \right) dx = \int_0^H b\delta v \, dx \qquad (3.2.5)$$

where δ is used to indicate the virtual quantities, and the other symbols have been defined previously. Substituting *(3.2.1)*, *(3.2.3)*, and *(3.2.4)* in *(3.2.5)* gives

$$\int_0^H \left(\delta Q_b{}^T \psi''{}^T M + \delta Q_s{}^T \Phi'^T V \right) dx \qquad (3.2.6)$$

$$= \int_0^H b \left(\delta Q_b{}^T \psi^T + \delta Q_s{}^T \Phi^T \right) dx$$

The force-deformation relations of Chapter Two relating the shear force to the shear deformation have to be modified for dynamic systems to include the effect of damping. Assuming linear viscoelastic damping proportional to the stiffness distribution, *(2.2.2.1)* becomes

$$V(x,t) = D_T(x)\,\gamma(x,t) + \alpha_s\, D_T(x)\,\dot{\gamma}(x,t) \qquad (3.2.7)$$

and similarly for the equation relating the bending moment to the bending deformation

$$M(x,t) = D_B(x)\,k(x,t) + \alpha_b\, D_B(x)\,\dot{k}(x,t) \qquad (3.2.8)$$

Then *(3.2.6)* leads to the following two sets of equations

$$\mathbf{K}_{bb}\mathbf{Q}_b + \alpha_b\,\mathbf{K}_{bb}\dot{\mathbf{Q}}_b = \mathbf{P}_b \qquad (3.2.9)$$

$$\mathbf{K}_{ss}\mathbf{Q}_s + \alpha_s\,\mathbf{K}_{ss}\dot{\mathbf{Q}}_s = \mathbf{P}_s \qquad (3.2.10)$$

where

$$\mathbf{K}_{bb} = \int_0^H \boldsymbol{\psi}''^{T} D_B \boldsymbol{\psi}''\, dx \qquad (3.2.11)$$

$$\mathbf{K}_{ss} = \int_0^H \boldsymbol{\Phi}'^{T} D_T \boldsymbol{\Phi}'\, dx \qquad (3.2.12)$$

$$\mathbf{P}_b = \int_0^H \boldsymbol{\psi}^T \mathbf{b}\, dx \qquad (3.2.13)$$

$$\mathbf{P}_s = \int_0^H \boldsymbol{\Phi}^T \mathbf{b}\, dx \qquad (3.2.14)$$

As for the $\mathbf{b}$, it consists of the external loads b_0 as well as an inertia component and a damping component and can be written as

$$\mathbf{b} = b_0 - m\ddot{v} - c\dot{v} \qquad (3.2.15)$$

For Civil Engineering structures, one is basically interested in wind and earthquake excitation. Thus

$$\mathbf{b} = b_w - m\ddot{a}_g - m\ddot{v} - c\dot{v} \qquad (3.2.16)$$

where b_w is a function expressing the wind load distribution along the height of the building and $m\ddot{a}_g$ is an equivalent earthquake load vector distributed along the height. For the stiffness proportional damping case, the damping term in the *(3.2.16)* drops out, and by substituting for $\ddot{v}$ from *(3.2.1)*, *(3.2.16)* becomes

$$\mathbf{b} = b_w - m\boldsymbol{\Phi}\ddot{Q}_s - m\boldsymbol{\psi}\ddot{Q}_b - m\ddot{a}_g \qquad (3.2.17)$$

Using *(3.2.17)*, the load terms of *(3.2.13)* and *(3.2.14)* expand to

$$\mathbf{P}_b = \mathbf{P}_{bw} - \mathbf{M}_{bb}\ddot{\mathbf{Q}}_b - \mathbf{M}_{bs}\ddot{\mathbf{Q}}_s - \ddot{a}_g\mathbf{P}_{be} \qquad (3.2.18)$$

$$\mathbf{P}_s = \mathbf{P}_{sw} - \mathbf{M}_{sb}\ddot{\mathbf{Q}}_b - \mathbf{M}_{ss}\ddot{\mathbf{Q}}_s - \ddot{a}_g\mathbf{P}_{se} \qquad (3.2.19)$$

where

$$\mathbf{M}_{bb} = \int_0^H m\,\boldsymbol{\psi}^T\boldsymbol{\psi}\,dx \qquad (3.2.20)$$

$$\mathbf{M}_{bs} = \mathbf{M}_{sb}^T = \int_0^H m\,\boldsymbol{\psi}^T\boldsymbol{\Phi}\,dx \qquad (3.2.21)$$

$$\mathbf{M}_{ss} = \int_0^H m\,\boldsymbol{\Phi}^T\boldsymbol{\Phi}\,dx \qquad (3.2.22)$$

$$\mathbf{P}_{bw} = \int_0^H \boldsymbol{\psi}^T b_w\,dx \qquad (3.2.23)$$

$$\mathbf{P}_{be} = \int_0^H m\,\boldsymbol{\psi}^T\,dx \qquad (3.2.24)$$

$$\mathbf{P}_{sw} = \int_0^H \boldsymbol{\Phi}^T b_w\,dx \qquad (3.2.25)$$

$$\mathbf{P}_{se} = \int_0^H m\,\boldsymbol{\Phi}^T\,dx \qquad (3.2.26)$$

Rewriting *(3.2.9)* and *(3.2.10)* in matrix form and substituting for the equivalent load vectors from *(3.2.18)* and *(3.2.19)* yields

$$\mathbf{M}\ddot{\mathbf{Q}} + \alpha\mathbf{K}\dot{\mathbf{Q}} + \mathbf{K}\mathbf{Q} = \mathbf{P}_w - \mathbf{P}_e\ddot{a}_g \qquad (3.2.27)$$

where

$$\mathbf{M} = \begin{bmatrix} \mathbf{M}_{ss} & \mathbf{M}_{sb} \\ \mathbf{M}_{bs} & \mathbf{M}_{bb} \end{bmatrix} \qquad (3.2.28)$$

$$\mathbf{K} = \begin{bmatrix} \mathbf{K}_{ss} & \mathbf{O} \\ \mathbf{O} & \mathbf{K}_{bb} \end{bmatrix} \qquad (3.2.29)$$

$$\mathbf{Q} = \begin{bmatrix} \mathbf{Q}_s \\ \mathbf{Q}_b \end{bmatrix} \qquad (3.2.30)$$

$$\alpha = \begin{bmatrix} \alpha_s \mathbf{I}_s & \mathbf{O} \\ \mathbf{O} & \alpha_b \mathbf{I}_b \end{bmatrix} \qquad (3.2.31)$$

$$\mathbf{P}_w = \begin{bmatrix} \mathbf{P}_{sw} \\ \mathbf{P}_{bw} \end{bmatrix} \qquad (3.2.32)$$

$$\mathbf{P}_e = \begin{bmatrix} \mathbf{P}_{se} \\ \mathbf{P}_{be} \end{bmatrix} \qquad (3.2.33)$$

The shear and bending displacement measures are coupled through the mass terms. Setting $\mathbf{Q}_b$ to zero reduces the formulation to that of a "shear beam" which will be the topic of Chapter Five. Similarly, setting $\mathbf{Q}_s$ to zero results in the formulation "bending beam" which will be the main topic of Chapter Six. Assuming a mixed mode behavior by taking $\mathbf{Q}_b = \lambda\mathbf{Q}_s$, and $\alpha_b = \alpha_s$, with $\mathbf{Q}_s$ as the independent variable, *(3.2.27)* takes the form

$$\mathbf{M}^*\ddot{\mathbf{Q}}_s + \alpha_s \mathbf{K}^*\dot{\mathbf{Q}}_s + \mathbf{K}^*\mathbf{Q}_s = \mathbf{P}_w^* - \mathbf{P}_e^*\ddot{a}_g \qquad (3.2.34)$$

where $$\mathbf{M}^* = \mathbf{M}_{ss} + \lambda\left(\mathbf{M}_{sb} + \mathbf{M}_{bs}\right) + \lambda^2\mathbf{M}_{bb} \qquad (3.2.35)$$

$$\mathbf{K}^* = \mathbf{K}_{ss} + \lambda^2\mathbf{K}_{bb} \qquad (3.2.36)$$

$$\mathbf{P}_w^* = \mathbf{P}_{sw} + \lambda\mathbf{P}_{bw} \qquad (3.2.37)$$

$$\mathbf{P}_e^* = \mathbf{P}_{se} + \lambda\mathbf{P}_{be} \qquad (3.2.38)$$

Additional simplifications are possible if one works with mutually orthogonal functions. Thus, knowing the shear mode shapes and the bending mode shapes, one can determine a factor that will incorporate bending in a shear beam formulation. Hence, one can combine the two to obtain the rigidity distributions of buildings that lie somewhere between those two extremes.

The next chapter provides an application of the general formulation developed herein to the case where only one mode is significant.

CHAPTER FOUR

FUNDAMENTAL MODE RESPONSE

4- 1 INTRODUCTION

This chapter presents the case where the spatial response can be reasonably approximated by the fundamental mode of the building. The approach is to define a stiffness distribution such that the deformation measures for the fundamental mode shape are constant over the height and satisfy *(2.2.1.33)*. The free vibration problem is considered first, followed by the development of the forced vibration problem specialized for earthquake excitation. Examples follow to illustrate how buildings with rigidity distributions based on the fundamental mode, respond to seismic excitation. The chapters that follow expand the analysis to handle multi-modal response.

4 - 2 *FUNDAMENTAL MODE - UNIFORM DEFORMATION*

First, the case of undamped free vibration with elastic force-deformation relations is considered. Thus the equivalent load consists only of the inertia term and *(3.2.15)* becomes

$$b = - m\ddot{v} \qquad (4.2.1)$$

The equilibrium equations for elastic behavior and inertia loading become

$$V(x,t) = - m \int_x^H \ddot{v}(x,t)\, dx = D_T(x)\, \gamma(x,t) \qquad (4.2.2)$$

$$M(x,t) = \int_x^H V(x,t)\, dx = D_B(x)\, k(x,t) \qquad (4.2.3)$$

Forcing the building to vibrate in a constant deformation fundamental mode, is equivalent to writing

$$\gamma(x,t) = \gamma^* e^{i\omega_1 t} \qquad (4.2.4)$$

$$k(x,t) = k^* e^{i\omega_1 t} \qquad (4.2.5)$$

where $i = \sqrt{-1}$ and ω_1 is the fundamental circular frequency of the structure. Making use of Equations *(2.2.1.18)* to *(2.2.1.22)* which were developed for the

single mode constant deformation case for the static problem and substituting *(4.2.4)* and *(4.2.5)* for γ^* and k^* respectively yields

$$\Phi = \bar{x} \qquad (4.2.6)$$

$$\psi = \frac{\bar{x}^2}{2} \qquad (4.2.7)$$

$$\bar{x} = \frac{x}{H} \qquad (4.2.8)$$

$$Q_s = \gamma^* H \, e^{i\omega_1 t} \qquad (4.2.9)$$

$$Q_b = k^* H^2 \, e^{i\omega_1 t} \qquad (4.2.10)$$

and hence *(2.2.1.14)* and *(2.2.1.15)* become

$$v = \gamma^* H \left[\bar{x} + \frac{1}{2} \left(\frac{k^* H}{\gamma^*} \right) \bar{x}^2 \right] e^{i\omega_1 t} \qquad (4.2.11)$$

$$\beta = \gamma^* H \left[\frac{1}{H} \left(\frac{k^* H}{\gamma^*} \right) \bar{x} \right] e^{i\omega_1 t} \qquad (4.2.12)$$

Making use of

$$a = \frac{k^* H}{\gamma^*} = \frac{H}{f B} \qquad (4.2.13)$$

and substituting in *(4.2.2)* and *(4.2.3)* yields

$$D_T(\bar{x}) = \frac{m\omega_1^2 H^2}{2}\left[1 - \bar{x}^2 + \frac{a}{3}\left(1 - \bar{x}^3\right)\right] \qquad (4.2.14)$$

$$D_B(\bar{x}) = \frac{m\omega_1^2 H^4}{2}\left[\frac{1}{4}\left(1 - \frac{4}{3}\bar{x} + \frac{1}{3}\bar{x}^4\right) + \frac{1}{3a}\left(2 - 3\bar{x} + \bar{x}^3\right)\right] \qquad (4.2.15)$$

Fig. 4.2.1 and Fig. 4.2.2 show plots for *(4.2.14)* and *(4.2.15)* respectively for a building with a period of 5 seconds and an $a = 3$. Fig. 4.2.3 shows a plot of the first five mode shapes of that same building with rigidity distributions given by *(4.2.14)* and *(4.2.15)* and uniform mass distribution.

D_T can be determined at $x = 0$ by specifying representative values of base shear and transverse shear deformation

$$D_T(0) = \frac{V(0)}{\gamma^*} \qquad (4.2.16)$$

The equation for fundamental frequency follows from *(4.2.14)*

$$D_T(0) = \frac{V(0)}{\gamma^*} = \frac{m\omega_1^2 H^2}{2}\left(1 + \frac{a}{3}\right) \qquad (4.2.17)$$

$$\omega_1 = \sqrt{\frac{2\,V(0)}{\gamma^* m H^2\left(1 + \frac{a}{3}\right)}} \qquad (4.2.18)$$

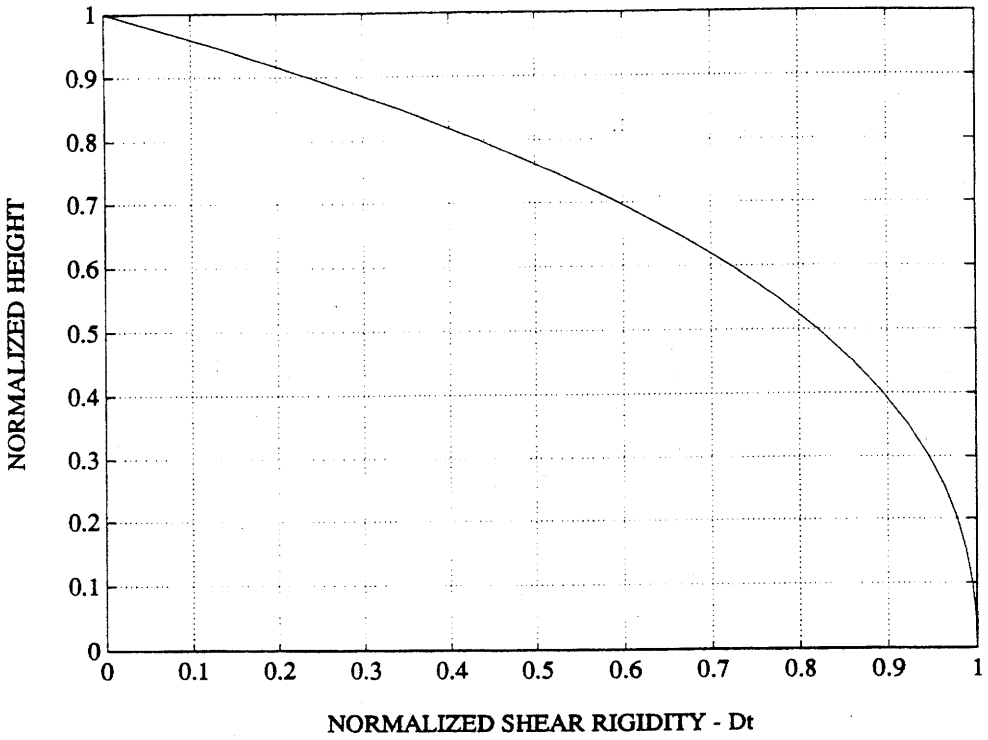

FIGURE 4.2.1: NORMALIZED SHEAR RIGIDITY DISTRIBUTION D_T

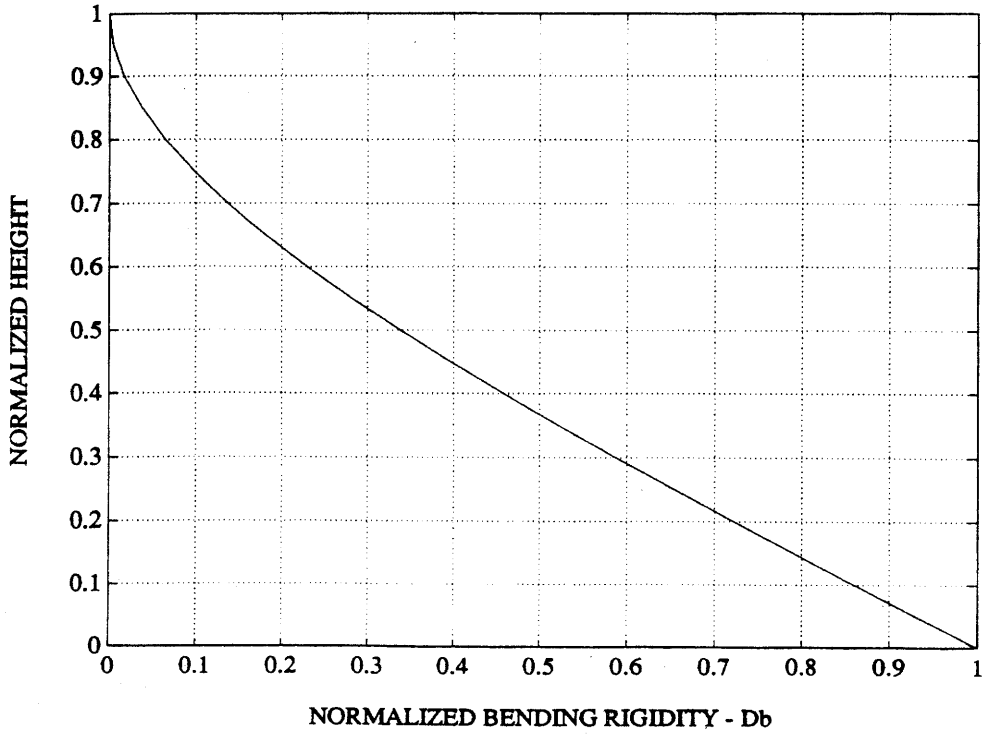

FIGURE 4.2.2: NORMALIZED BENDING RIGIDITY DISTRIBUTION D_B

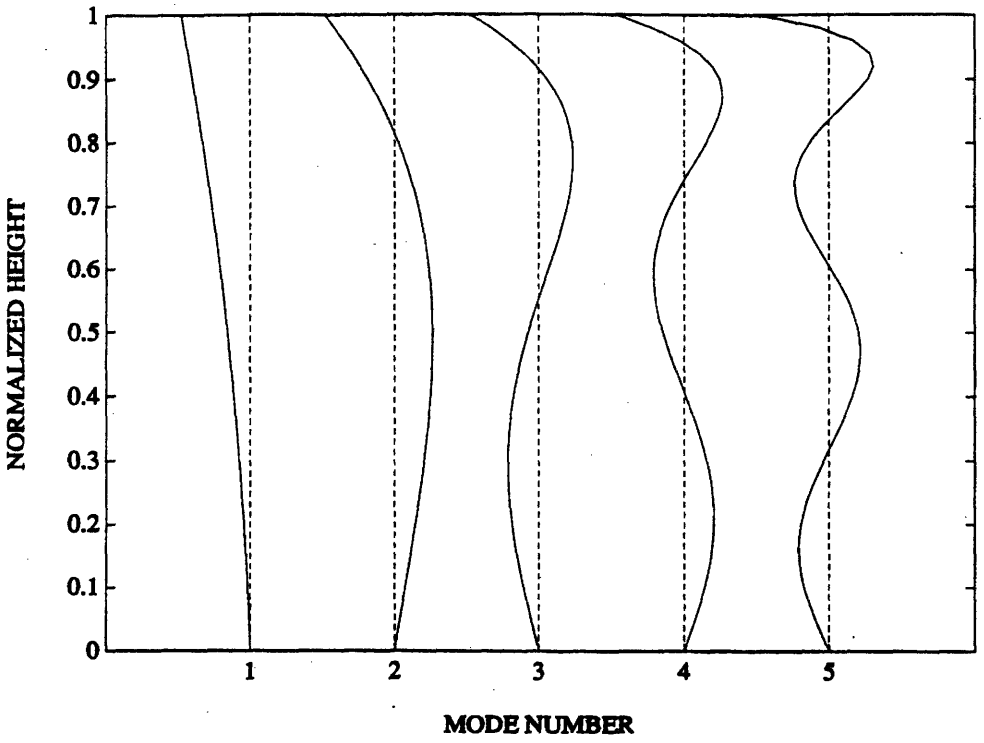

FIGURE 4.2.3: MODE SHAPES

It should be noted that the mode shape and frequency expressions are the exact solution for the fundamental modal response of the beam having the rigidity distributions defined by *(4.2.14)* and *(4.2.15)* . One obtains the solution for the "shear" beam by setting $a = 0$. For tall buildings a is around 2 .

4 - 3 SINGLE MODE - FORCED VIBRATION

As a first approximation, the fundamental mode shape defined by *(4.2.11)* and *(4.2.12)* is used to represent the spatial variation of the displacement response. For convenience, the equations are relisted here

$$v = Q_s\left(\bar{x} + \frac{1}{2} a \bar{x}^2\right) = Q_s \theta_s \qquad (4.3.1)$$

$$\beta = Q_s\left(\frac{a}{H}\bar{x}\right) = Q_s \theta_b \qquad (4.3.2)$$

$$\gamma = \frac{Q_s}{H} \qquad (4.3.3)$$

$$k = \frac{a}{H^2} Q_s \qquad (4.3.4)$$

$$a = \frac{Hk^*}{\gamma^*} \qquad (4.3.5)$$

Assume an equivalent load of

$$b = b_0 - m\ddot{v} - c\dot{v} \qquad (4.3.6)$$

What follows is very similar to the formulation of the previous chapter, however, since the damping is included in the load vector, one cannot obtain the results by directly substituting in the previously derived equations. Going back to the Principle of Virtual Displacements which takes the following form

$$\int_0^H \left(M\delta k + V\delta\gamma\right) dx = \int_0^H \left(b_0 - m\ddot{v} - c\dot{v}\right) \delta v \, dx \qquad (4.3.7)$$

Requiring that *(4.3.7)* be satisfied for arbitrary δv yields

$$M^* \ddot{Q}_s + C^* \dot{Q}_s + K^* Q_s = P^* \qquad (4.3.8)$$

where $$M^* = \int_0^H m\,\theta_s^2\,dx = mH\left(\frac{1}{3} + \frac{a}{4} + \frac{a^2}{20}\right) \qquad (4.3.9)$$

$$P^* = \int_0^H \theta_s\, b\, dx = \frac{b_0 H}{2}\left(1 + \frac{a}{3}\right) \quad \text{for constant } b_0 \qquad (4.3.10)$$

$$K^* = \int_0^H \left[\frac{a^2}{H^4} D_B + \frac{1}{H^2} D_T\right] dx = \omega_1^2 M^* \qquad (4.3.11)$$

$$C^* = \int_0^H \left[c\,\theta_s^2 + \frac{a^2}{H^4} D_B^* + \frac{1}{H^2} D_T^*\right] dx \qquad (4.3.12)$$

Assuming the viscous damping terms can be related to the mass and stiffness by the following equations

$$c = \alpha m \qquad (4.3.13)$$

$$D_T^* = \beta D_T \qquad (4.3.14)$$

$$D_B^* = \beta D_B \qquad (4.3.15)$$

then $$C^* = \alpha M^* + \beta K^* \qquad (4.3.16)$$

Finally, if C^* is expressed in terms of the modal damping ratio ξ_1

$$C^* = 2\,\xi_1\,\omega_1\,M^* \qquad (4.3.17)$$

one can solve for ξ_1

$$\xi_1 = \frac{1}{2}\left(\frac{\alpha}{\omega_1} + \beta\ \omega_1\right) \qquad (4.3.18)$$

The equilibrium equation then takes the form

$$\ddot{Q}_s + 2\,\xi_1\,\omega_1\,\dot{Q}_s + \omega_1^2\,Q_s = \frac{P^*}{M^*} \qquad (4.3.19)$$

Specializing *(4.3.19)* further for earthquake excitation, one can introduce the following substitution

$$b_0 = -\,m\,\ddot{a}_g \qquad (4.3.20)$$

and *(4.3.10)* becomes

$$P^* = -\,\frac{mH}{2}\,\ddot{a}_g\left(1 + \frac{a}{3}\right) \qquad (4.3.21)$$

Substituting *(4.3.21)* in *(4.3.19)* leads to

$$\ddot{Q}_s + 2\,\xi_1\,\omega_1\,\dot{Q}_s + \omega_1^2\,Q_s = -\,\Gamma_1\tilde{P}^* \qquad (4.3.22)$$

where
$$\Gamma_1 = \frac{\int_0^H m\,\theta_s\,dx}{\int_0^H m\,\theta_s^2\,dx} = \frac{1+\frac{a}{3}}{\frac{2}{3}+\frac{a}{2}+\frac{a^2}{10}} \qquad (4.3.23)$$

Table 4.3.1 shows the variation of Γ_1 with a .

a	0	1	2	3	4	5
Γ_1	1.50000	1.05263	0.80645	0.65217	0.54688	0.47059

TABLE 4.3.1: VARIATION OF Γ_1 WITH a .

4 - 4 CALIBRATION OF FUNDAMENTAL MODE MODEL

A response spectrum can be used, such as the one shown in Fig. A.2.3 to obtain an estimate of the maximum value of Q_s for a specific level of ground motion. Given ω_1 and ξ_1, one finds the pseudo-spectral velocity S_v from the spectrum. The maximum value of Q_s and the total acceleration are related to S_v by

$$Q_{s,max} = \frac{\Gamma_1\, S_v(\xi_1,\omega_1)}{\omega_1} \qquad (4.4.1)$$

$$\left(\ddot{a}_g + \ddot{Q}_s\right)_{max} \approx \omega_1^2\, Q_{s,max} = \Gamma_1\, \omega_1\, S_v(\xi_1,\omega_1) \qquad (4.4.2)$$

Once $Q_{s,max}$ is known, the deformation measures can be evaluated, and consequently, the transverse shear and the bending moment can also be evaluated. However, the fundamental frequency depends on a "reference" shear force which, as has been shown, also depends on the fundamental frequency. One can resolve the problem by establishing an expression for the reference base shear using only the first mode results and then equating the two expressions.

The transverse shear force distribution can be obtained by specializing *(A.4.9)* for the current problem

$$V_{1,max}(x) = \Gamma_1 \, \omega_1 \, S_v(\xi_1,\omega_1) \int_x^H m \, \theta_s \, dx \qquad (4.4.3)$$

and the base shear becomes, considering only the first mode

$$V_{max}(0) = \Gamma_1 \, \omega_1 \, S_v(\xi_1,\omega_1) \frac{mH}{2}\left(1 + \frac{a}{3}\right) \qquad (4.4.4)$$

Equating *(4.4.4)* and *(4.2.17)* yields the desired expression for ω_1

$$\omega_1 = \frac{S_v(\xi_1,\omega_1)}{\gamma^* H} \Gamma_1 \qquad (4.4.5)$$

$$T_1 = 2\pi \frac{\gamma^* H}{\Gamma_1 \, S_v(\xi_1,\omega_1)} \qquad (4.4.6)$$

Equation *(4.4.6)* is used for the range where S_v is constant. This depends on the level of damping and the construction of the spectrum. A typical range is $0.5\,s < T < 5\,s$. When $T < 0.5\,s$, the pseudo-spectral velocity is considered to vary linearly with ω

$$S_v = \frac{1}{\omega} S_a \qquad (4.4.7)$$

and S_a is constant. Equation *(4.4.6)* takes an equivalent form

$$\omega_1 = \sqrt{\frac{\Gamma_1 S_a(\xi_1,\omega_1)}{\gamma^* H}} \qquad (4.4.8)$$

$$T_1 = 2\pi \sqrt{\frac{\gamma^* H}{\Gamma_1 S_a(\xi_1,\omega_1)}} \qquad (4.4.9)$$

4 - 5 EXAMPLES

The design procedure consists of specifying an m and an H, and deciding on the values of γ^* and S_v to be used for the service load design. Equation *(4.4.6)* gives the fundamental period. The reference base shear follows from *(4.4.4)*. Lastly, the shear and bending rigidity distributions are generated using *(4.2.14)* and *(4.2.15)*.

In the examples that follow, the mass, γ^* and, S_v are specified. Then, four fundamental periods are chosen to cover the spectrum, and the

corresponding building heights are calculated using *(4.4.6)* and are listed in Table 4.5.1. All the buildings used have a modal damping ratio of 2% in the fundamental mode. The mass distribution is 20000 kg/m height. The rigidities of those buildings are calculated using *(4.2.14)* and *(4.2.15)*. The determined rigidities are discretized following the procedure described in Appendix C and

PERIOD	a	S_v	H
0.6*s*	0.75	1.5 *m/s*	33 *m*
1.2*s*	1.00	1.5 *m/s*	60 *m*
3.0*s*	3.00	1.5 *m/s*	116 *m*
5.0*s*	3.00	1.5 *m/s*	155 *m*

TABLE 4.5.1: BUILDING EXAMPLES

the mode shapes of the lumped parameter MDOF system are hence determined. The discrete model is then subjected to earthquake excitation to determine the maximum encountered deformations with the proposed rigidity distributions. Two accelerograms are used, El Centro S00E and Taft N21E (Appendix B), both scaled to a maximum pseudo-spectral velocity of 1.5 m/s. Fig. 4.5.1 through 4.5.16 show the different rigidity distributions and the resulting maximum deformations for the different periods and values of a . The dotted lines in the rigidity diagrams consist of the modal rigidity contributions, and the solid lines show the rigidity distributions as determined by *(4.2.14)* and *(4.2.15)*. As to the deformation diagrams, the dashed vertical line indicates the target maximum

deformation and the solid line gives the maximum deformation under El Centro excitation whereas the other dashed line gives the maximum deformation under Taft excitation. It is seen that as the fundamental period increases, the effect of the higher modes becomes more significant and the deflection at the top increases. The following chapters help identify the reasons behind this kind of behavior.

This approach assumes that the response can be represented by a single displacement function (i.e. a single mode). From the accompanying figures, it can be seen that for buildings with very low fundamental periods subjected to seismic excitation, this approximation holds and with the proposed rigidity distributions, the deformations are quite uniform. However, the target deformation is not quite achieved for the following reasons:

- The higher modes contribute to the displaced shape, resulting in non-uniform deformation.

- The magnitude of the maximum deformation is sensitive to the magnitude and distribution of damping.

- The magnitude of the maximum deformation is sensitive the excitation and the accompanying scaling procedures.

Finally, the difference in the behavior of the five second building under the two excitations is mainly due to the difference in the spectra. For the El Centro

Spectrum, at a period of five seconds, S_v is much less than the assumed 1.5m/s which occurs at a period close to that of the second mode. This results in an overestimation of the first mode excitation leading to a reduction in deformation at the base where the contribution from the first mode is dominant. The Taft spectrum shows that the design S_v occurs at the fundamental mode period which is why the actual deformation is so close to the target deformation.

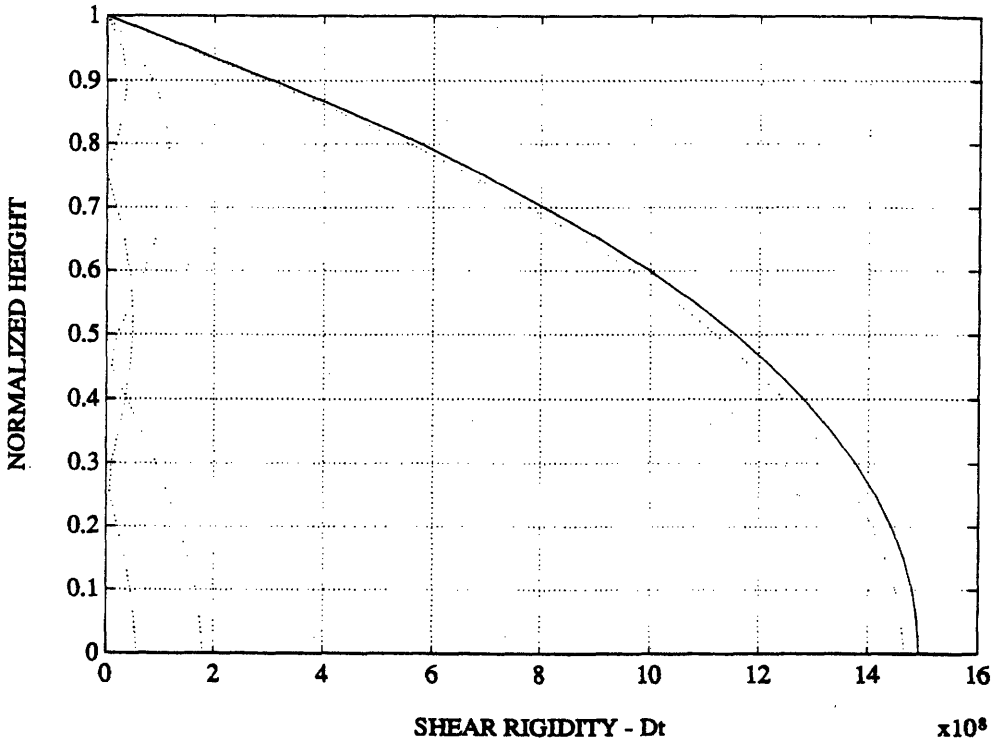

FIGURE 4.5.1: SHEAR RIGIDITY D_T *(T=0.6s - a=0.75)*

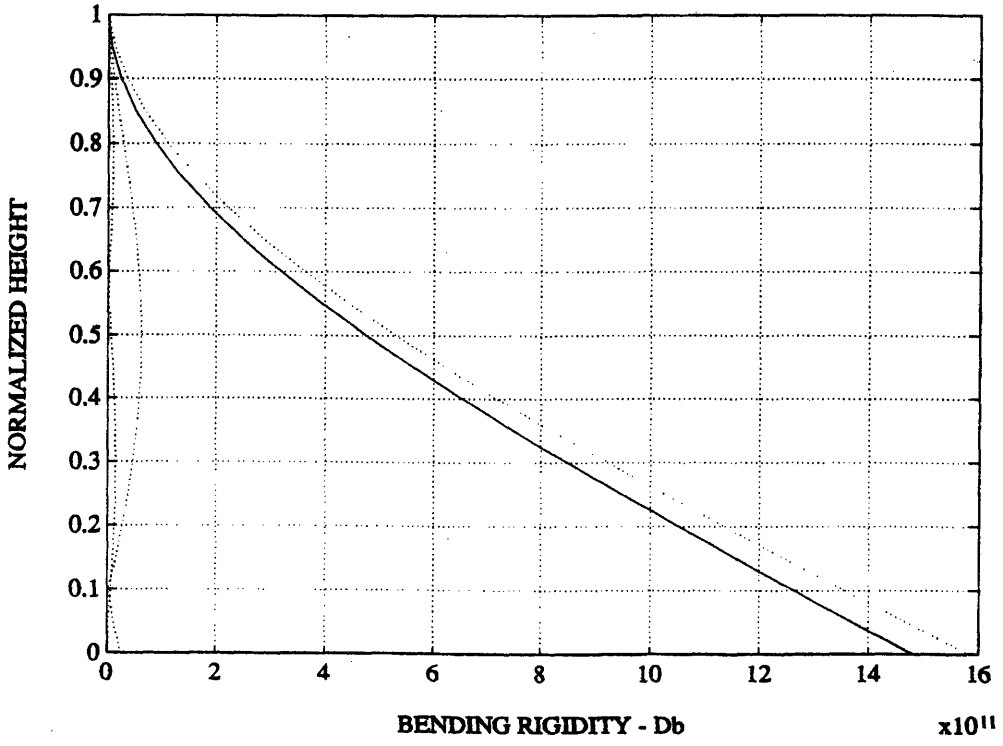

FIGURE 4.5.2: BENDING RIGIDITY D_B *(T=0.6s - a=0.75)*

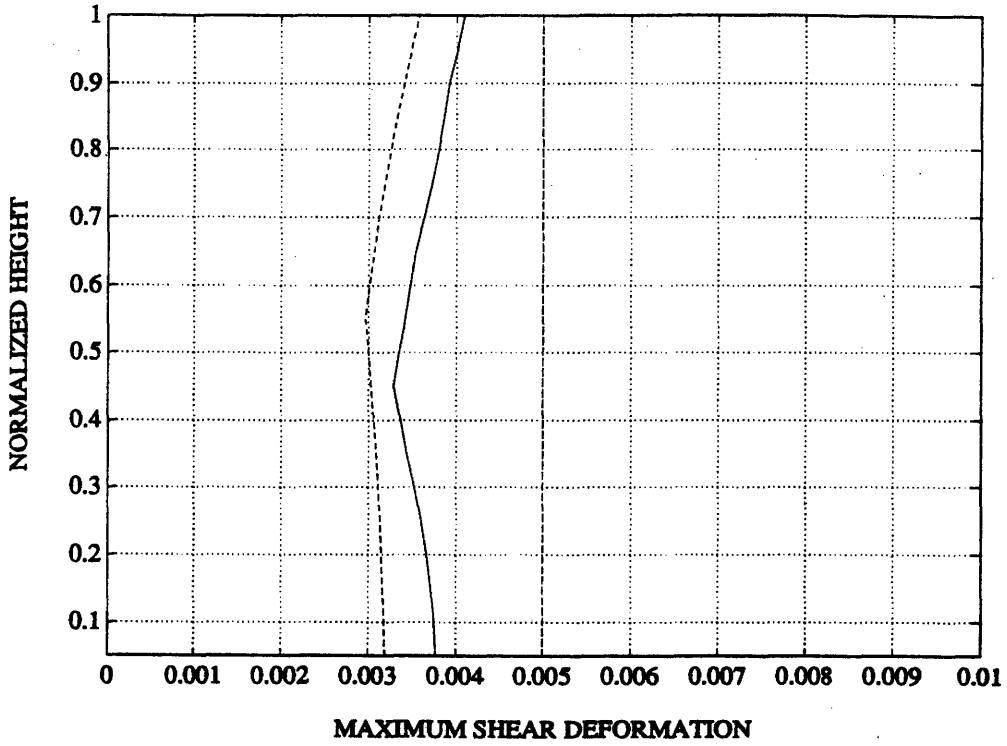

FIGURE 4.5.3: SHEAR DEFORMATION (T=0.6s - a=0.75)

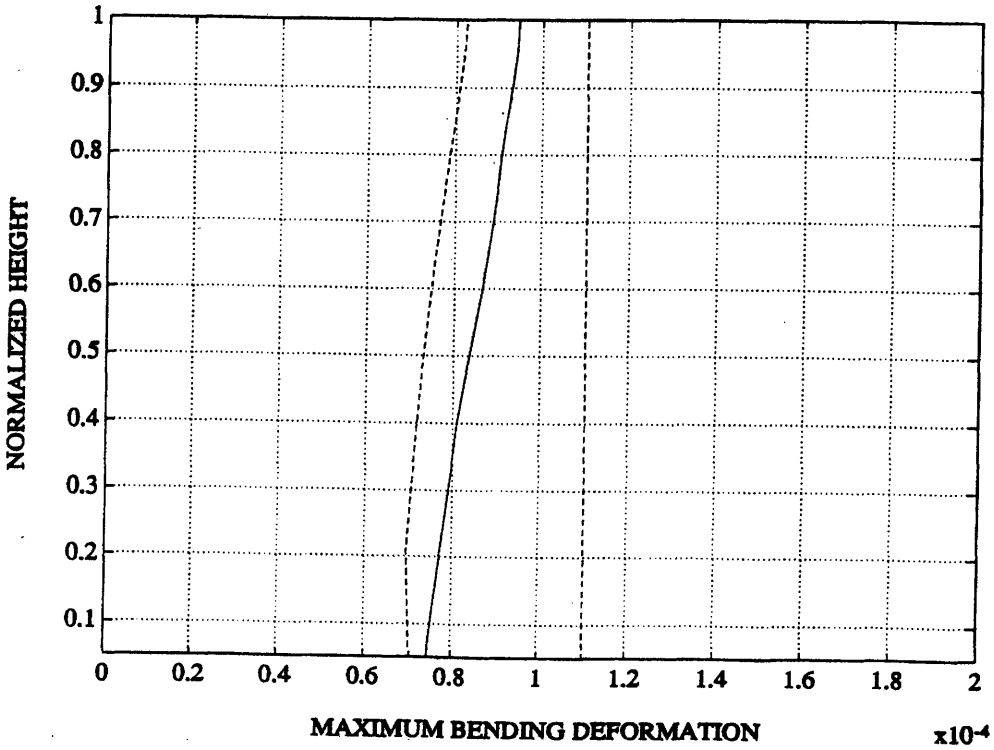

FIGURE 4.5.4: BENDING DEFORMATION (T=0.6s - a=0.75)

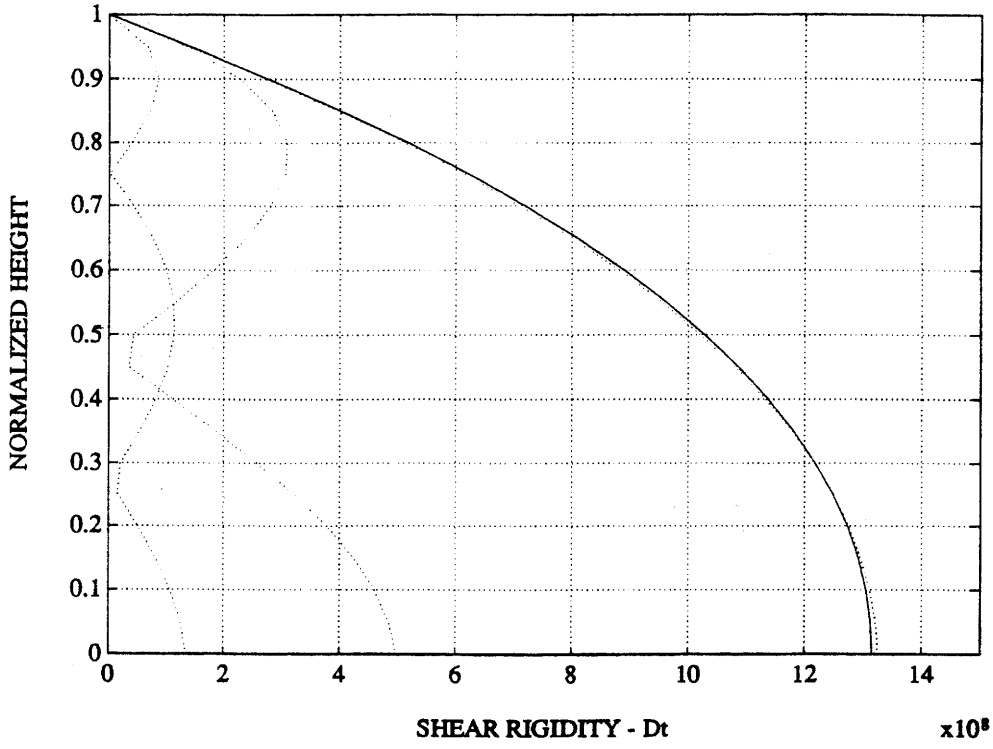

FIGURE 4.5.5: SHEAR RIGIDITY D_T *(T=1.2s - a=1.0)*

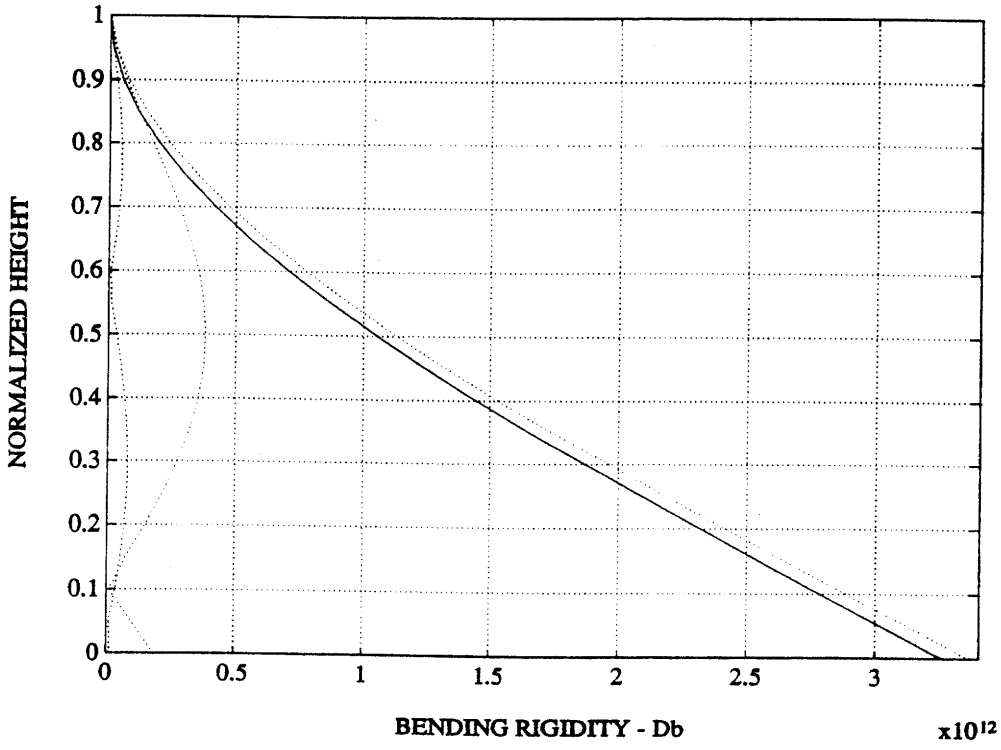

FIGURE 4.5.6: BENDING RIGIDITY D_B *(T=1.2s - a=1.0)*

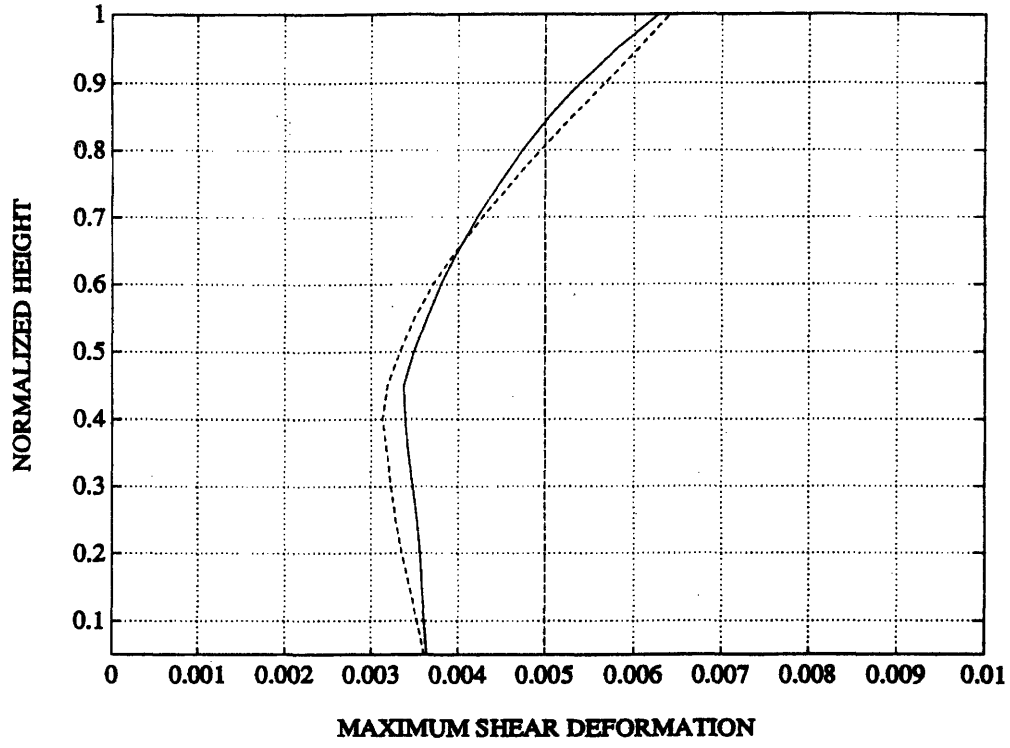

FIGURE 4.5.7: SHEAR DEFORMATION (T=1.2s - a=1.0)

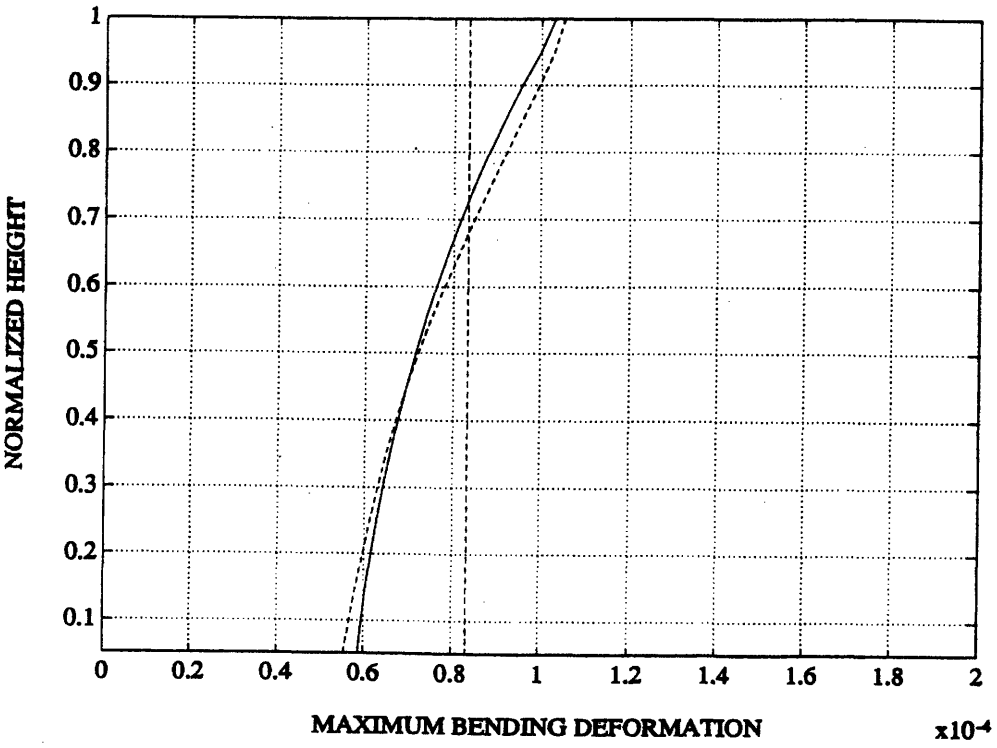

FIGURE 4.5.8: BENDING DEFORMATION (T=1.2s - a=1.0)

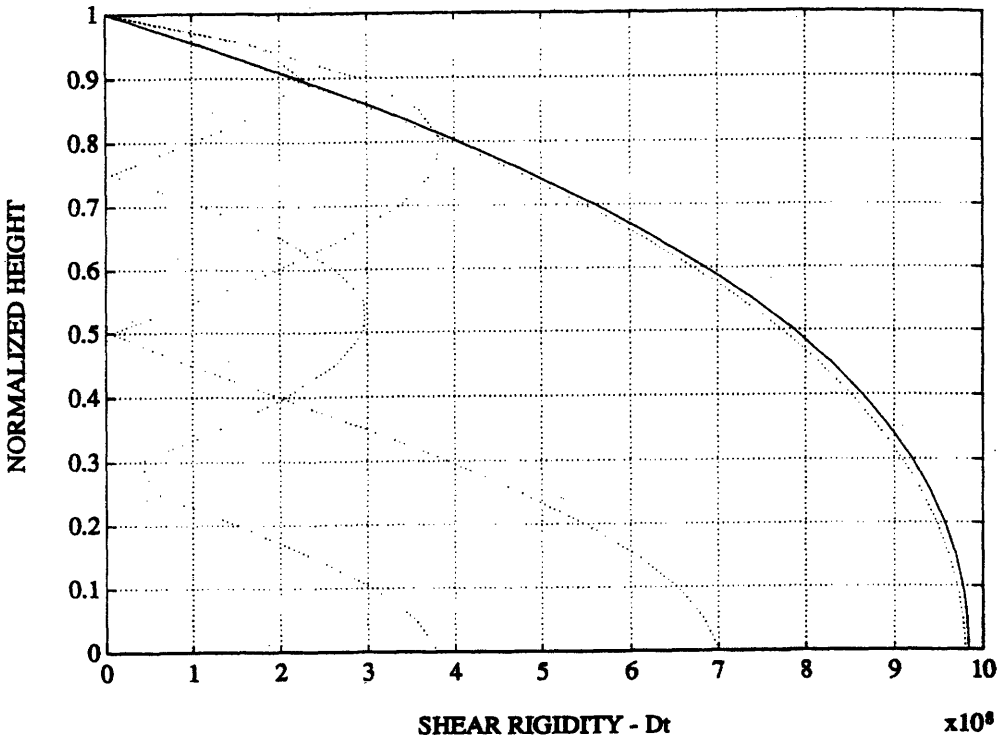

FIGURE 4.5.9: SHEAR RIGIDITY D_T (T=3.0s - a=3.0)

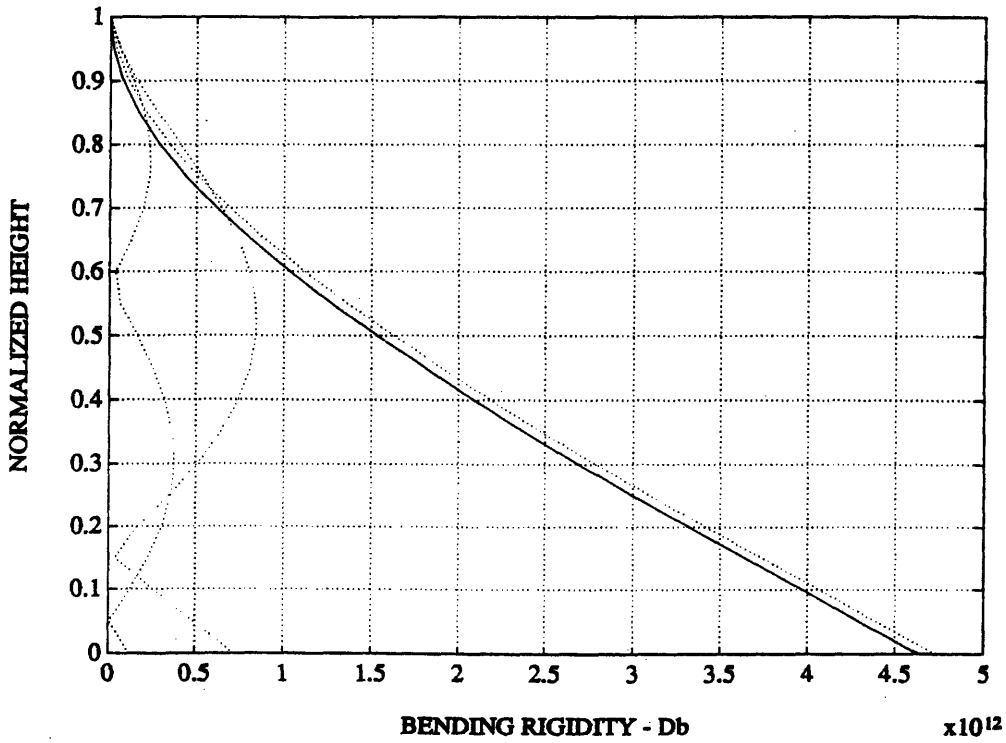

FIGURE 4.5.10: BENDING RIGIDITY D_B (T=3.0s - a=3.0)

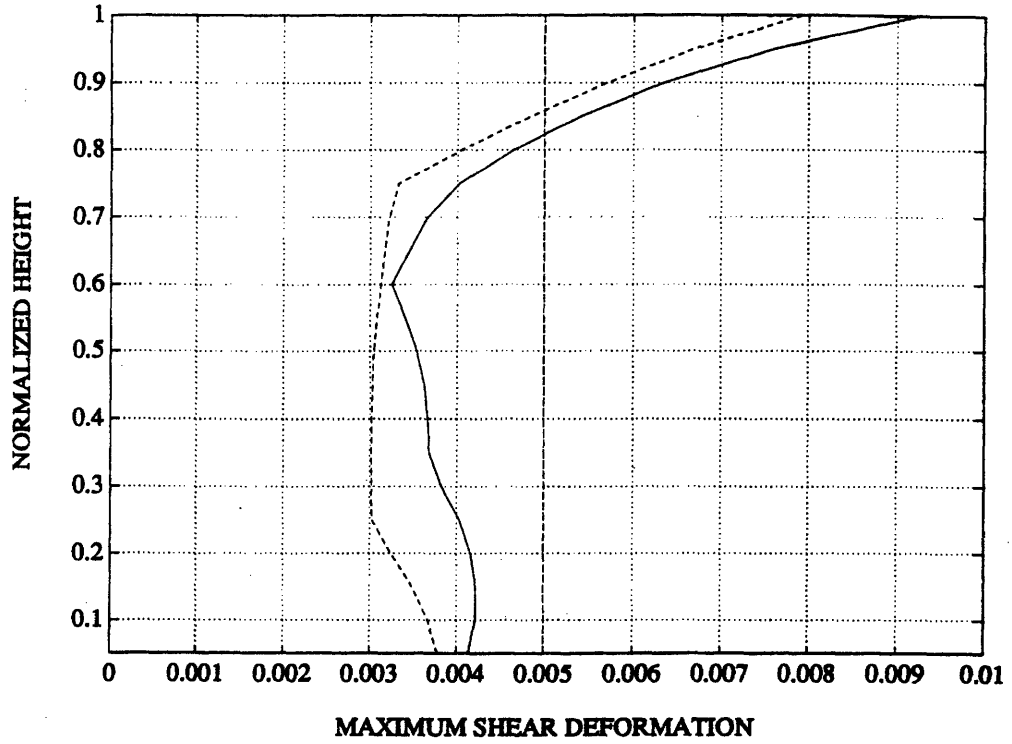

FIGURE 4.5.11: SHEAR DEFORMATION (T=3.0s - a=3.0)

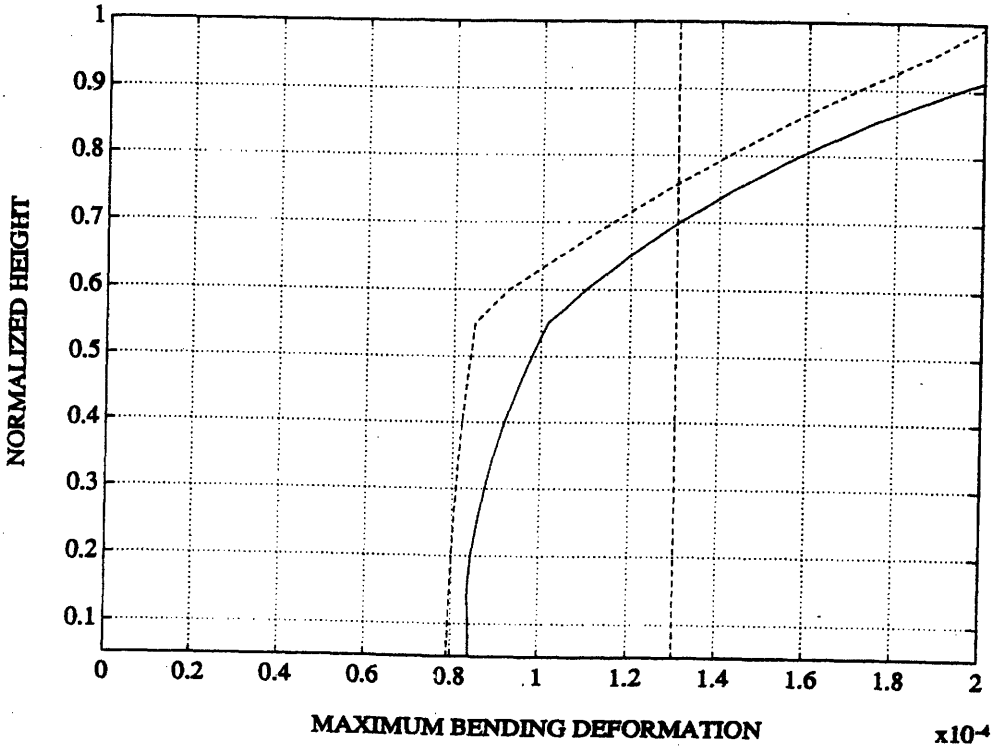

FIGURE 4.5.12: BENDING DEFORMATION (T=3.0s - a=3.0)

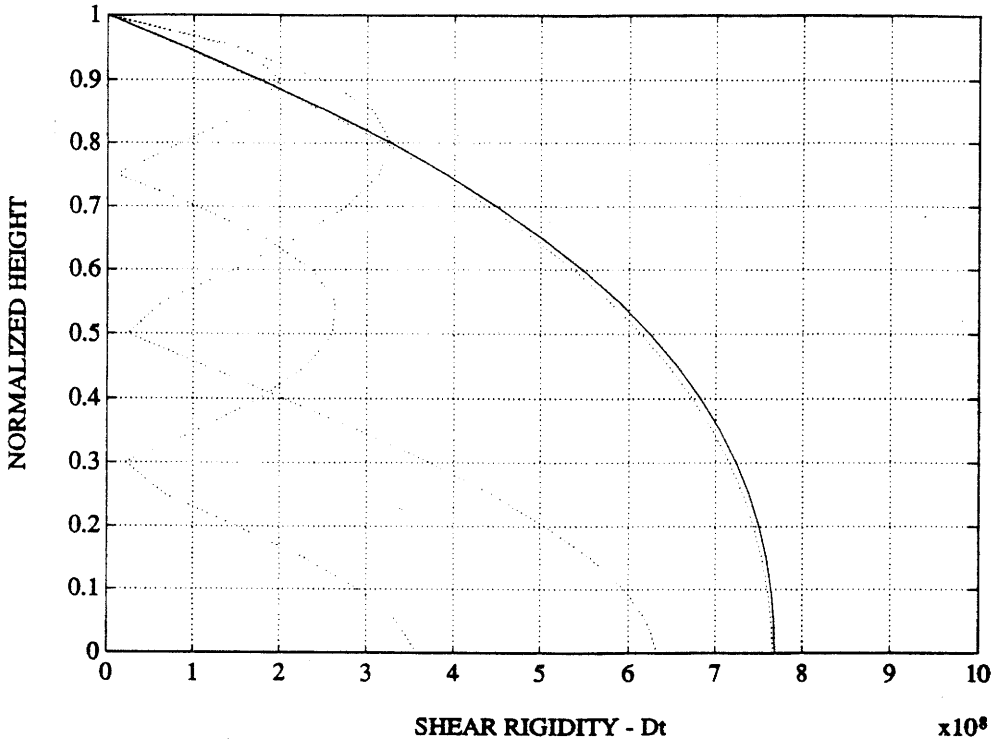

FIGURE 4.5.13: SHEAR RIGIDITY D_T *(T=5.0s - a=3.0)*

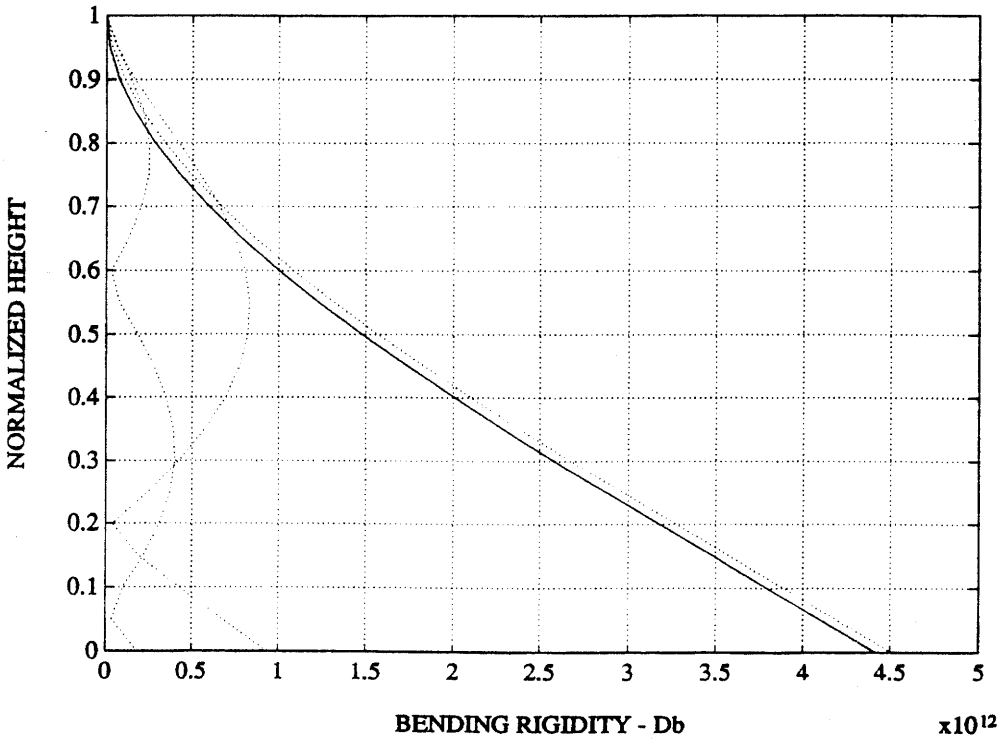

FIGURE 4.5.14: BENDING RIGIDITY D_B *(T=5.0s - a=3.0)*

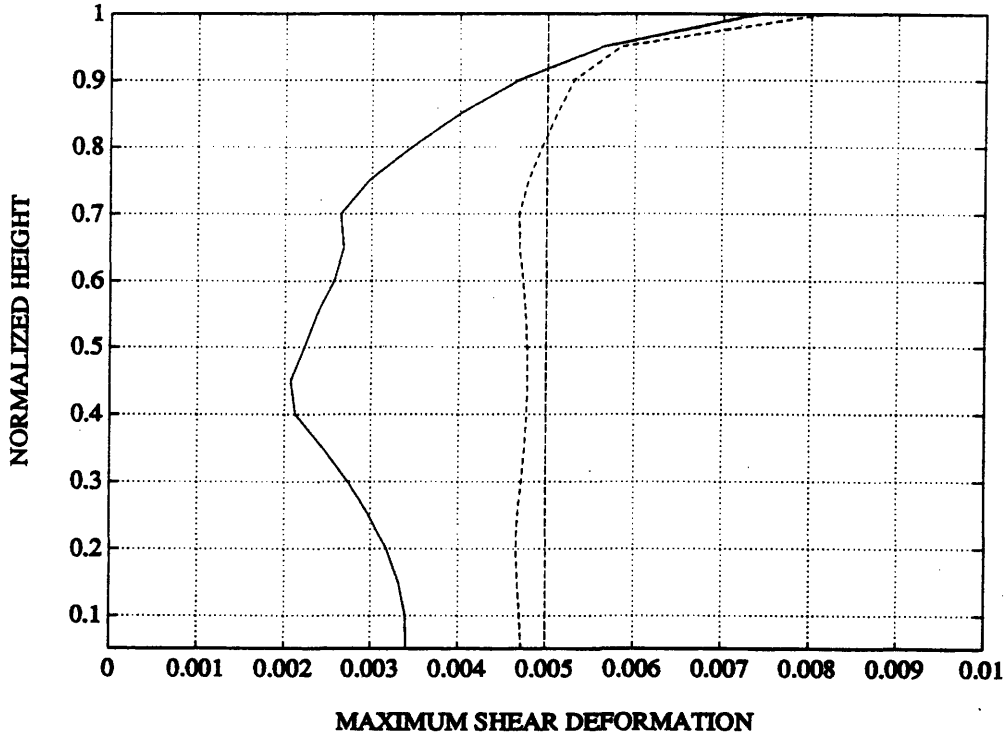

FIGURE 4.5.15: SHEAR DEFORMATION (T=5.0s - a=3.0)

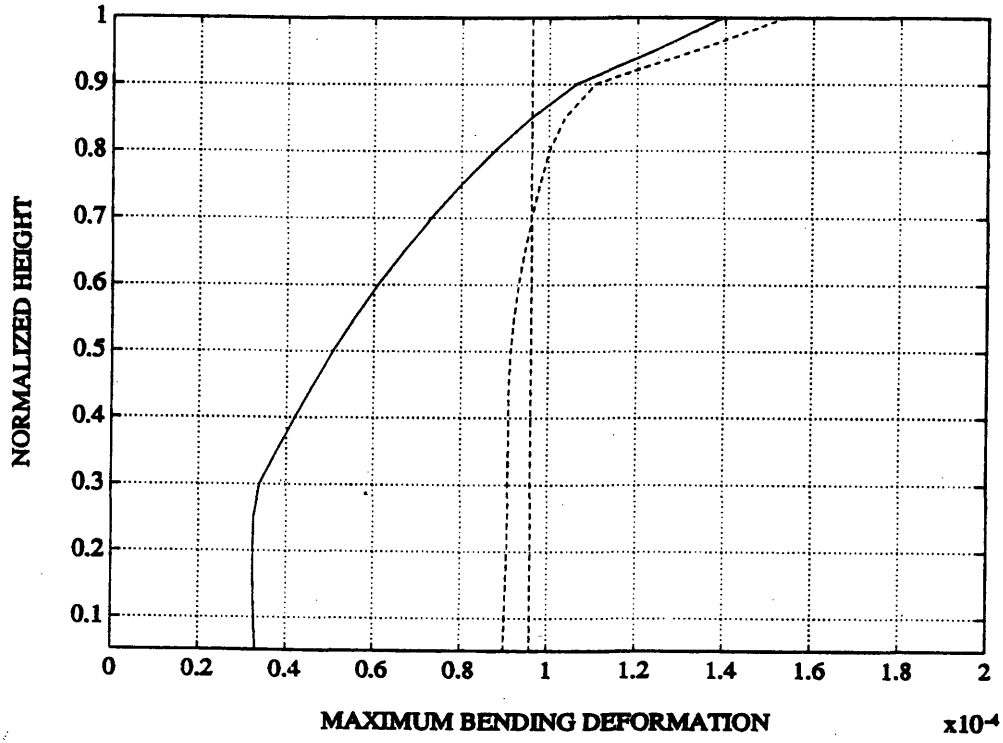

FIGURE 4.5.16: BENDING DEFORMATION (T=5.0s - a=3.0)

CHAPTER FIVE

MULTI-MODAL SHEAR BEAM BASED STIFFNESS

5 - 1 INTRODUCTION

The main purpose of this chapter and the following one is the establishment of analytical expressions that provide further insight as to how buildings behave in the limiting cases of very short and very tall ones. Low rise buildings essentially display a pseudo-shear beam behavior meaning that the rotation of their cross-sections is negligible and only shear deformation needs to be considered. This is equivalent to having very high bending rigidity that prevents any rotation from taking place. The shear beam models closely buildings with low aspect ratios and periods less than 1 second and is the topic of this chapter. On the other hand, the following chapter analyzes the other extreme

of the spectrum, the high rise buildings which display negligible shear deformation as compared to the bending deformation. Numerous buildings lie somewhere in between those two extremes where both bending and shear deformation are significant and will be dealt with later on.

The objective of this chapter is the development of a simple method that allows the estimation of the shear rigidity distribution, based on the superposition of the modes of a uniformly distributed parameter shear beam model. Only seismic loading is considered for illustrative purposes. After exposing the formulation and developing the necessary equations, a couple of buildings with different periods are designed using the proposed procedures and their behavior is tested under earthquake loading to demostrate the effectiveness of the proposed method.

5 - 2 FREE VIBRATIONS OF A CANTILEVER SHEAR BEAM

The free vibration equation of motion of an undamped prismatic shear beam, with uniform mass and shear rigidity distributions and an infinite bending rigidity over its length, is given by

$$m\frac{\partial^2 v}{\partial t^2} - D_T\frac{\partial^2 v}{\partial x^2} = 0 \qquad (5.2.1)$$

Assuming a solution of the form

$$v(x,t) = \Phi(x)\, Q(t) \qquad (5.2.2)$$

equation *(5.2.1)* becomes

$$m\,\Phi(x)\,\ddot{Q}(t) - D_t\, Q(t)\,\Phi''(x) = 0 \qquad (5.2.3)$$

Dividing by $\Phi(x)\,Q(t)$ yields the desired separation of the independent variables

$$\frac{\ddot{Q}(t)}{Q(t)} = \frac{D_T}{m}\frac{\Phi''(x)}{\Phi(x)} = -\omega^2 \qquad (5.2.4)$$

The two ordinary differential equations become

$$\Phi''(x) + \frac{m\,\omega^2}{D_T}\Phi(x) = 0 \qquad (5.2.5)$$

$$\ddot{Q}(t) + \omega^2 Q(t) = 0 \qquad (5.2.6)$$

Solving *(5.2.5)* yields the eigenvalues and the eigenfunctions (mode shapes) of the beam. The solution to *(5.2.5)* is of the form

$$\Phi(x) = A_1 \cos ax + A_2 \sin ax \qquad (5.2.7)$$

where $$a^2 = \frac{m\,\omega^2}{D_T} \qquad (5.2.8)$$

Enforcing the boundary conditions for a cantilever beam

$$\Phi(0) = 0 \qquad (5.2.9)$$

$$V(H) = D_T \Phi'(H) = 0 \qquad (5.2.10)$$

requires $\cos a_n H = 0$ (5.2.11)

for the system to admit a non trivial solution . The solution of *(5.2.11)* provides the values of aH

$$a_n H = \frac{(2n-1)\,\pi}{2} \qquad n = 1, 2, 3, \ldots \qquad (5.2.12)$$

where n represents the mode number. The frequencies and periods thus follow by substituting *(5.2.12)* in *(5.2.8)*

$$\omega_n = \frac{(2n-1)\,\pi}{2H}\sqrt{\frac{D_T}{m}} \qquad (5.2.13)$$

$$T_n = \frac{4H}{(2n-1)}\sqrt{\frac{m}{D_T}} \qquad (5.2.14)$$

The eigenvectors on the other hand, scaled to a magnitude of one, take the form

$$\Phi_n(x) = \sin\frac{(2n-1)\,\pi}{2H}x \qquad (5.2.15)$$

The ratio of the period of the n th mode with respect to the fundamental one is given by

$$\frac{T_n}{T_1} = \frac{1}{2n\text{-}1} \qquad (5.2.16)$$

Table 5.2.1 gives the values of a_nH for the first ten modes as well as the ratios of the periods corresponding to the higher modes relative to the fundamental period. Fig. 5.2.1 shows the mode shapes scaled to a maximum amplitude of one.

MODE #	a_nH	$\frac{T_n}{T_1}$
1	1.57080	1.00000
2	4.71239	0.33333
3	7.85398	0.20000
4	10.99557	0.14286
5	14.13717	0.11111
6	17.27876	0.09091
7	20.42035	0.07692
8	23.56194	0.06667
9	26.70354	0.05882
10	29.84513	0.05263

TABLE 5.2.1: CANTILEVER SHEAR BEAM PARAMETERS

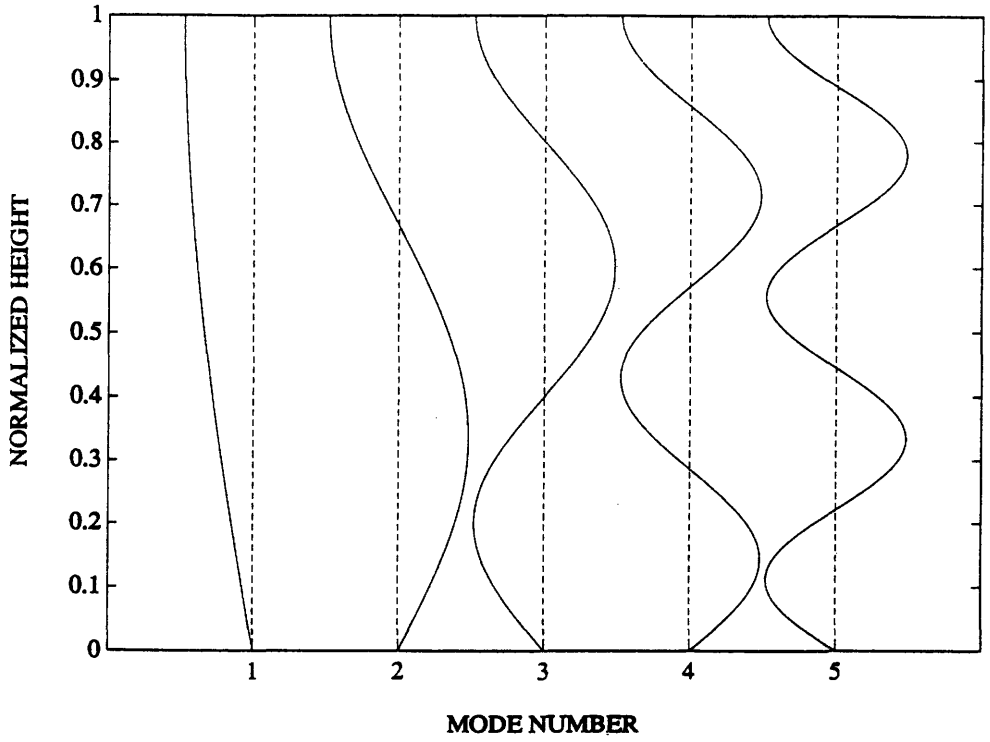

FIGURE 5.2.1: MODE SHAPES OF A UNIFORM PARAMETER SHEAR BEAM

5 - 3 MULTI-MODAL SHEAR BEAM BASED STIFFNESS:

The ultimate goal is the determination of a stiffness distribution leading to uniform maximum interstory deformations. The approach consists of combining the shear contributions of the different modes of the uniform shear beam at every level. Then by specifying a desired deformation γ^* , one can determine the rigidity distribution D_T by

$$D_T = \frac{V_{max}(x)}{\gamma^*} \qquad (5.3.1)$$

In order to determine the shear contribution of the different modes, one has first

to determine the participation factors which can be evaluated using *(A.4.2)*

$$\int_0^H m\,\Phi_n(x)\,dx = \frac{2mH}{(2n\text{-}1)\,\pi} \qquad (5.3.2)$$

and

$$\int_0^H m\,\Phi_n^2(x)\,dx = \frac{mH}{2} \qquad (5.3.3)$$

leading to

$$\Gamma_n = \frac{\int_0^H m\,\Phi_n(x)\,dx}{\int_0^H m\,\Phi_n^2(x)\,dx} = \frac{4}{(2n\text{-}1)\,\pi} \qquad (5.3.4)$$

The next step is determining the shear force distribution which may be obtained by summing up the inertia forces above the desired location The inertia force at x is given by

$$b_{n,max}(x) = m\,\Phi_n(x)\,\Gamma_n\,\omega_n\,S_v(\xi_n,\omega_n)$$

$$= \frac{2\sqrt{D_T m}}{H} S_v(\xi_n,\omega_n)\sin\left(\frac{(2n\text{-}1)\,\pi}{2H}x\right) \qquad (5.3.5)$$

and the shear follows from *(A.4.9)*

$$V_{n,max}(x) = \frac{4\sqrt{D_T\,m}}{(2n\text{-}1)\,\pi} S_v(\xi_n,\omega_n)\cos\left(\frac{(2n\text{-}1)\,\pi}{2H}x\right) \qquad (5.3.6)$$

Integrating leads to the moments

$$M_{n,max}(x) = \frac{8H\sqrt{D_T\, m}}{(2n\text{-}1)^2\,\pi^2} S_v(\xi_n,\omega_n)\left\{(-1)^{n+1} - \sin\left(\frac{(2n\text{-}1)\,\pi}{2H}x\right)\right\} \qquad (5.3.7)$$

Table 5.3.1 lists the values of the participation factors for the lowest ten modes.

MODE #	a_nH	Γ_n	$\left(\frac{1}{2n-1}\right)$	$\left(\frac{1}{2n-1}\right)^2$
1	1.57080	1.27324	1.00000	1.00000
2	4.71239	0.42441	0.33333	0.11111
3	7.85398	0.25465	0.20000	0.04000
4	10.99557	0.18189	0.14286	0.02041
5	14.13717	0.14147	0.11111	0.01235
6	17.27876	0.11575	0.09091	0.00826
7	20.42035	0.09794	0.07692	0.00592
8	23.56194	0.08488	0.06667	0.00444
9	26.70354	0.07490	0.05882	0.00346
10	29.84513	0.06701	0.05263	0.00277

TABLE 5.3.1: CANTILEVER SHEAR BEAM PARAMETERS

Assuming equal modal damping ratios, for the case where $S_v(\xi_n, \omega_n)$ is constant (periods larger than 0.6 seconds), the fourth column gives the relative shears with respect to that of the fundamental mode. Column five gives the relative shears in the region where $S_a(\xi_n, \omega_n)$ is constant (periods smaller than 0.6 seconds). One can see that as the period increases, the higher periods become more dominant since $S_a(\xi_n, \omega_n)$ tends to increase before stabilizing. This explains the results obtained in the previous chapter. However, it is the higher damping present in the higher modes that reduces the effect of those higher modes.

5 - 4 CALIBRATION OF EQUIVALENT SHEAR BEAM

It remains to calibrate the shear rigidity of the "equivalent" shear beam with the beam of the previous chapter (the beam with quadratic shear rigidity and cubic bending rigidity). One possible approach would be to require both beams to have the same peak transverse shear deformation γ_{max} at the base. Using *(5.3.6)* and *(5.2.14)* with $n = 1$, one obtains for the constant rigidity shear beam

$$T_{SB1} = \frac{\pi H \gamma_{max}}{S_v(\xi_1, \omega_1)} \qquad (5.4.1)$$

$$D_{T,SB1}(0) = \frac{16 H^2 m}{T_{SB1}^2} = \frac{16 m S_v(\xi_1, \omega_1)}{\pi^2 \gamma_{max}^2} \qquad (5.4.2)$$

The corresponding equations for the quadratic shear rigidity beam are listed below

$$T_{QSD1} = 2\pi \frac{H \gamma_{max}}{\Gamma_1 S_v(\xi_1,\omega_1)} \tag{5.4.3}$$

$$D_{T,QSD1}(0) = \frac{2\pi^2 H^2 m}{T_{QSD1}^2}\left(1+\frac{a}{3}\right) \tag{5.4.4}$$

$$= \frac{m(S_v(\xi_1,\omega_1)^2}{2\gamma_{max}^2}\Gamma_1^2\left(1+\frac{a}{3}\right) \tag{5.4.5}$$

$$= \frac{m(S_v(\xi_1,\omega_1)^2}{2\gamma_{max}^2}\left\{\frac{\left(1+\frac{a}{3}\right)^3}{\left(\frac{2}{3}+\frac{a}{2}+\frac{a^2}{10}\right)^2}\right\} \tag{5.4.6}$$

Another approach would be to require the maximum shear forces to be equal. Using only the first mode terms, the base shear force for the uniform shear beam is given by *(5.3.6)* evaluated at $x = 0$

$$V_{SB1,max}(0) = \frac{4\sqrt{D_T m}}{\pi} S_v(\xi_1,\omega_1) \tag{5.4.7}$$

For the beam with a quadratic shear rigidity, the base shear is given by *(4.3.27)*

$$V_{QSD,max}(0) = \Gamma_1 \omega_1 S_v(\xi_1,\omega_1)\frac{mH}{2}\left(1+\frac{a}{3}\right) \tag{5.4.8}$$

$$= \frac{(\Gamma_1 S_v(\xi_1,\omega_1)^2}{\gamma_{max}} \frac{m}{2}\left(1+\frac{a}{3}\right) \qquad (5.4.9)$$

Equating *(5.4.7)* and *(5.4.9)* , one can determine an expression for D_T

$$D_T(0) = \frac{m\, S_v^2(\xi_1,\omega_1)}{\gamma_{max}^2}\left\{\frac{\pi}{8}\Gamma_1^2\left(1+\frac{a}{3}\right)\right\}^2 \qquad (5.4.10)$$

$$T_1 = \frac{4\, H\, \gamma_{max}}{S_v(\xi_1,\omega_1)\left\{\frac{\pi}{8}\Gamma_1^2\left(1+\frac{a}{3}\right)\right\}^2} \qquad (5.4.11)$$

In this work, *(5.4.10)* and *(5.4.11)* are used since it is more logical to match forces than deformations.

5 - 5 EXAMPLES

Similar examples to the ones used in the previous chapter were tested to verify the proposed approach. The fundamental periods of the buildings used are 0.6s and 1.2s . Once the height of the buildings is determined based on the values of a , S_v , γ^*, and T , the rigidity distribution is determined by calculating the modal shear force distributions using *(5.3.6)*, and superposing the shears using one of the methods listed in Appendix A. The shear forces are then divided by the specified deformation to obtain the new rigidity distribution. This rigidity distribution is then discretized as was done in the previous chapter, after which the building is seismically excited. Fig. 5.5.1 through 5.5.4 show the results

where the superposition is based on the sum of absolute values which was found to provide the best solution for the cases considered. The SAV is represented by the rightmost dotted line, which is preceded by the MSRSS with a coefficient of 2 (solid line), which in turn is preceded by the SRSS (dashed line).

By examining *(5.3.6)* carefully and using Table 5.3.1, one can see that for a constant S_v, the contribution at the base of the second mode is a third of the contribution of the first. However for the building with a fundamental period of $0.6s$, S_v drops down very quickly (the second period is $0.2s$, and looking at the design spectrum scaled to a maximum S_v of $1.5\,m/s$, S_v drops by a factor of five, thus the contribution of the second mode at the base is $1/15$ of the first.) Thus one can reasonably approximate the response by that of the first mode. For the second case considered (fundamental period is $1.2s$), the shear contribution from the second mode is more than the one for the first case, but still a bit low. As one goes still higher, the situation tends to become worse and the higher modes tend to become as dominant as the first as will be seen in the next chapter. The maximum deformation plots show that the building takes off at the top as opposed to the rigidity distribution of the previous chapter. This is due to the difference in shape of the integral of the modes of the previous chapter and the current one. Although this analytic formulation is restricted to very simple cases, it clarifies the physics of the behavior of buildings.

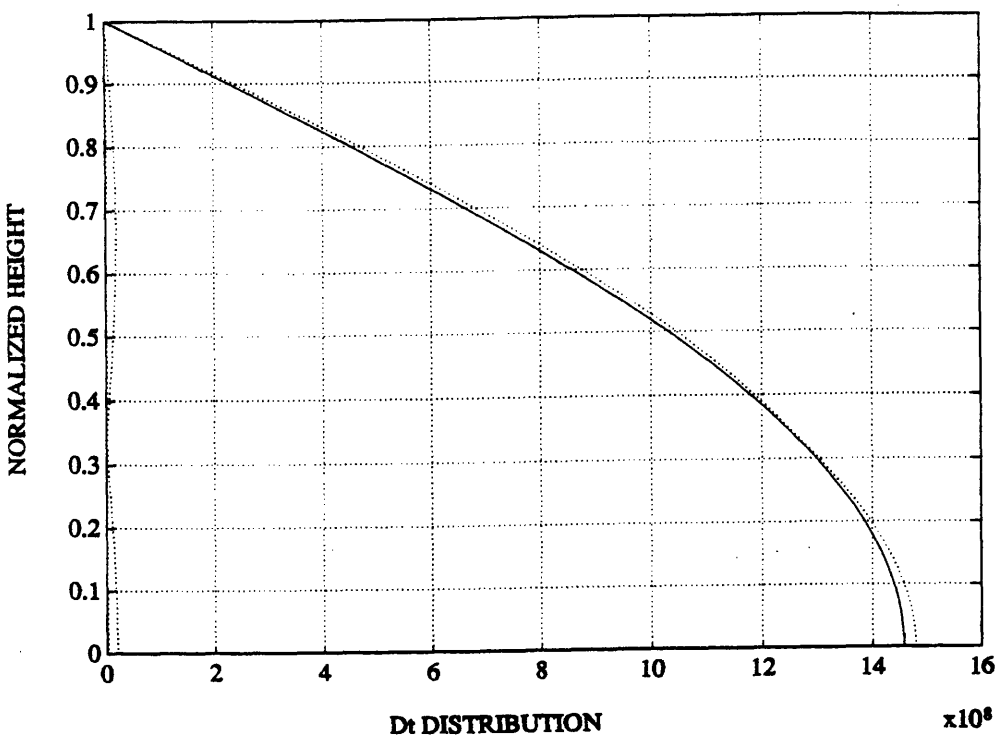

FIGURE 5.5.1: SHEAR RIGIDITY D_T *(T=0.6s - a=0.75)*

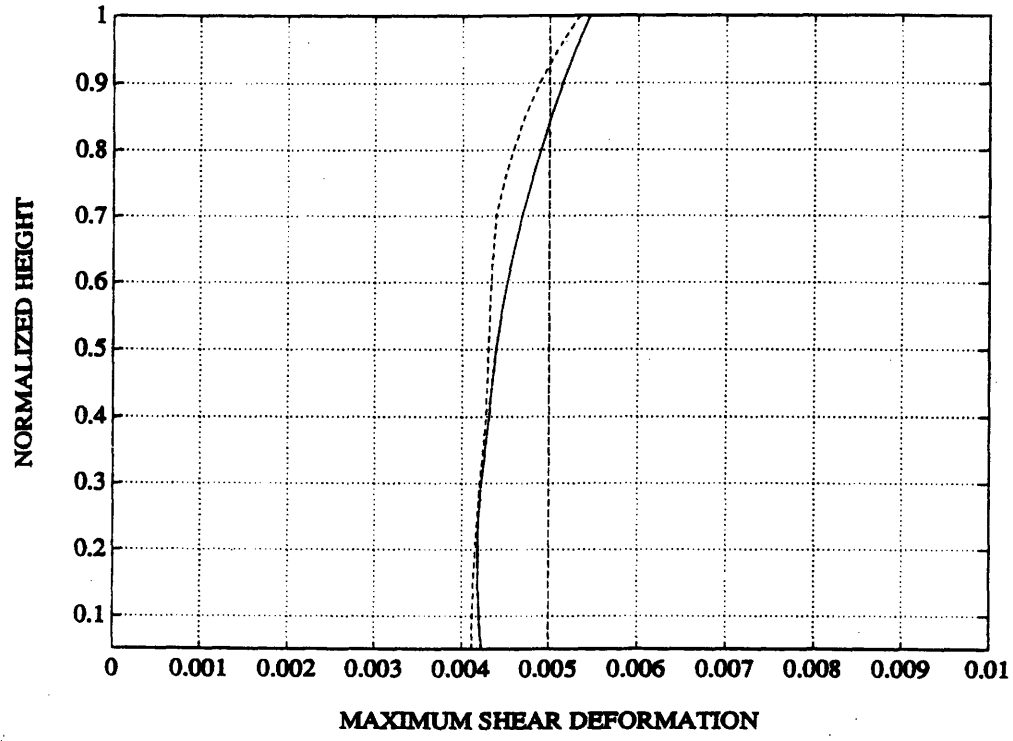

FIGURE 5.5.2: SHEAR DEFORMATION (T=0.6s - a=0.75)

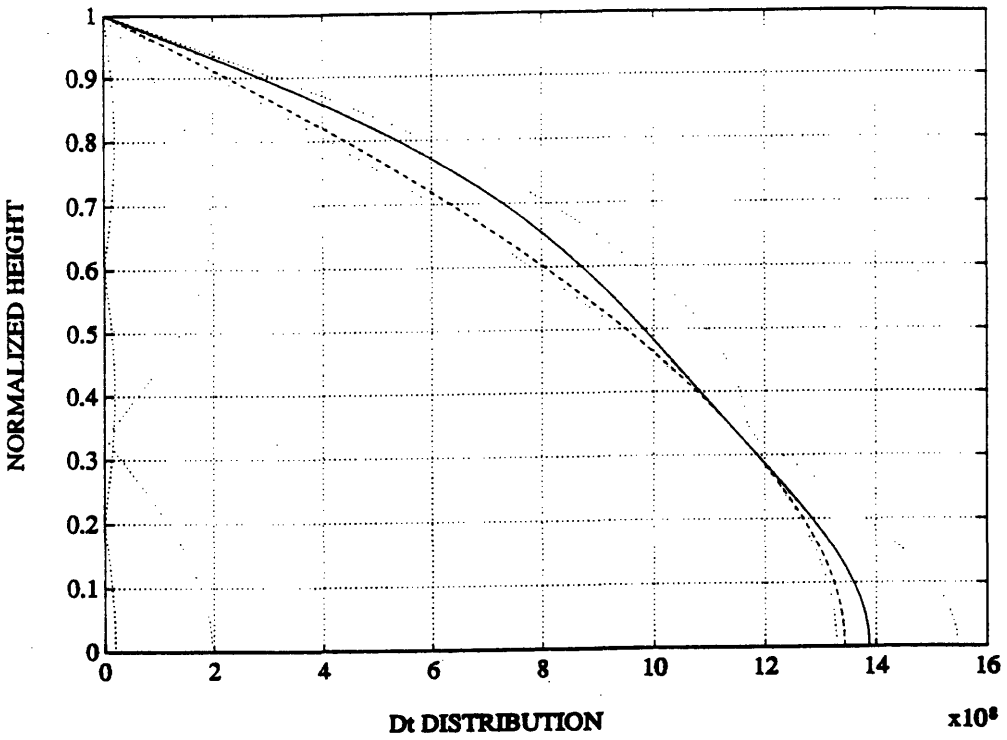

FIGURE 5.5.3: SHEAR RIGIDITY D_T (T=1.2s - a=1.0)

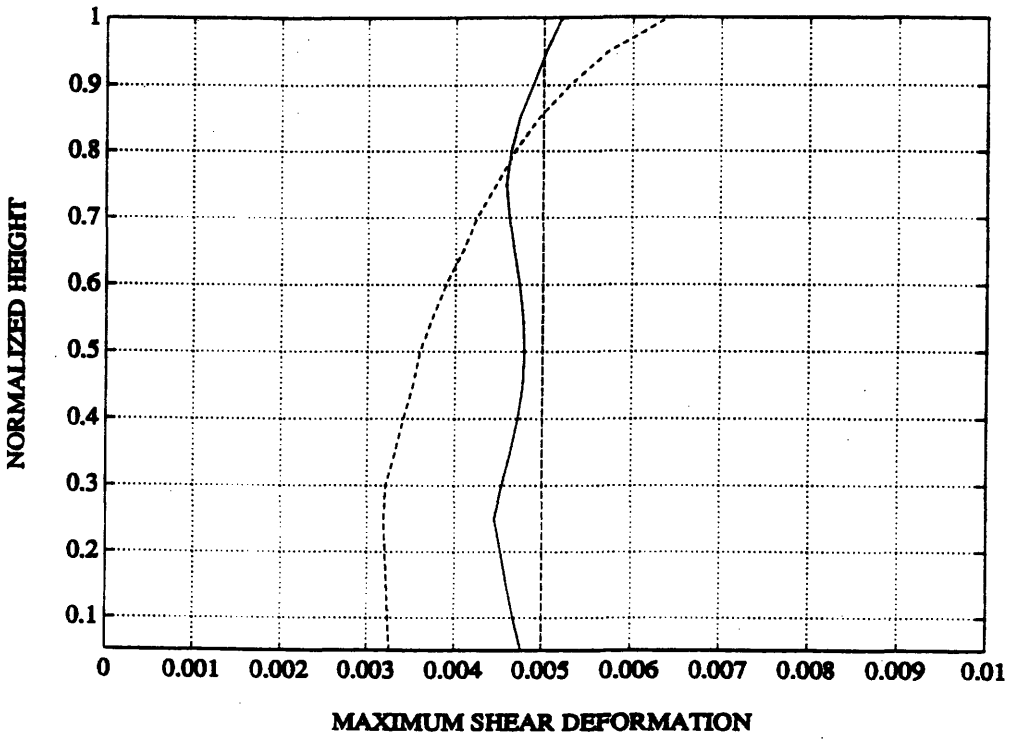

FIGURE 5.5.4: SHEAR DEFORMATION (T=1.2s - a=1.0)

CHAPTER SIX

MULTI-MODAL BENDING BEAM BASED STIFFNESS

6 - 1 INTRODUCTION

In parallel to the previous chapter where an analytical solution was established for buildings with small aspect ratios, this chapter develops an analytical solution for bending beams, used to model high rise buildings with very large aspect ratios. The shear deformation of such beams can be neglected in comparison to the bending deformation. The formulation of the bending beam problem follows the same steps as that of the shear beam problem to determine rigidity distributions based on superposing the modes of the bending beam. Already, it has been established that for buildings subjected to seismic excitation,

the higher modes become more significant. The current chapter adds insight as to how buildings behave at the other extreme of the spectrum.

6 - 2 FREE VIBRATIONS OF A CANTILEVER BENDING BEAM

The equation of motion for a prismatic bending beam with uniform properties along its length, neglecting shear deformation and rotatory inertia, can be written as

$$EI \frac{\partial^4 v}{\partial x^4} + m \frac{\partial^2 v}{\partial t^2} = 0 \qquad (6.2.1)$$

where EI is the bending rigidity. Expressing *(6.2.1)* in terms of dots and primes and dividing throughout by EI results in

$$v^{iv} + \frac{m}{EI} \ddot{v} = 0 \qquad (6.2.2)$$

Assuming a solution of the form

$$v(x,t) = \psi(x)\, Q(t) \qquad (6.2.3)$$

(6.2.2) becomes

$$\psi^{iv}(x)\, Q(t) + \frac{m}{EI} \psi(x)\, \ddot{Q}(t) = 0 \qquad (6.2.4)$$

which upon dividing by $\psi(x)\,Q(t)$ achieves the desired seperation

$$\frac{\psi^{iv}(x)}{\psi(x)} = -\frac{m}{EI}\frac{\ddot{Q}(t)}{Q(t)} = a^4 \qquad (6.2.5)$$

leading to two ordinary differential equations, one involving each variable. a is a constant raised to the fourth power for convenience. The two ordinary differential equations are

$$\psi^{iv}(x) - a^4\psi(x) = 0 \qquad (6.2.6)$$

$$\ddot{Q}(t) + \omega^2 Q(t) = 0 \qquad (6.2.7)$$

where $$\omega^2 = \frac{a^4 EI}{m} \qquad (6.2.8)$$

Thus the frequencies and the periods of the system are respectively given by

$$\omega = (aH)^2\sqrt{\frac{EI}{mH^4}} \qquad (6.2.9)$$

$$T = \frac{2\pi}{(aH)^2}\sqrt{\frac{mH^4}{EI}} \qquad (6.2.10)$$

Solving *(6.2.6)* yields the eigenvalues and eigenfunctions (mode shapes) of the beam. Assuming a solution of the form

$$\psi(x) = C\, e^{sx} \qquad (6.2.11)$$

and substituting into *(6.2.6)* gives

$$(s^4 - a^4) C\, e^{sx} = 0 \qquad (6.2.12)$$

from which

$$s = \pm a\,,\ \pm i\, a \qquad (6.2.13)$$

and the corresponding eigenfunctions expressed in terms of hyperbolic and trigonometric functions become

$$\psi(x) = A_1 \sin ax + A_2 \cos ax + A_3 \sinh ax + A_4 \cosh ax \qquad (6.2.14)$$

where the four constants A_i are determined using the boundary conditions. For a cantilever beam

$$\psi(0) = 0 \qquad (6.2.15)$$

$$\psi'(0) = 0 \qquad (6.2.16)$$

$$M(H) = EI\, \psi''(H) = 0 \qquad (6.2.17)$$

$$V(H) = EI\, \psi'''(H) = 0 \qquad (6.2.18)$$

Enforcing the boundary conditions dictates that in order for the system to admit a non trivial solution, the following transcendental equations has to be satisfied

$$1 + \cos a_n H \cosh a_n H = 0 \qquad (6.2.19)$$

where n is the mode number. The modal shapes are hence given by

$$\psi(x) = A \left(\sin a_n x - \sinh a_n x + g_n (\cosh a_n x - \cos a_n x)\right) \qquad (6.2.20)$$

where $$g_n = \frac{\sin a_n H + \sinh a_n H}{\cos a_n H + \cosh a_n H} \qquad (6.2.21)$$

The solution of *(6.2.19)* provides the values of aH from which the frequencies of vibration and hence the periods, as well as the mode shapes can be determined. Table 6.2.1 gives the values of $a_n H$ and g_n for the first ten modes as well as the ratio of the higher periods corresponding to the higher modes relative to the period of the fundamental mode. Fig. 6.2.1 is a plot of the mode shapes scaled to a maximum amplitude of one.

One should note that for the second and higher modes, the following approximations hold

$$a_n H = \frac{(2n - 1)\pi}{2} \qquad n = 2, 3 \ldots \qquad (6.2.22)$$

$$g_n = 1 \qquad (6.2.23)$$

MODE #	a_nH	g_n	$\frac{T_n}{T_1}$
1	1.875104	1.362221	1.000000
2	4.694091	0.981867	0.159569
3	7.854757	1.000776	0.056988
4	10.995541	0.999966	0.029081
5	14.137168	1.000001	0.017592
6	17.278760	1.000000	0.011777
7	20.420352	1.000000	0.008432
8	23.561945	1.000000	0.006333
9	26.703538	1.000000	0.004931
10	29.845130	1.000000	0.003947

TABLE 6.2.1: CANTILEVER BENDING BEAM PARAMETERS

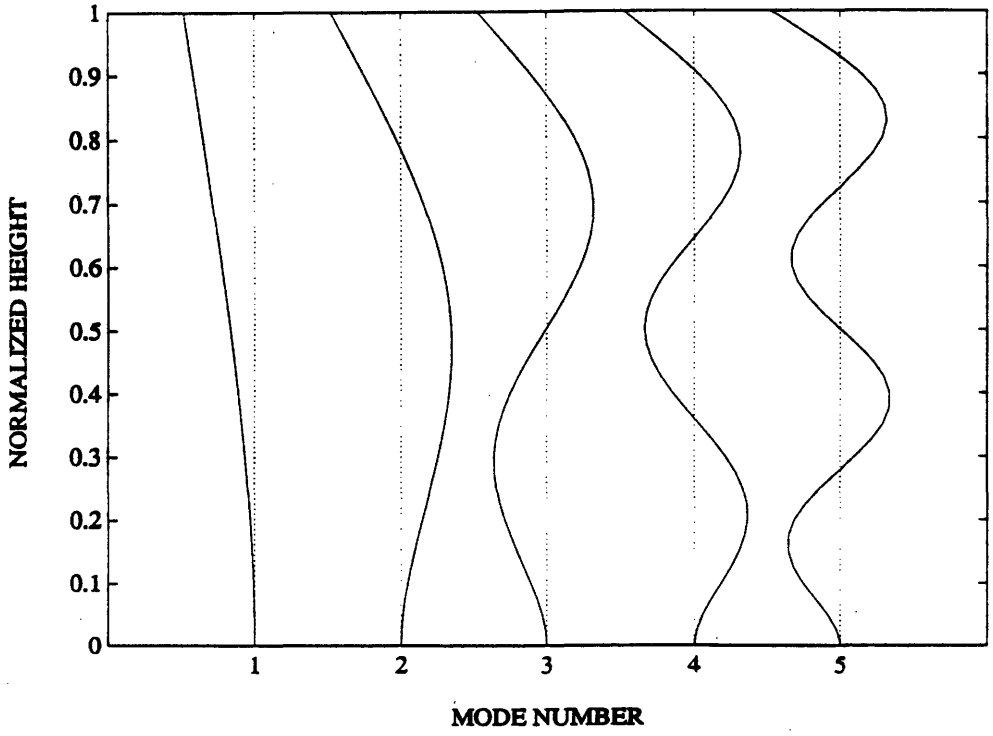

FIGURE 6.2.1: MODE SHAPES OF A UNIFORM PARAMETER BENDING BEAM

6 - 3 *MULTI-MODAL BASED STIFFNESS:*

Following the same approach used for the shear beam, one can express the lateral force due to earthquake excitation in terms of the "modal" pseudo-spectral velocity *(A.4.8)*

$$F_{n,max}(x) = m\,\omega_n\,\Gamma_n\,S_v(\xi_n,\omega_n)\,\psi_n(x) \qquad (6.3.1)$$

The participation factors for the different modes can be determined by solving *(A.4.2)* for the particular problem. Using *(6.2.19)*, the numerator of *(A.4.2)* gives

$$\int_0^H m\,\psi_n(x)\,dx = mH\,\frac{2}{a_nH} \qquad (6.3.2)$$

and the denominator gives

$$\begin{aligned}\int_0^H m\,\psi_n^2\,dx = \frac{mH}{D}\{\,&1 + 4\,s\,e^{-a_nH} - 2\,(2\,c^2 - 1)\,e^{-2a_nH} \\ &- 4\,s\,e^{-3a_nH} + e^{-4a_nH}\,\} \\ -\frac{mH}{a_nH\,D}\{&(3\,s\,c - 3\,c^2) \\ &+ 6\,(s - c)\,e^{-a_nH} + 6\,c\,s\,e^{-2a_nH} \\ &+ 6\,(s + c)\,e^{-3a_nH} + 3\,(c\,s + c^2)\,e^{-4\,a_nH}\}\end{aligned} \qquad (6.3.3)$$

where $$D = 1 + 4\,c\,e^{-a_n H} + 2\,(2\,c^2 + 1)\,e^{-2a_n H} + 4\,c\,e^{-3a_n H} + e^{-4a_n H} \qquad (6.3.4)$$

and $$c = \cos a_n H$$

$$s = \sin a_n H$$

One can write the integral in *(6.3.3)* as

$$\int_0^H m\,\psi^2(x)\,dx = mH\,\beta_n \qquad (6.3.5)$$

and thus the participation factors of the different modes become

$$\Gamma_n = \frac{\int_0^H m\,\psi_n(x)\,dx}{\int_0^H m\,\psi_n^2(x)\,dx} = \frac{2}{\beta_n\,a_n H} \qquad (6.3.6)$$

Table 6.3.1 contains results for the first 10 modes. Note that $\beta_n \approx 1$ for $n \geq 2$.

The shear force distribution is obtained by substituting the bending beam parameters in *(A.4.9)* and integrating

$$V_{n,max}(x) = mH\,A_n\,\psi_{s,n}(x) \qquad (6.3.7)$$

where $$A_n = \frac{2}{\beta_n}\sqrt{\frac{EI}{mH^4}}\, S_v(\xi_n,\omega_n) \qquad (6.3.8)$$

and $$\psi_{s,n}(x) = \cos a_n x + \cosh a_n x + g_n (\sin a_n x - \sinh a_n x) \qquad (6.3.9)$$

and the bending moment is obtained by integrating the shear

$$M_{n,max}(x) = mH^2 B_n \ \psi_{b,n}(x) \qquad (6.3.10)$$

where $$B_n = \frac{A_n}{a_n H} = \frac{2}{\beta_n a_n H}\sqrt{\frac{EI}{mH^4}}\, S_v(\xi_n,\omega_n) \qquad (6.3.11)$$

and $$\psi_{b,n}(x) = \sin a_n x + \sinh a_n x - g_n (\cos a_n x + \cosh a_n x) \qquad (6.3.12)$$

The last two columns of Table 6.3.2 give the relative contributions of the different modes for the shear and bending assuming that the value of $S_v(\xi_n, \omega_n)$ remains unchanged (i.e. assuming periods higher than 0.6s and uniform damping in all the modes. One can see that the participation of the higher modes in shear is almost the same and is twice that of the fundamental mode. On the other hand, the contribution to the bending decays rather quickly. So damping is really very important in controlling the higher modes. Assuming that modal damping varies linearly with frequency,

$$\xi_n = \frac{T_1}{T_n}\xi_1 = \frac{(2n-1)^2}{1.425}\xi_1 \qquad n = 2, 3, \ldots \qquad (6.3.13)$$

MODE #	$a_n H$	$\frac{2}{a_n H}$	β_n	Γ_n	$\frac{A_n}{A_1}$	$\frac{B_n}{B_1}$
1	1.875104	1.066607	2.127599	0.501320	1.000000	1.000000
2	4.694091	0.426068	0.964387	0.441801	2.206167	0.055377
3	7.854757	0.254623	1.001553	0.254228	2.124299	0.031862
4	10.995541	0.181892	0.999933	0.181904	2.127741	0.022798
5	14.137168	0.141471	1.000003	0.141471	2.127592	0.017731
6	17.278760	0.115749	1.000000	0.115749	2.127599	0.014507
7	20.420352	0.097942	1.000000	0.097942	2.127599	0.012275
8	23.561945	0.084883	1.000000	0.084883	2.127599	0.010638
9	26.703538	0.074896	1.000000	0.074896	2.127599	0.009387
10	29.845130	0.067013	1.000000	0.067013	2.127599	0.008399

TABLE 6.3.1: CANTILEVER BENDING BEAM PARAMETERS

since from *(7.1.22)*

$$\frac{T_1}{T_n} = \frac{(2n-1)^2\pi^2}{4}\frac{1}{(1.875)^2} = \frac{(2n-1)^2}{1.425} \qquad (6.3.14)$$

Equation *(6.3.13)* shows that damping is more significant for bending beams versus shear beams with respect to the pseudo-spectral velocity.

6 - 4 *CALIBRATING THE EQUIVALENT BENDING BEAM*

Following the same procedure as in Chapter Five, it remains to calibrate the equivalent "bending" beam. It is required that the base shear generated from the fundamental mode of the bending beam be equal to that obtained from the beam with the quadratic shear rigidity distribution of Chapter Four. Thus the base shear from the bending beam is

$$V_{BB1,max}(0) = 2A_1 mH = \frac{4mH}{\beta_1}\sqrt{\frac{EI}{mH^4}}\, S_v(\xi_1,\omega_1) \qquad (6.4.1)$$

and from the beam with the quadratic shear rigidity distribution

$$V_{QSD,max}(0) = \frac{m}{2\gamma^*}\left(1+\frac{a}{3}\right)\left[\Gamma_1 S_v(\xi_1,\omega_1)\right]^2 \qquad (6.4.2)$$

Equating *(6.4.1)* and *(6.4.2)* assuming that $S_v(\xi_1,\omega_1)$ is the same for both terms, and substituting for β_1 using from Table 6.3.2 leads to

$$EI = mH^2\left(\frac{0.26595}{\gamma^*}\left(1+\frac{a}{3}\right)\Gamma_1^2 S_v(\xi_1,\omega_1)\right)^2 \qquad (6.4.3)$$

Table 6.4.1 lists the values of $\Gamma_1^2\left(1+\frac{a}{3}\right)$ versus a . It is of interest to compare the fundamental periods of the two beams, thus

$$T_{BB1} = 2\pi\,\frac{1}{(a_1 H)^2}\sqrt{\frac{mH^4}{EI}} \qquad (6.4.4)$$

a	0	1	2	3	4	5
$\Gamma_1\left(1+\frac{a}{3}\right)$	1.50000	1.40351	1.34409	1.30435	1.27604	1.25490
$\Gamma_1^2\left(1+\frac{a}{3}\right)$	2.25000	1.47738	1.08394	0.85066	0.69784	0.59054

TABLE 6.4.1: VARIATION OF $\Gamma_1^2\left(1+\frac{a}{3}\right)$ *WITH* a .

$$T_{QSD1} = 2\pi \frac{H\gamma^*}{\Gamma_1 S_v(\xi_1,\omega_1)} \qquad (6.4.5)$$

Making use of *(6.4.3)* , one obtains

$$\frac{T_{BB1}}{T_{QSD1}} = \frac{1}{\Gamma_1\left(1+\frac{a}{3}\right)\left[0.26595\,(a_1 H)^2\right]} = \frac{1.06942}{\Gamma_1\left(1+\frac{a}{3}\right)} \qquad (6.4.6)$$

Taking $a = 3$ as typical value leads to

$$\frac{T_{BB1}}{T_{QSD1}} = 0.81989 \qquad (6.4.7)$$

Thus, assuming one is dealing with a tall building with a fundamental period in the region of 5 seconds, *(6.4.7)* shows that it is reasonable to assume $S_v(\xi_1,\omega_1)$ the same for both models for the same damping ratio. The illustrative examples for this formulation have not yet been generated, however this chapter

was included for completeness since it illustrates the significant amplification in the participation of the higher modes.

CHAPTER SEVEN

MULTI-MODAL ITERATIVE BASED STIFFNESS

7 - 1 INTRODUCTION

Only very few simple problems can be solved analytically. Already in superposing modal contributions, a computer was utilized to crunch the numbers. So why not develop a computer based solution where the desired rigidity distributions are established based on an iterative scheme. The disadvantage of such an approach is the need for a computer accompanied by a tendency to overlook the physics of the problem which the simple analytic solutions of the previous two chapters established. The developed analytic solutions help bracket the problem and serve as a check on the computer output. This iterative scheme makes use of Chapter Four where the rigidity distributions based on the single mode response is used as a starting solution. Then one iterates to converge on an acceptable solution meeting the requirements and the

degree of accuracy sought (remembering that a lot of uncertainty exists in earthquake excitation). One advantage of this numerical scheme is the ability of handling buildings over a range of periods and parameters. Results are provided to illustrate the different behavior for different periods..

7 - 2 STEP BY STEP ITERATION PROCEDURE

What follows summarizes the proposed numerical scheme.

STEP 1: Given the mass of the building and its height, one decides on an S_v , a desired deformation limit, and an 'a' which relates the bending and shear deformations. Also specify some desired modal damping which will be achieved by the damping present in the system supplemented with energy absorbing and dissipating devices.

STEP 2: The period of the building can then be computed using *(4.4.6)* and a starting rigidity distribution based on the first mode can be determined using *(4.2.14)* and *(4.2.15)*.

STEP3: Discretize the rigidities and establish the lumped stiffness and mass matrices of the MDOF system.

STEP 4: Solve the eigenvalue problem to determine the frequencies and the mode shapes.

STEP 5: Establish the modal shear and bending moment contributions based on some specified design spectrum.

STEP 6: Combine the modal shears and bending moments using SRSS or any other method found appropriate, and divide by the desired deformations to obtain the rigidity approximation.

STEP 7: Run several excitations to evaluate the behavior of your system.

STEP 8: Iterate starting from *STEP 3*.

7 - 3 EXAMPLES

To illustrate the proposed scheme, the rigidities developed based on the fundamental mode for the different cases in Chapter Four are used to kick off the described procedure. Fig. 7.3.1 through 7.3.20 illustrate the rigidity distributions and the maximum deformations under the excitations used previously. In superposing the modal contributions, the Square Root Sum of Squares was used (dashed line). The Sum of Absolute Values was found to over correct the rigidities attracting more load in certain cases resulting in larger deformations. The results presented are based on either one or two trials as indicated. And the maximum deformation graphs show that in a couple of cycles, the deformations were reduced below the specified maximum value.

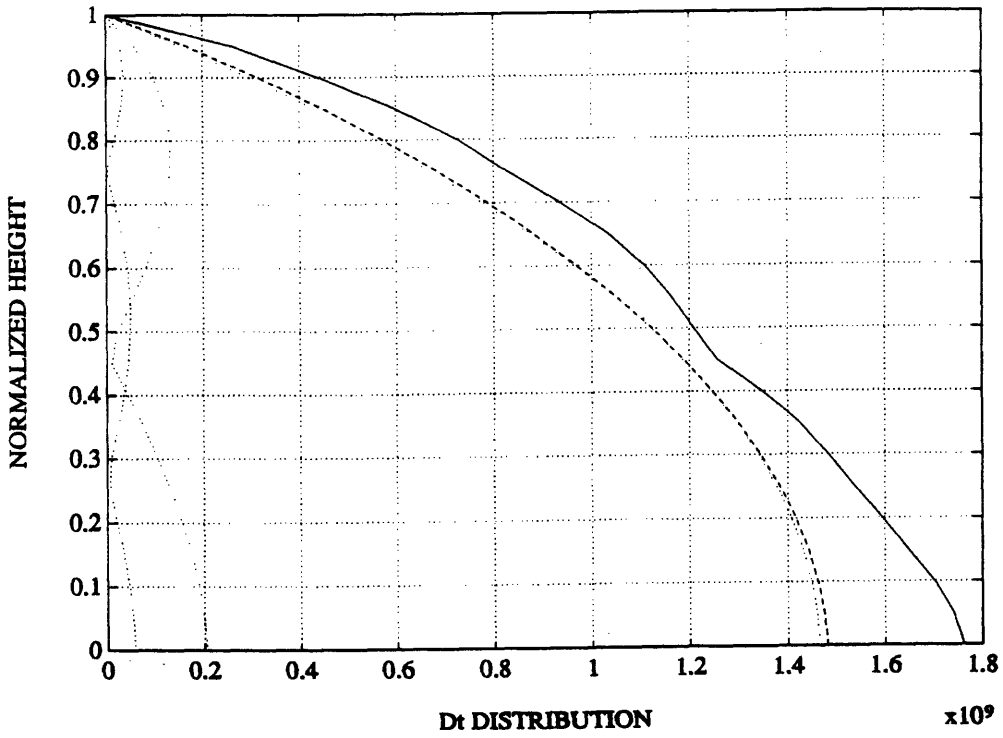

FIGURE 7.3.1: SHEAR RIGIDITY D_T (T=0.6s - a=0.75 - TRIAL1)

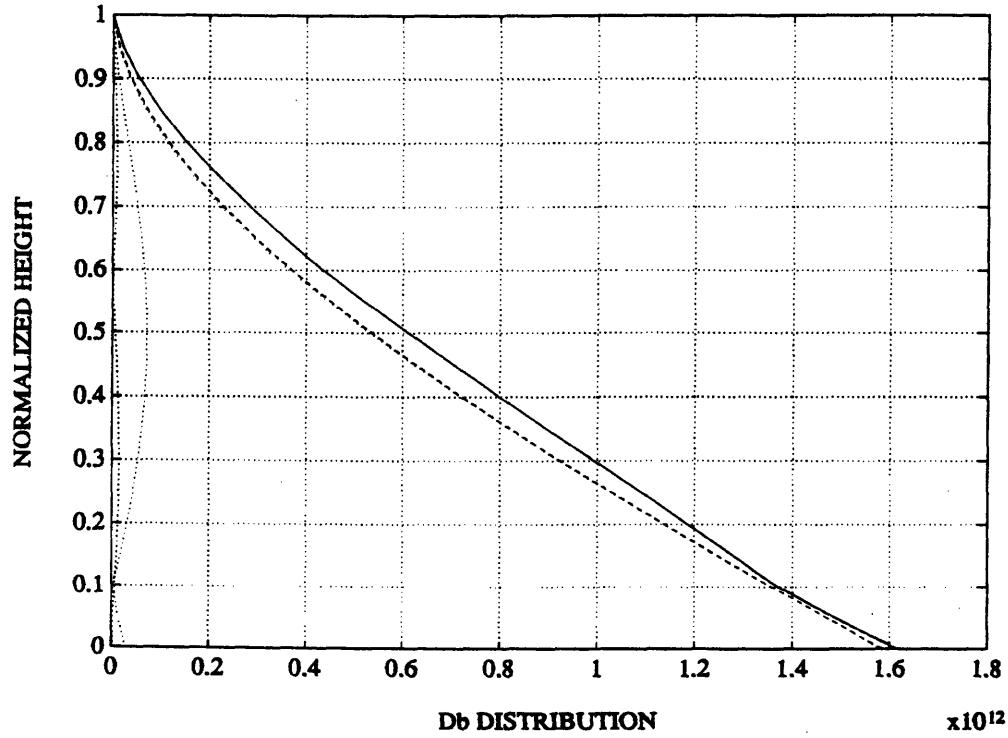

FIGURE 7.3.2: BENDING RIGIDITY D_B (T=0.6s - a=0.75 - TRIAL1)

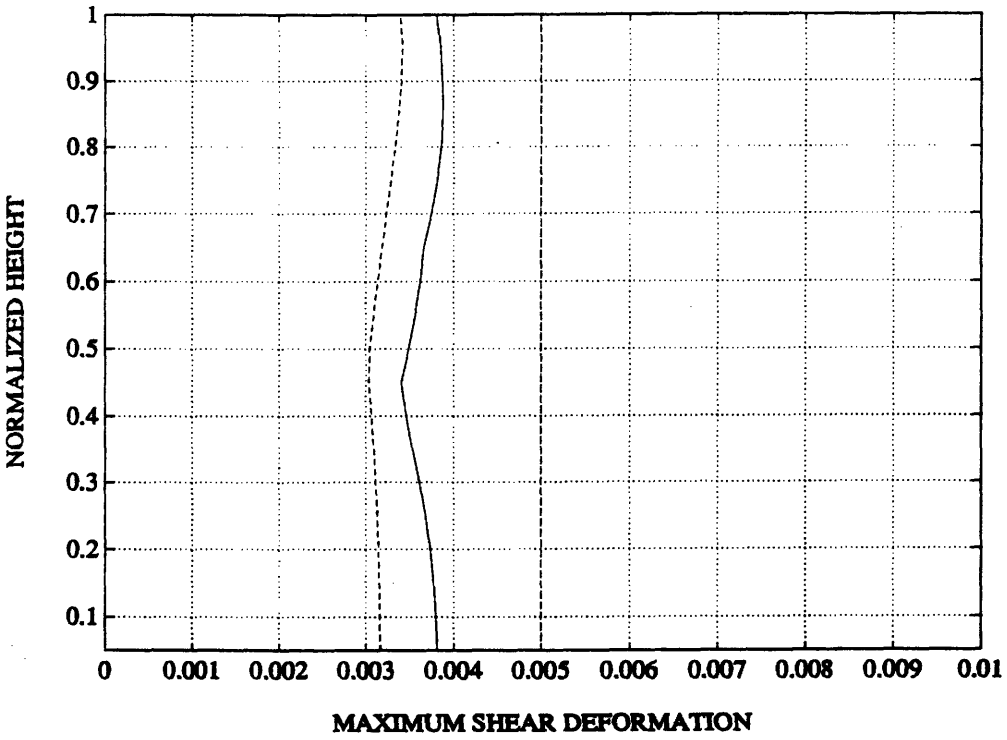

FIGURE 7.3.3: SHEAR DEFORMATION (T=0.6s - a=0.75 - TRIAL1)

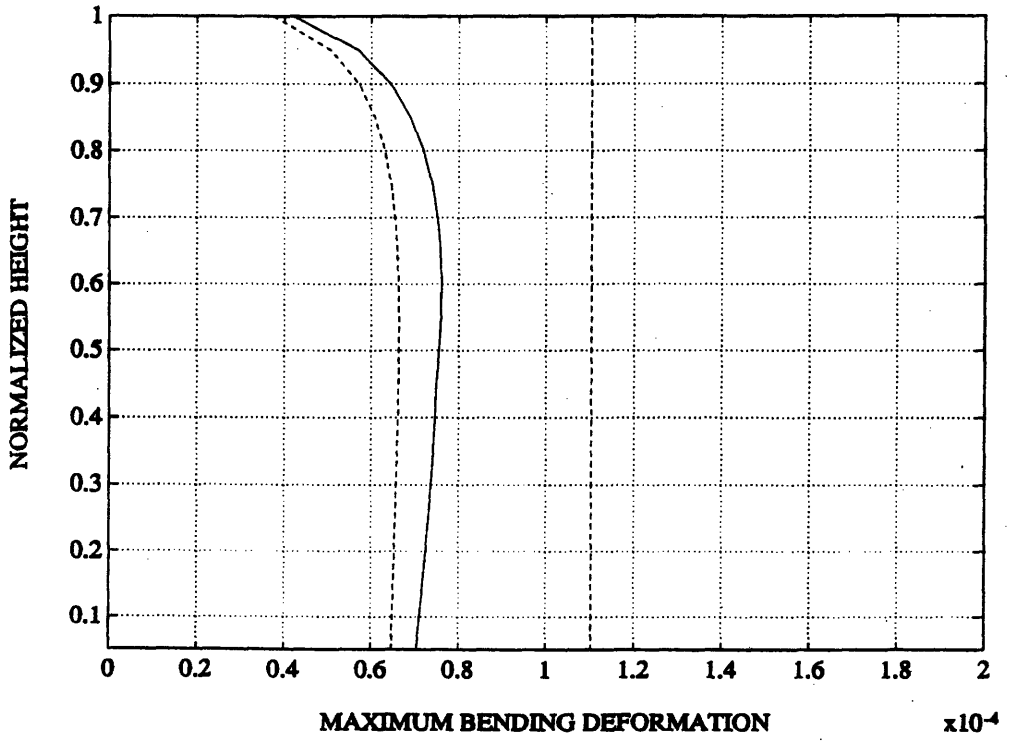

FIGURE 7.3.4: BENDING DEFORMATION (T=0.6s - a=0.75 - TRIAL1)

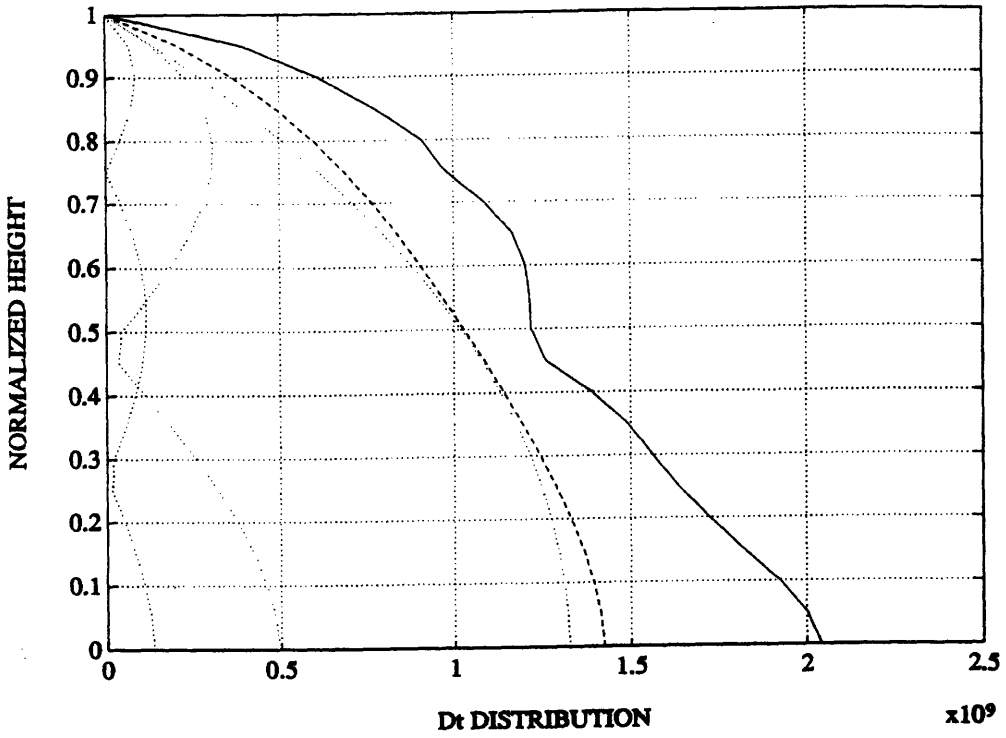

FIGURE 7.3.5: SHEAR RIGIDITY D_T (T=1.2s - a=1.0 - TRIAL1)

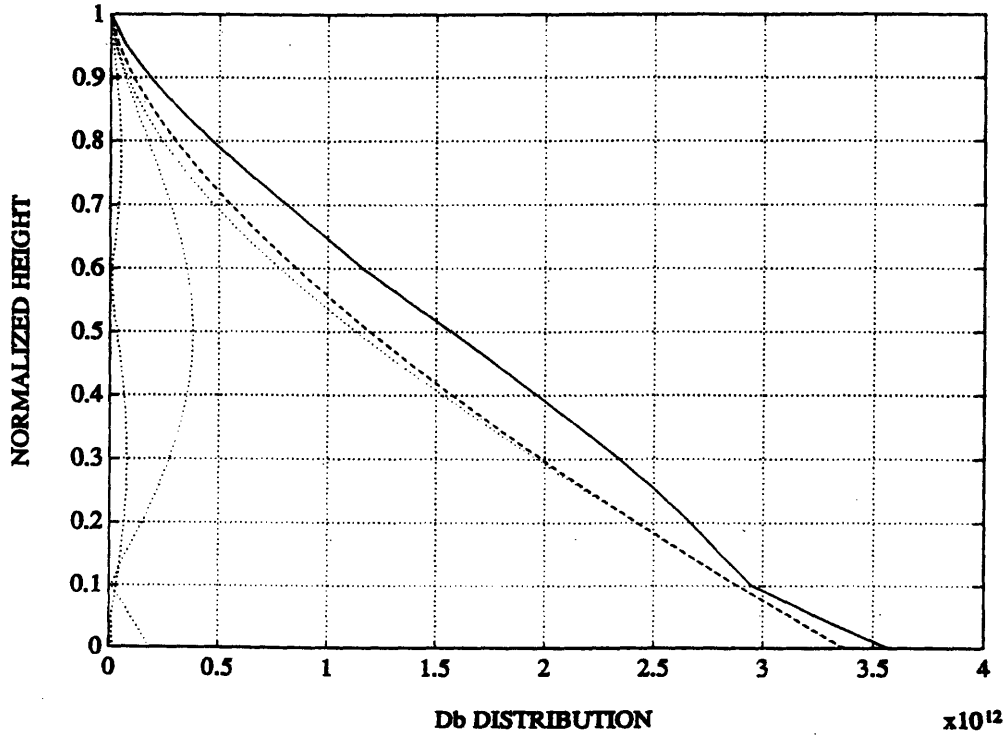

FIGURE 7.3.6: BENDING RIGIDITY D_B (T=1.2s - a=1.0 - TRIAL1)

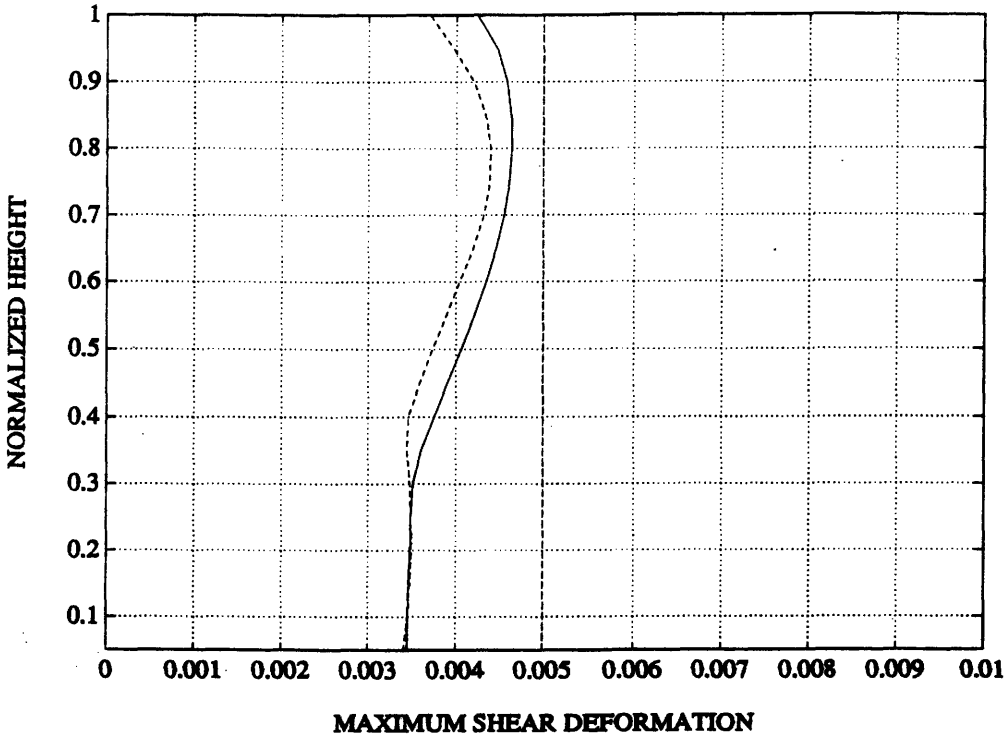

FIGURE 7.3.7: SHEAR DEFORMATION (T=1.2s - a=1.0 - TRIAL1)

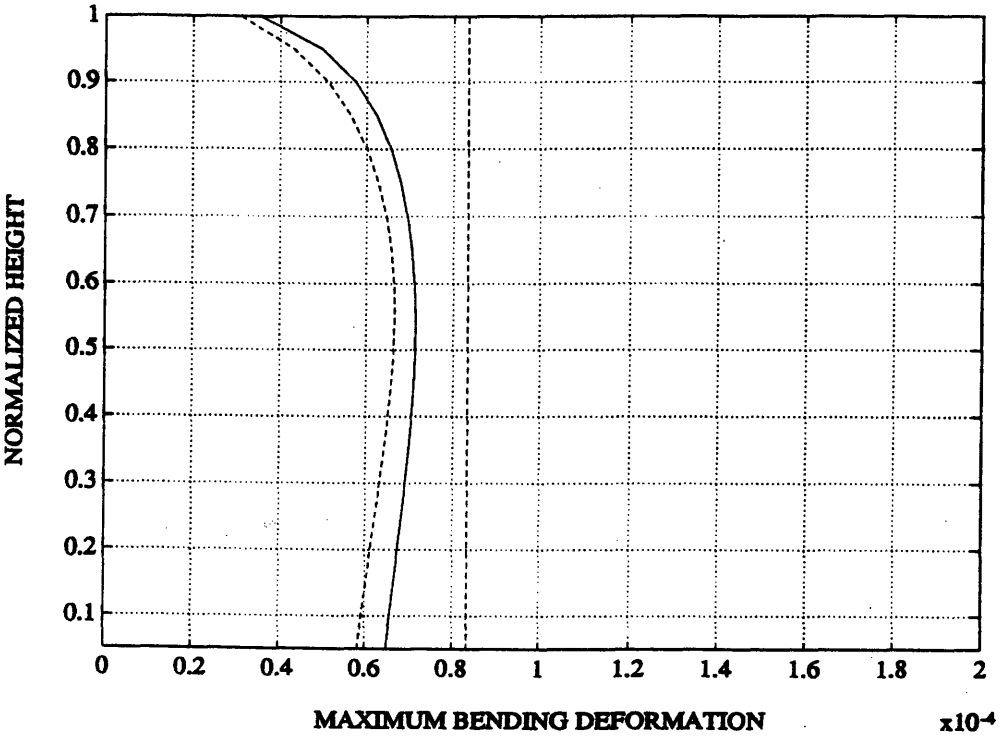

FIGURE 7.3.8: BENDING DEFORMATION (T=1.2s - a=1.0 - TRIAL1)

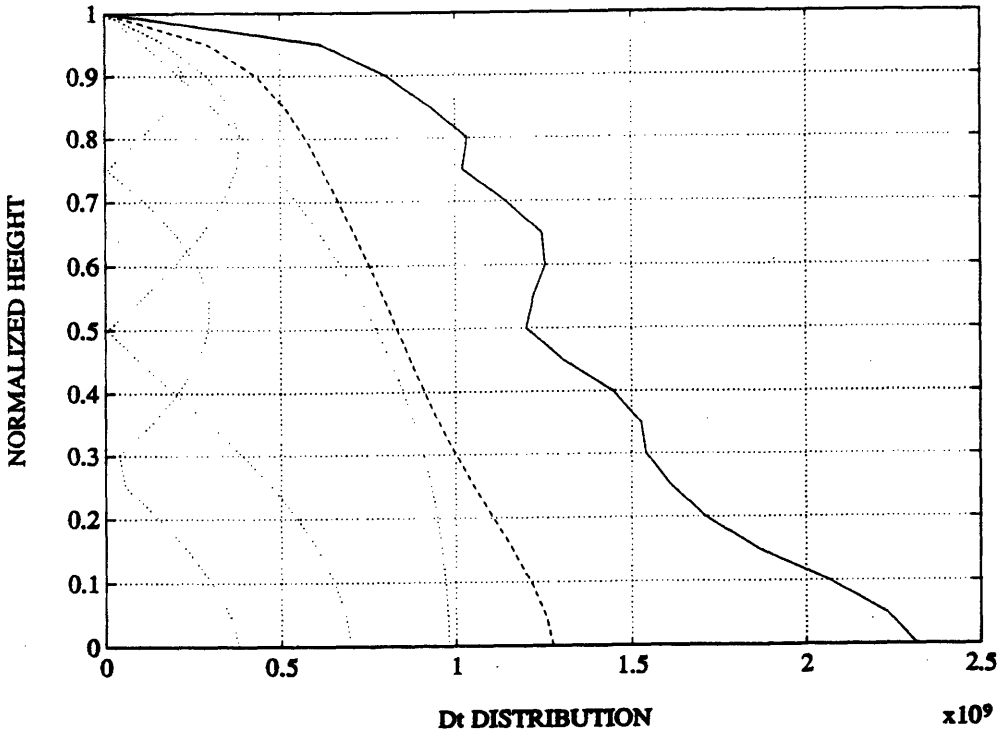

FIGURE 7.3.9: SHEAR RIGIDITY D_T *(T=3.0s - a=3.0 - TRIAL1)*

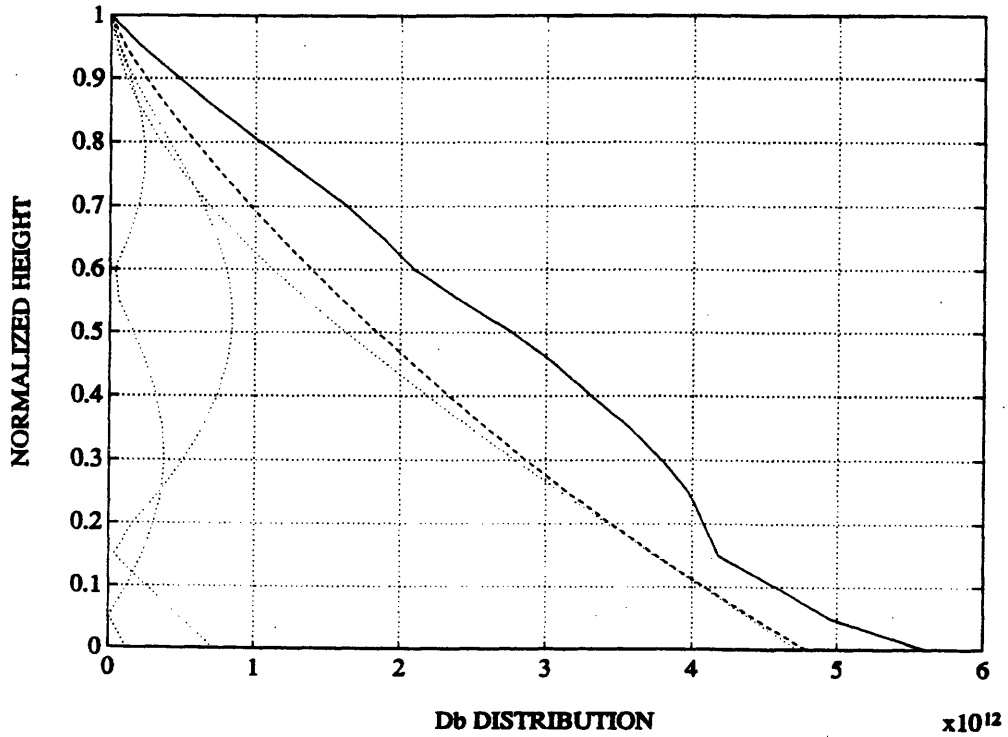

FIGURE 7.3.10: BENDING RIGIDITY D_B *(T=3.0s - a=3.0 - TRIAL1)*

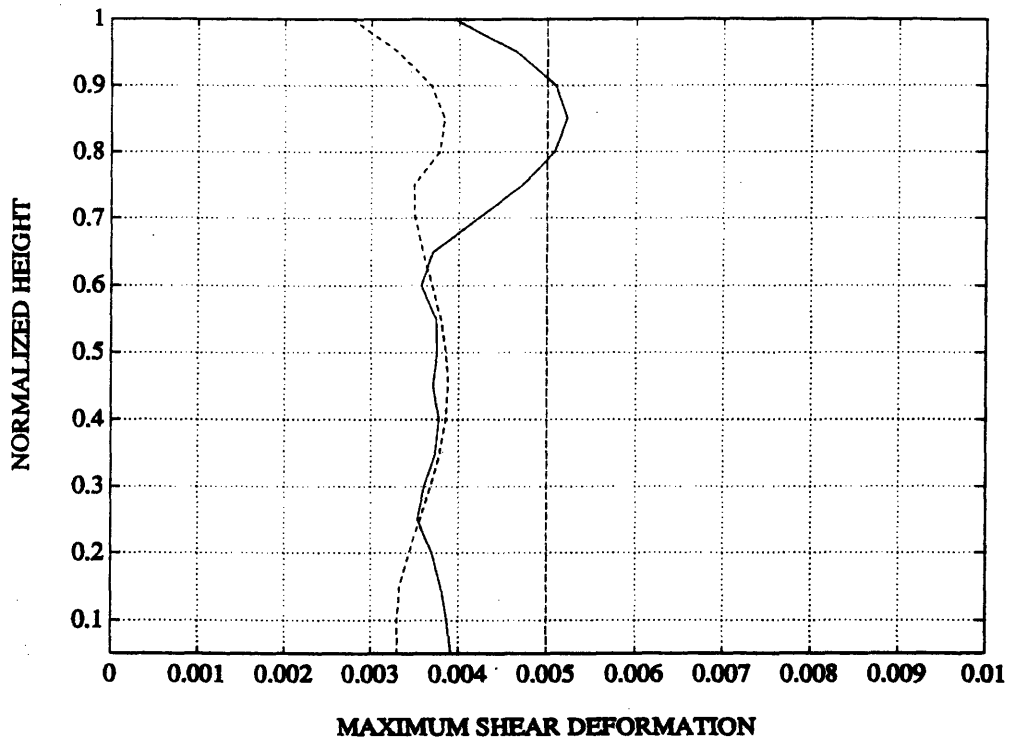

FIGURE 7.3.11: SHEAR DEFORMATION (T=3.0s - a=3.0 - TRIAL1)

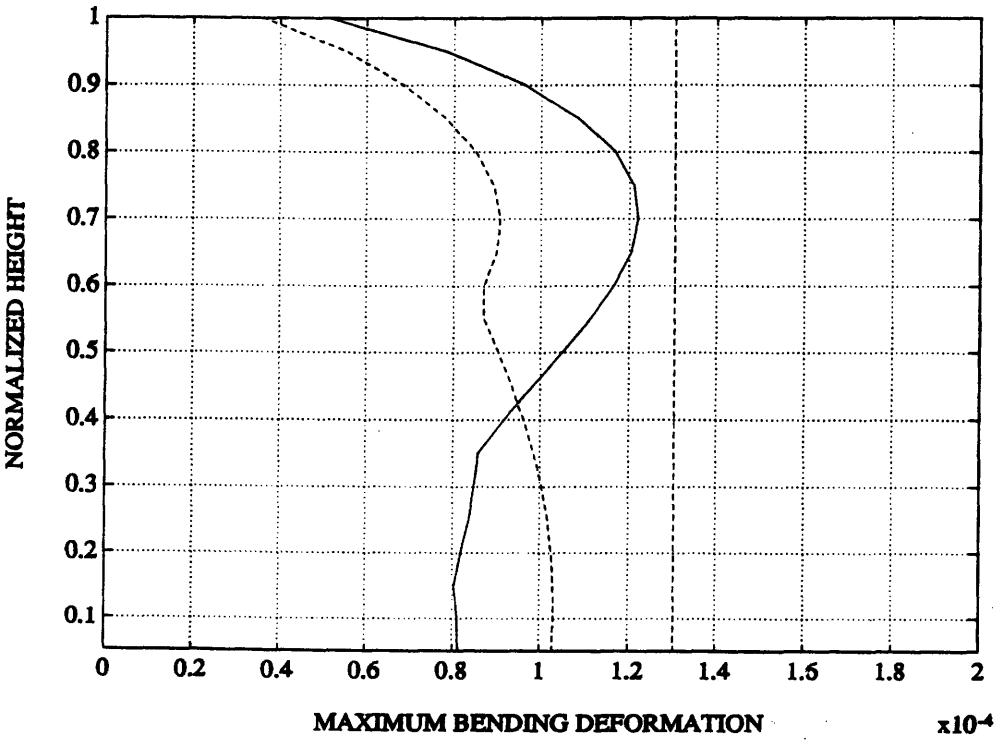

FIGURE 7.3.12: BENDING DEFORMATION (T=3.0s - a=3.0 - TRIAL1)

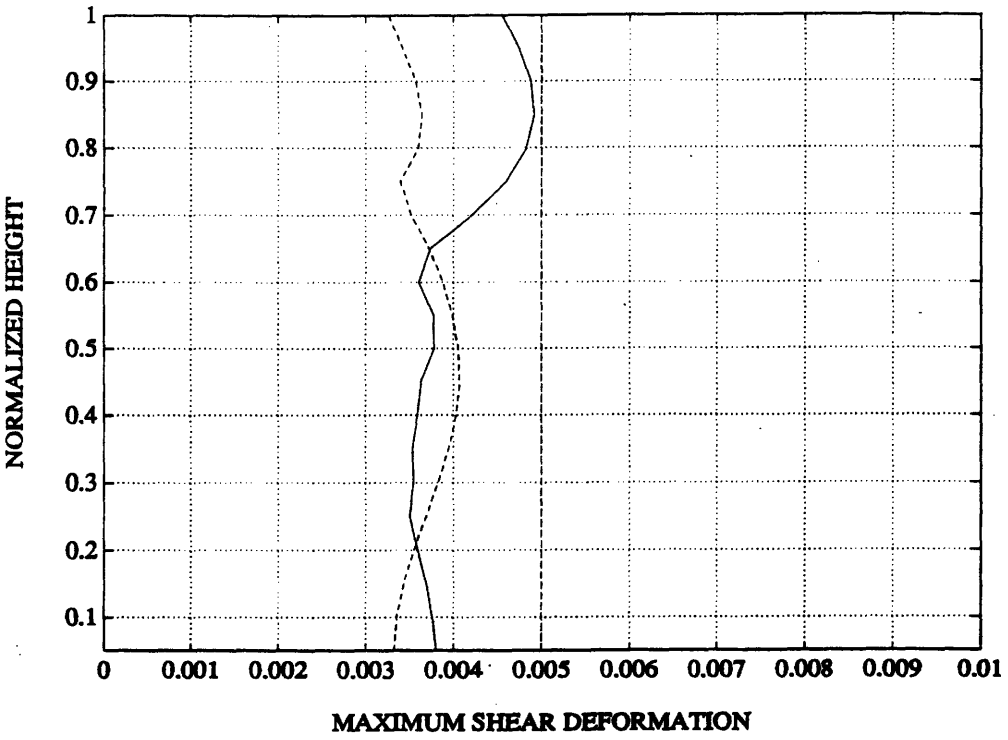

FIGURE 7.3.13: SHEAR DEFORMATION (T=3.0s - a=3.0 - TRIAL2)

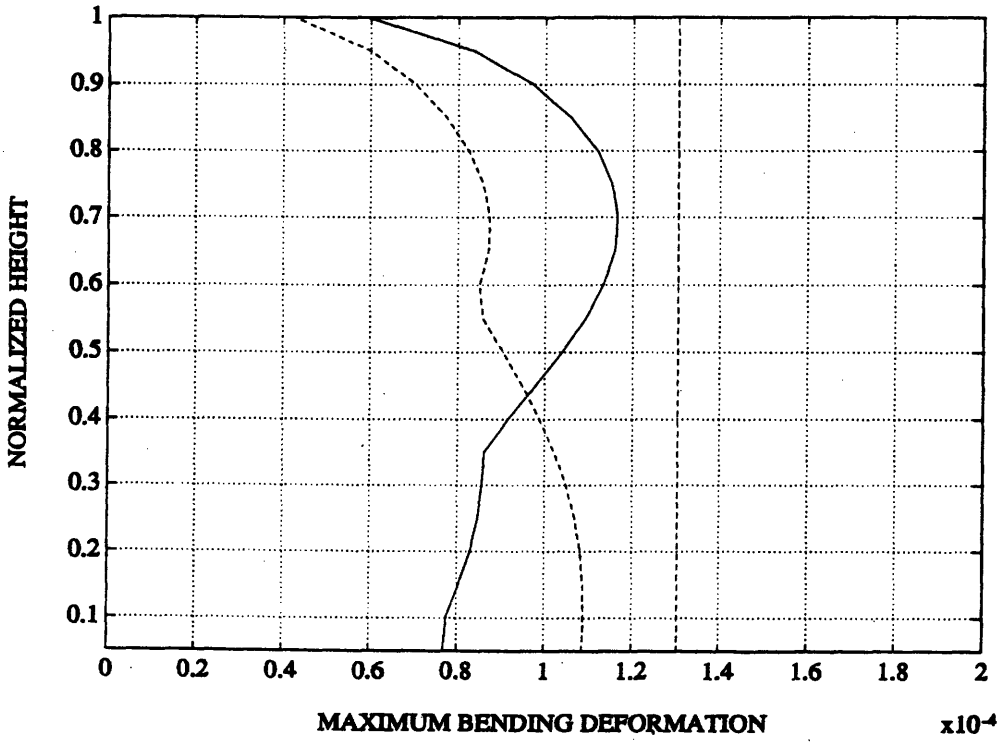

FIGURE 7.3.14: BENDING DEFORMATION (T=3.0s - a=3.0 - TRIAL2)

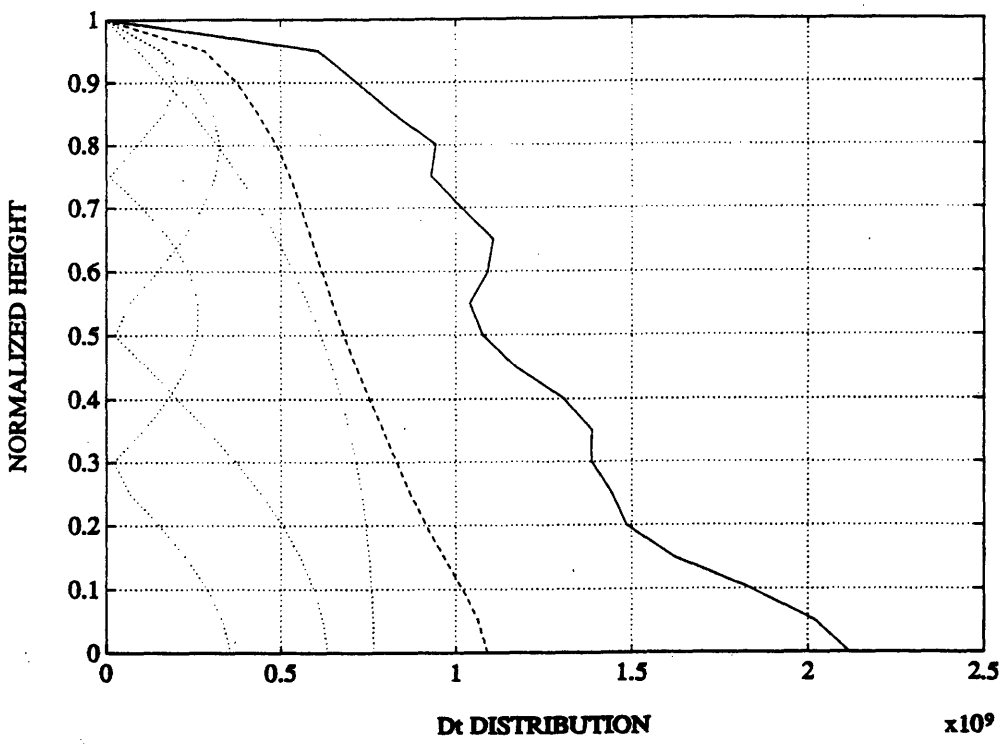

FIGURE 7.3.15: SHEAR RIGIDITY D_T (T=5.0s - a=3.0 - TRIAL1)

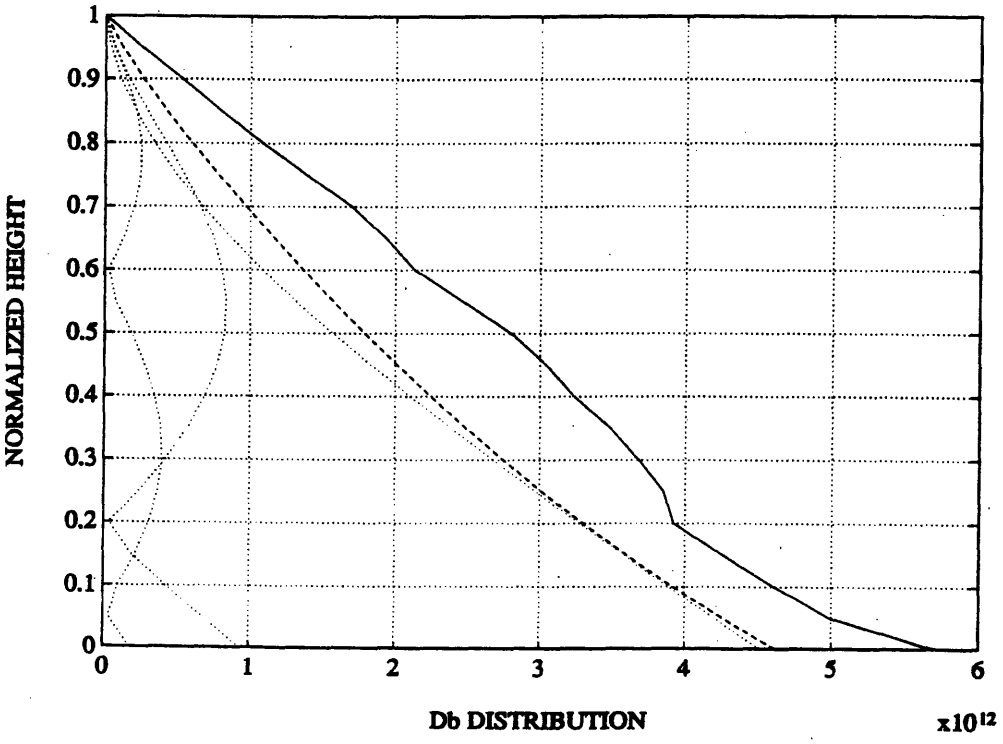

FIGURE 7.3.16: BENDING RIGIDITY D_B (T=5.0s - a=3.0 - TRIAL1)

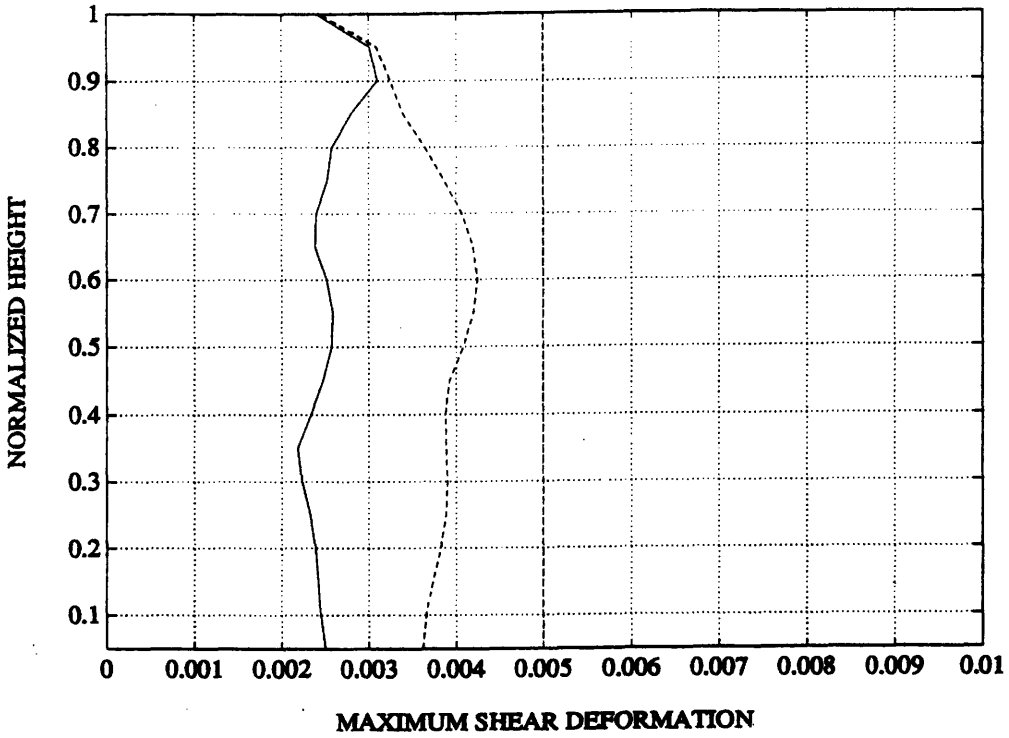

FIGURE 7.3.17: SHEAR DEFORMATION (T=5.0s - a=3.0 - TRIAL1)

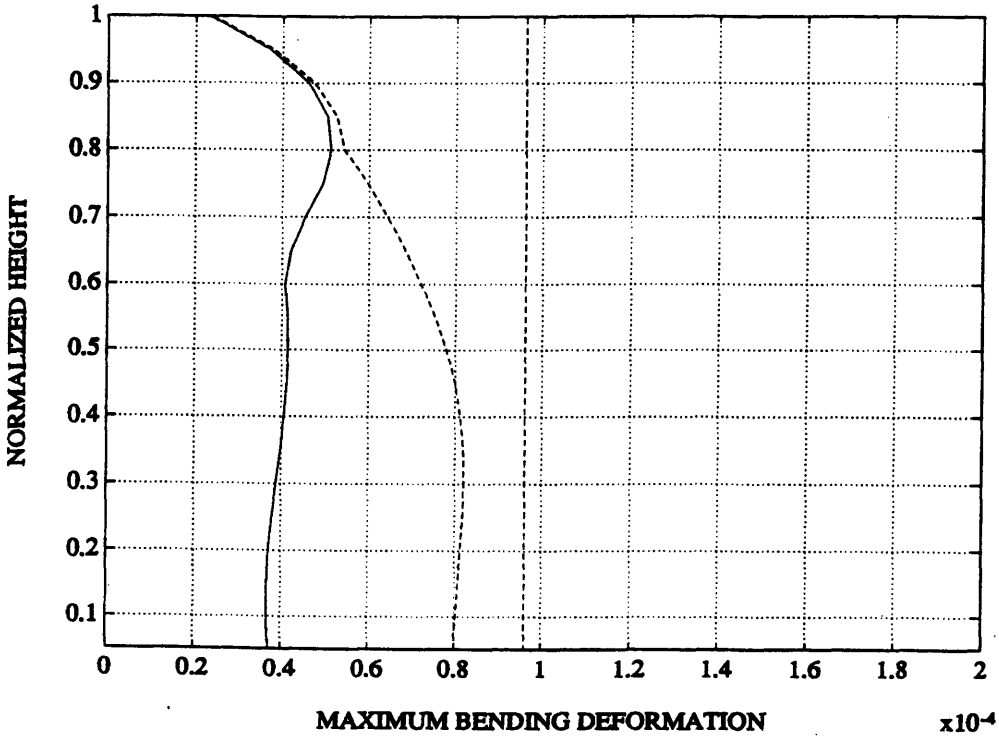

FIGURE 7.3.18: BENDING DEFORMATION (T=5.0s - a=3.0 - TRIAL1)

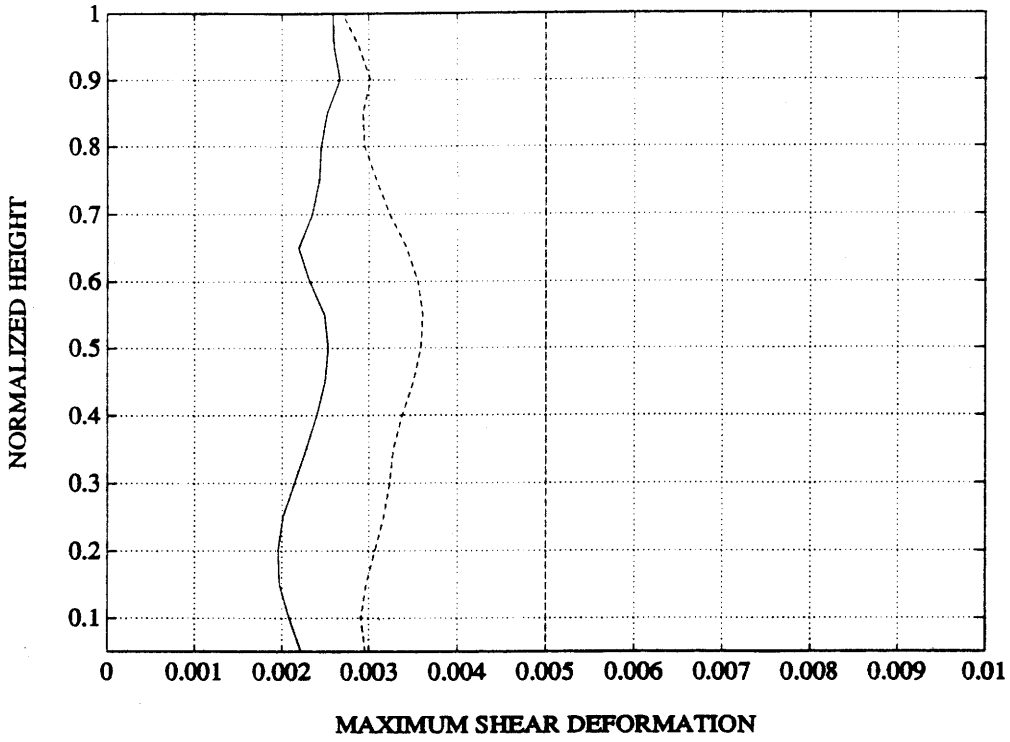

FIGURE 7.3.19: SHEAR DEFORMATION (T=5.0s - a=3.0 - TRIAL2)

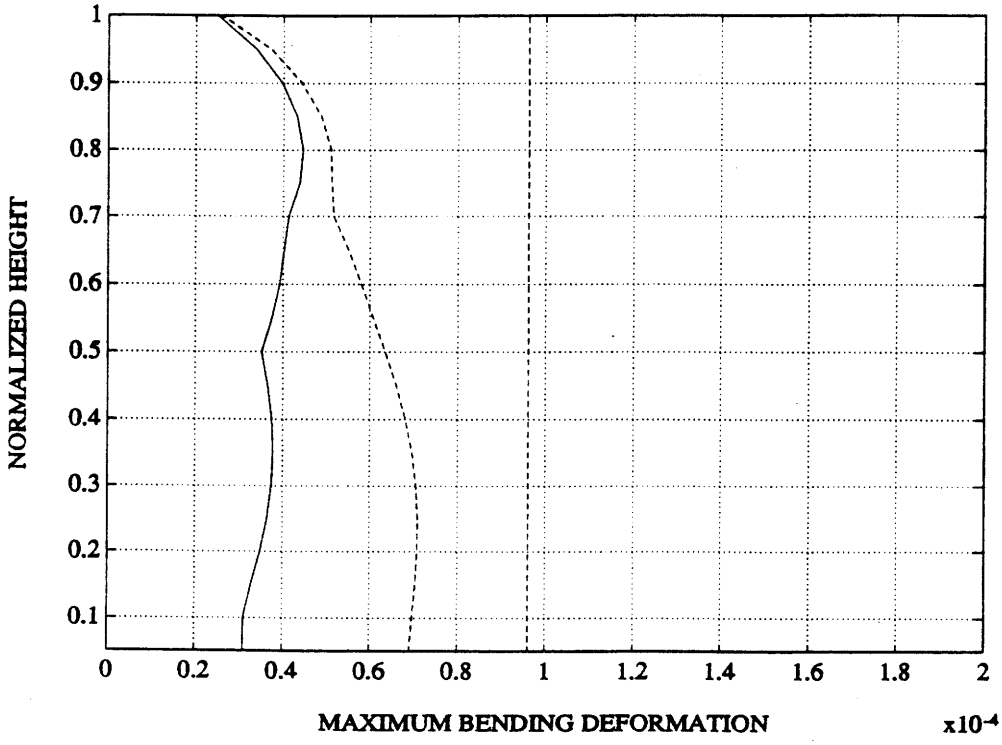

FIGURE 7.3.20: BENDING DEFORMATION (T=5.0s - a=3.0 - TRIAL2)

CHAPTER EIGHT
CONCLUSION

Since the ultimate goal of this research program is the development of a rational design strategy that optimally integrates passive and active control systems, this thesis has provided a solid foundation for pursuing that task. A strain based approach for handling loading has been developed. For the static case, where the loads are applied very slowly with respect to the period of the system, one can determine a stiffness distribution that leads to a uniform strain state along the height provided the loading is known. Moving on to the dynamic case, several alternatives are proposed. First, a strategy for handling the case where the response of the structure can be approximated by the fundamental mode response is proposed. This method is extended to handle multi-mode responses when the higher modes have a significant effect. A numerical scheme is proposed which starts off with the rigidities of the single mode response and superposes the modes obtained by the use of a discretized model to obtain new rigidity distributions. The iteration shows fast convergence in getting a

satisfactory rigidity distribution for preliminary design. Accompanying this numerical method, two analytical methods are developed providing further insight as to how buildings behave. Those methods consist of a shear beam model used to model the behavior of low rise buildings, and a bending beam model used for modeling high rise building behavior. Those analytical problems show how the importance of the higher modes varies with the period of the structure. As the period decreases, buildings behave more like shear beams and at very low periods, a single mode response seems adequate. However, as the periods increase, then the other modes become significant, and in the extreme case where the building behaves essentially as a bending beam, the higher periods become as significant as the fundamental one if not more. The developed methodology for distributing stiffness still needs some refinement and a linear distribution may provide very good estimate considering the wide uncertainty that exists in the loading. Also, some design charts need to be proposed to make the proposed strategy more practical and useful.

The second task is the distribution of damping throughout the building. And finally there's the issue of active control and whether it is practical to consider it for Civil Engineering structures. A lot of research is being done in this area, but still that field is far from being mature. The results encountered in this research suggest that the top of the building is very critical and one may want to consider applying some active control there.

APPENDIX A

EARTHQUAKE RESPONSE SPECTRA ANALYSIS

A - 1 INTRODUCTION

This appendix provides a brief description of the Response Spectra Design Method, one of the currently used methods for designing civil engineering structures subjected to earthquake loading among others. The formulation of the equations for the maximum displacement, maximum elastic force, maximum shear, and maximum bending moment distributions along the height of the building in terms of the spectral coordinates (to be defined in the following section) are derived for the case where the building is discretized into a multidegree-of-freedom (MDOF) lumped-parameter system as well as for the case where it is treated as a continuously distributed-parameter system. This is followed by a small section illustrating some of the different methods of combining the modal contributions of the desired quantities leading to the values

used in the design. Although this formulation is found in many books on earthquake engineering and structural dynamics, including it here was considered essential for the completeness of the discussion, since the proposed methods are applied to seismically excited structures and make extensive use of the Response Spectra Method in superposing modal contributions.

A - 1 RESPONSE SPECTRA

One design method that has gained wide acceptance in structural dynamics practice, particularly in earthquake engineering, is based on the concept of response spectra. The response spectrum is a plot of the maximum response (maximum displacement, velocity, acceleration, or any other quantity of interest) to a specified load function for all possible single degree-of-freedom (SDOF) systems. The abscissa of the spectrum is the natural frequency or period of the system, and the ordinate, the maximum response.

Consider the single degree-of-freedom shown in Fig. A.1.1. The equation of motion for that system subjected to earthquake excitation in terms of absolute displacements assuming that the stiffness is proportional to the relative displacement, and that the damping is proportional to the relative velocity with respect to ground, is given by

$$m\ddot{y}(t)+ c\left(\dot{y}(t) - \dot{y}_g(t)\right) + k\left(y(t) - y_g(t)\right) = 0 \qquad (A.2.1)$$

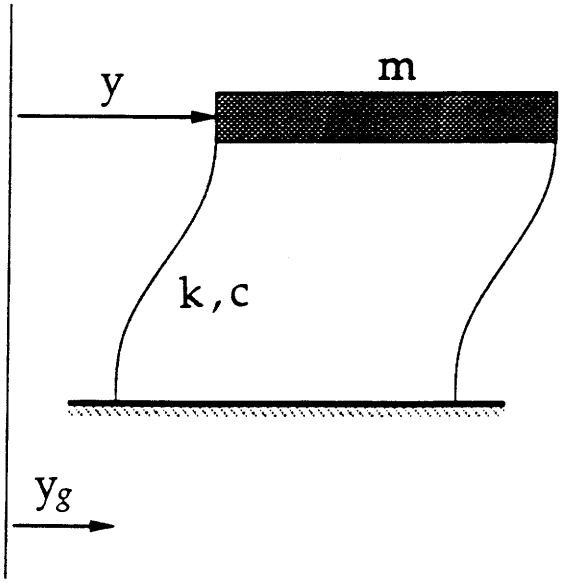

FIGURE A.2.1: SDOF SYSTEM SUBJECTED TO BASE TRANSLATION

which in terms of displacements relative to ground, becomes

$$m\ddot{v}(t) + c\dot{v}(t) + kv(t) = -m\ddot{a}_g(t) \qquad (A.2.2)$$

where

- m is the mass of the system.
- c is the damping.
- k is the stiffness.
- y denotes the absolute displacement (the "dots" indicate differentiation with respect to time).
- y_g denotes the ground displacement.
- v is the relative displacement $= y - y_g$.
- $\ddot{a}_g$ is the ground acceleration $= \ddot{y}_g$.
- t is the independent time variable.

The response of this system to a specified ground acceleration $\ddot{a}_g(t)$ may be expressed by means of the Duhamel integral with an effective loading of $-m\ddot{a}_g(t)$ by

$$v(t) = \frac{1}{m\omega_d} \int_0^t -m\ddot{a}_g(\tau)\, e^{-\xi\omega_n(t-\tau)} \sin\left(\omega_d(t-\tau)\right) d\tau \qquad (A.2.3)$$

where ω_d is the damped frequency $= \omega_n \sqrt{1-\xi^2}$.

ω_n is the undamped frequency.

ξ denotes the damping ratio.

For civil engineering structures where $\xi << 20\%$, the difference between the damped and the undamped frequencies can be neglected and *(A.2.3)* reduces to

$$v(t) = \frac{1}{\omega_n} \int_0^t -\ddot{a}_g(\tau)\, e^{-\xi\omega_n(t-\tau)} \sin\left(\omega_n(t-\tau)\right) d\tau \equiv \frac{1}{\omega_n}\vartheta(t) \qquad (A.2.4)$$

The "spectral displacement" S_d , defined as the maximum value of the response relative to the ground is usually taken as a measure of the earthquake intensity. From *(A.2.4)* , one can write

$$S_d = v_{max} = \frac{1}{\omega_n} S_v \qquad (A.2.5)$$

in which S_v is given by

$$S_v(\omega_n, \xi) = \left(\int_0^t - \ddot{a}_g(\tau)\, e^{-\xi\omega_n(t-\tau)} \sin\left(\omega_n(t-\tau)\right) d\tau \right)_{max} \qquad (A.2.6)$$

and is referred to as the "spectral pseudo-velocity". In addition, the "spectral acceleration", which is very close to the absolute acceleration of the mass, is related to the previously defined spectral quantities by

$$S_a = \omega_n S_v = \omega_n^2 S_d \qquad (A.2.7)$$

and is a measure of the maximum spring force developed in the system

$$F_{max} = k S_d = \omega_n^2 m S_d = m S_a \qquad (A.2.8)$$

The simple relationships between the three spectral quantities allows one to plot them on four-way log paper producing what is known as a "tripartite response spectra" which is widely used in designing structures for earthquake loadings. Fig. A.2.2 shows a the response spectrum for the El-Centro earthquake (Comp S00E) for different damping ratios.

As earthquakes consist of a series of essentially random ground motions, and as presently there is no accurate method available to predict the particular motion that a site can be expected to experience in future earthquakes, a "design response spectrum" averaging several response spectra is a reasonable spectrum to use in design. Fig. A.2.3 is an example of a design response

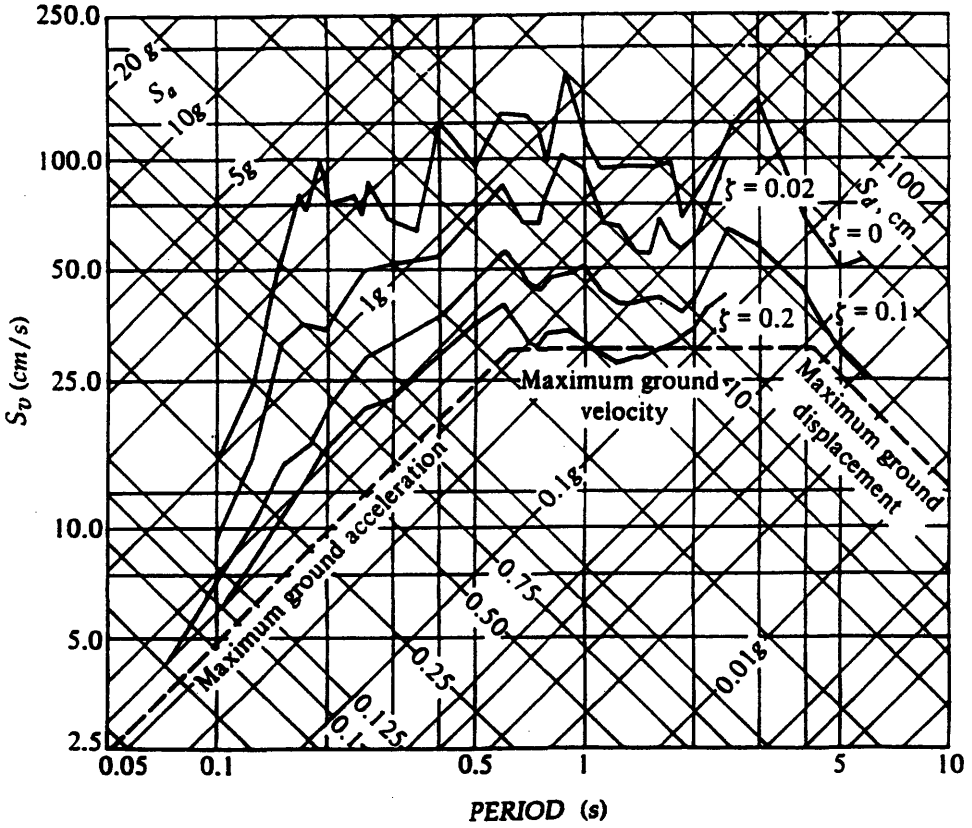

FIGURE A.2.1: RESPONSE SPECTRA FOR EL CENTRO EARTHQUAKE

spectrum normalized for a maximum ground acceleration of 1g, and Table A.2.1 gives the amplification factors for the different damping ratios. For a particular structure, the engineer decides on a certain peak ground acceleration that will govern the design, scales the design response spectrum by acceleration, and hence can determine the spectral coordinates for the different frequencies and damping ratios, which in turn are used in determining the maximum quantities of interest such as displacements, elastic forces, shears, bending moments, . . . along the height of the structure. The spectrum of Figure A.2.3 is the design spectrum used in this thesis although the formulation applies to any other spectrum.

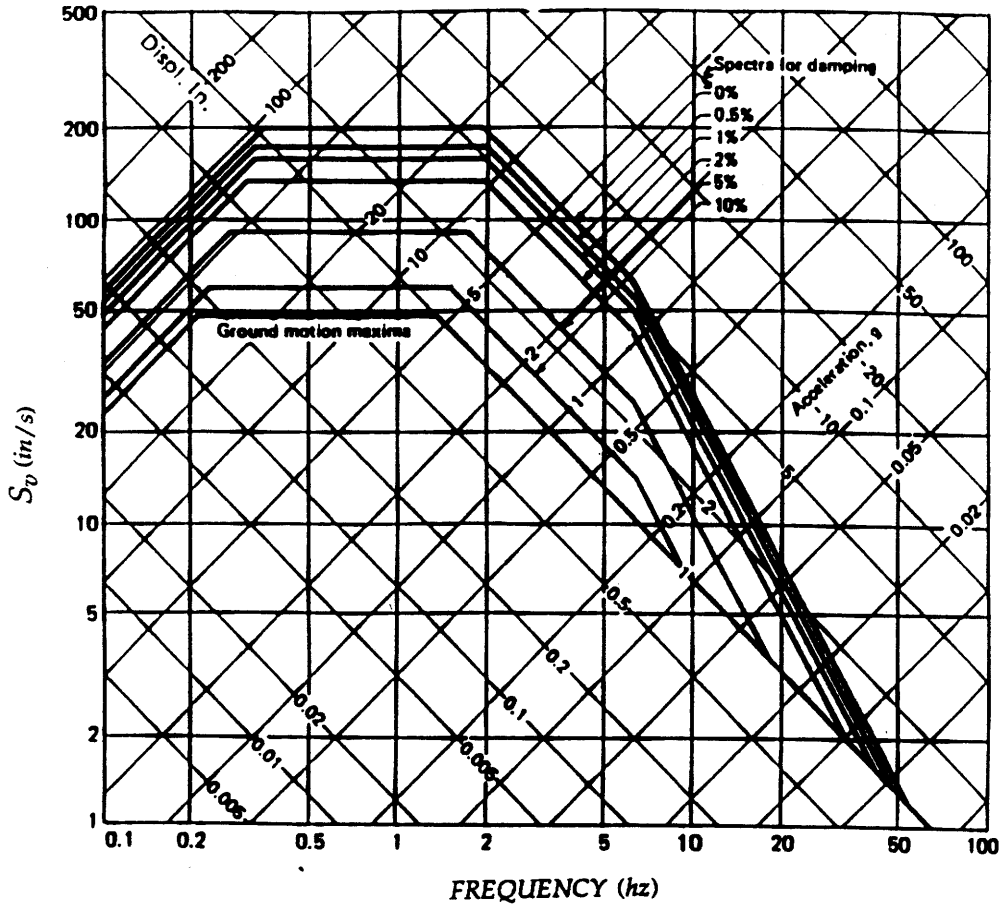

FIGURE A.2.3: ELASTIC DESIGN SPECTRUM SCALED TO 1g.

PERCENT DAMPING	AMPLIFICATION FACTORS		
	DISPLACEMENT	VELOCITY	ACCELERATION
0.0	2.5	4.0	6.4
0.5	2.2	3.6	5.8
1.0	2.0	3.2	5.2
2.0	1.8	2.8	4.3
5.0	1.4	1.9	2.6
7.0	1.2	1.5	1.9
10.0	1.1	1.3	1.5
20.0	1.0	1.1	1.2

TABLE A.2.1: RELATIVE VALUES SPECTRUM AMPLIFICATION FACTORS

A - 3 EARTHQUAKE RESPONSE ANALYSIS : LUMPED MDOF SYSTEMS

This section consists of the formulation of the response of lumped-parameter multidegree-of-freedom systems to earthquake translational excitations, which will then be specialized to incorporate the spectral parameters in order to determine the maximum quantities of interest.

Analogous to the equation of motion of the SDOF system subjected to ground acceleration *(A.2.2)*, the equation of motion for a MDOF system subjected to ground excitation can be expressed in matrix form as

$$\mathbf{M}\ddot{\mathbf{Y}}(t) + \mathbf{C}\dot{\mathbf{Y}}(t) + \mathbf{K}\mathbf{Y}(t) = \mathbf{P}_{eff}(t) = -\mathbf{M}\mathbf{E}\,\ddot{a}_g(t) \qquad (A.3.1)$$

where
- $\mathbf{M}$ is an nxn mass matrix
- $\mathbf{C}$ is an nxn damping matrix
- $\mathbf{K}$ is an nxn stiffness matrix
- $\mathbf{Y}$ is an $nx1$ displacement vector
- $\dot{\mathbf{Y}}$ is an $nx1$ velocity vector
- $\ddot{\mathbf{Y}}$ is an $nx1$ acceleration vector
- $\mathbf{E}$ is an $nx1$ vector expressing the displacements of all degrees of freedom in the structure produced by a unit static translation of the base

Transforming the above system of equations to a system of normal modal

coordinates by substituting

$$\mathbf{Y}(t) = \mathbf{\Phi}\,\mathbf{Q}(t) \qquad (A.3.2)$$

where $\mathbf{Q}$ is an $rx1$ vector of normal modal coordinates which are functions of time and $\mathbf{\Phi}$ is an nxr matrix containing in its columns the r mode shapes one wishes to consider, obtained by solving the eigenvalue problem

$$\mathbf{K}\,\mathbf{\Phi}_j = \omega_j^2\ \mathbf{M}\,\mathbf{\Phi}_j \qquad (A.3.3)$$

resulting from solving the undamped free vibration problem

$$\mathbf{M}\ddot{\mathbf{Y}} + \mathbf{K}\mathbf{Y} = \mathbf{O} \qquad (A.3.4)$$

results in $$\mathbf{M}\mathbf{\Phi}\,\ddot{\mathbf{Q}} + \mathbf{C}\mathbf{\Phi}\,\dot{\mathbf{Q}} + \mathbf{K}\mathbf{\Phi}\,\mathbf{Q} = -\mathbf{M}\mathbf{E}\,\ddot{a}_g \qquad (A.3.5)$$

Premultiplying *(A.3.5)* by $\mathbf{\Phi}^T$ gives

$$\mathbf{\Phi}^T\mathbf{M}\mathbf{\Phi}\,\ddot{\mathbf{Q}} + \mathbf{\Phi}^T\mathbf{C}\mathbf{\Phi}\,\dot{\mathbf{Q}} + \mathbf{\Phi}^T\mathbf{K}\mathbf{\Phi}\,\mathbf{Q} = -\mathbf{\Phi}^T\mathbf{M}\mathbf{E}\,\ddot{a}_g \qquad (A.3.6)$$

which upon applying the orthogonality conditions

$$\mathbf{\Phi}^T\mathbf{K}\mathbf{\Phi} = \mathbf{\Omega}^2\,\mathbf{\Phi}^T\mathbf{M}\mathbf{\Phi} = \mathbf{\Omega}^2\begin{bmatrix} \mathbf{\Phi}_1^T\mathbf{M}\mathbf{\Phi}_1 & \cdots & \mathbf{O} \\ \vdots & \ddots & \vdots \\ \mathbf{O} & \cdots & \mathbf{\Phi}_r^T\mathbf{M}\mathbf{\Phi}_r \end{bmatrix} \qquad (A.3.7)$$

uncouples the equations assuming a damping matrix proportional to the mass and stiffness matrices

$$\mathbf{C} = \alpha \mathbf{M} + \beta \mathbf{K} \qquad (A.3.8)$$

$\mathbf{\Omega}^2$ is a diagonal matrix containing the eigenvalues of *(A.3.3)*. One can then express $\mathbf{C}$ in terms of modal damping ratios

$$\mathbf{\Phi}^T\mathbf{C}\mathbf{\Phi} = \begin{bmatrix} 2\xi_1\omega_1\mathbf{\Phi}_1^T\mathbf{M}\mathbf{\Phi}_1 & \cdots & \mathbf{O} \\ \vdots & \ddots & \vdots \\ \mathbf{O} & \cdots & 2\xi_r\omega_r\mathbf{\Phi}_r^T\mathbf{M}\mathbf{\Phi}_r \end{bmatrix} \qquad (A.3.9)$$

Dividing every equation j of the system of equations in *(A.3.6)* by the corresponding j th modal mass $\mathbf{\Phi}_j^T\mathbf{M}\mathbf{\Phi}_j$, which shall be denoted by $\widehat{M}_j$, one obtains

$$\ddot{Q}_j + 2\xi_j\omega_j\dot{Q}_j + \omega_j^2 Q_j = -\frac{\mathbf{\Phi}_j^T\mathbf{M}\mathbf{E}}{\widehat{M}_j}\ddot{a}_g \qquad (A.3.10)$$

where the participation factor of the j th mode shall be defined as

$$\Gamma_j = \frac{\mathbf{\Phi}_j^T\mathbf{M}\mathbf{E}}{\widehat{M}_j} \qquad (A.3.11)$$

The response of each mode of the MDOF system is given by

$$Q_n(t) = \frac{\Gamma_j}{\omega_j}\vartheta_j(t) \qquad (A.3.12)$$

where $\vartheta_j(t)$ is given by the integral of equation *(A.2.4)* and is dependent on the modal damping ratio ξ_j and the j th mode of vibration. The relative displacement vector produced by the j th mode is then given by

$$\mathbf{Y}_j(t) = \mathbf{\Phi}_j \frac{\Gamma_j}{\omega_j}\vartheta_j(t) \qquad (A.3.13)$$

and the relative displacement vector due to all modal responses is obtained by superposition

$$\mathbf{Y}(t) = \mathbf{\Phi}\,\mathbf{Q}(t) = \sum_{j=1}^{r} \mathbf{\Phi}_j \frac{\Gamma_j}{\omega_j}\vartheta_j(t) \qquad (A.3.14)$$

The elastic forces associated with the relative displacements can be obtained directly by premultiplying by the stiffness matrix

$$\mathbf{F}(t) = \mathbf{K}\,\mathbf{Y}(t) = \mathbf{K}\mathbf{\Phi}\,\mathbf{Q}(t) \qquad (A.3.15)$$

which can also be expressed as

$$\mathbf{F}(t) = \mathbf{M}\mathbf{\Phi}\mathbf{\Omega}^2\mathbf{Q}(t) = \mathbf{M}\mathbf{\Phi}\begin{Bmatrix}\Gamma_1\,\omega_1\vartheta_1(t)\\ \vdots \\ \Gamma_r\,\omega_r\vartheta_r(t)\end{Bmatrix} = \sum_{j=1}^{r}\mathbf{M}\mathbf{\Phi}_j\,\Gamma_j\,\omega_j\vartheta_j(t)$$

(A.3.16)

by using the equivalence of the elastic and inertia forces which is expressed by the eigenvalue relationship *(A.3.3)*. Vector $\mathbf{F}$ contains both the elastic forces and moments at every lumped mass.

The shear force below mass x when one considers a lumped-mass vertical cantilever beam can be obtained by summing up the elastic inertia forces above the point where the shear force is being determined. Thus

$$V(x,t) = \sum_{i=x}^{n} F_i^I(t) = \sum_{j=1}^{r} \sum_{i=x}^{n} \left(\mathbf{M}\Phi_j \Gamma_j \omega_j \vartheta_j(t)\right)_i \qquad (A.3.17)$$

where F_i^I is the elastic translational force at mass i and the interior summation gives the contribution of mode j to the total shear force below mass x. Similarly, the resulting moment at level x due to the elastic translational forces is given by

$$M(x,t) = \sum_{i=x}^{n} x_i F_i^I(t) = \sum_{j=1}^{r} \sum_{i=x}^{n} x_i \left(\mathbf{M}\Phi_j \Gamma_j \omega_j \vartheta_j(t)\right)_i \qquad (A.3.18)$$

where x_i is the height of mass i above the point where the moment is being calculated. In general, the elastic moments developed due to the rotation of the story are relatively much smaller than the moments given by *(A.3.18)* and are usually neglected.

To evaluate the earthquake response of a lumped MDOF system at any time t involves the evaluation of the earthquake response integral at that time

for each significant response mode. In order to determine the maximum response, one can make use of the approximate response-spectra method where for each mode, the maximum response can be obtained directly from the response spectrum as described for the SDOF systems. So from *(A.3.13)*, the maximum displacement in mode j is given by

$$\mathbf{Y}_{j,max} = \mathbf{\Phi}_j \frac{\Gamma_j}{\omega_j} S_v(\xi_j, \omega_j) \qquad (A.3.19)$$

where $S_v(\xi_j, \omega_j)$ is the spectral pseudo velocity corresponding to the damping and frequency of the j th mode. Similarly, the j th mode contribution to the elastic force vector is

$$\mathbf{F}_{j,max} = \mathbf{M}\mathbf{\Phi}_j \Gamma_j \omega_j S_v(\xi_j, \omega_j) = \mathbf{M}\mathbf{\Phi}_j \Gamma_j S_a(\xi_j, \omega_j) \qquad (A.3.20)$$

where $S_v(\xi_j, \omega_j)$ and $S_a(\xi_j, \omega_j)$ are the spectral pseudo-velocity and spectral acceleration respectively. From *(A.3.19)* one can determine the shear and moment contributions of the j th mode given by

$$V_{j,max}(x) = \sum_{i=x}^{n} \left(\mathbf{M}\mathbf{\Phi}_j \Gamma_j \omega_j S_v(\xi_j, \omega_j)\right)_i \qquad (A.3.21)$$

and

$$M_{j,max}(x) = \sum_{i=x}^{n} x_i \left(\mathbf{M}\mathbf{\Phi}_j \Gamma_j \omega_j S_v(\xi_j, \omega_j)\right)_i \qquad (A.3.22)$$

A - 4 EARTHQUAKE RESPONSE ANALYSIS : DISTRIBUTED PARAMETER SYSTEMS

The formulation of the earthquake response equations for systems having continuously distributed properties can be carried out by procedures which are completely analogous to those of the lumped MDOF systems. The decoupled modal equations of motion take the same form as the lumped mass system and may be expressed as

$$\ddot{Q}_j + 2\xi_j\omega_j \dot{Q}_j + \omega_j^2 Q_j = \Gamma_j \ddot{a}_g \qquad (A.4.1)$$

where

$$\Gamma_j = \frac{\int_0^H m(x)\,\Phi_j(x)\,dx}{\int_0^H m(x)\,\Phi_j^2(x)\,dx} \qquad (A.4.2)$$

The displacement at x is given by

$$y(x,t) = \sum_{j=1}^{r} \Phi_j(x) Q_j(t) = \sum_{j=1}^{r} \Phi_j(x) \frac{\Gamma_j}{\omega_j} \vartheta_j(t) \qquad (A.4.3)$$

and the elastic force distribution is given by an expression analogous to *(A.3.16)*

$$F(x,t) = \sum_{j=1}^{r} m(x)\Phi_j(x)\omega_j^2 Q_j(t) = \sum_{j=1}^{r} m(x)\Phi_j(x)\,\Gamma_j\,\omega_j\,\vartheta_j(t) \qquad (A.4.4)$$

Similarly, the shear force at level x is found to be

$$V(x,t) = \int_x^H F(x,t)\,dx = \sum_{j=1}^{r} \omega_j^2 Q_j(t) \int_x^H m(x)\Phi_j(x)\,dx$$

$$= \sum_{j=1}^{r} \Gamma_j \omega_j \vartheta_j(t) \int_x^H m(x)\Phi_j(x)\,dx \qquad (A.4.5)$$

and the moment becomes

$$M(x,t) = \int_x^H x\,F(x,t)\,dx = \sum_{j=1}^{r} \omega_j^2 Q_j(t) \int_x^L x\,m(x)\Phi_j(x)\,dx$$

$$= \sum_{j=1}^{r} \Gamma_j \omega_j \vartheta_j(t) \int_x^L x\,m(x)\Phi_j(x)\,dx \qquad (A.4.6)$$

And the maximum modal response values for the distributed parameter systems can be determined in a similar manner as for the lumped MDOF systems giving

$$y_{j,max}(x) = \Phi_j(x) \frac{\Gamma_j}{\omega_j} S_v(\xi_j, \omega_j) \qquad (A.4.7)$$

$$F_{j,max}(x) = m(x)\,\Phi_j(x)\,\Gamma_j\,\omega_j\,S_v(\xi_j, \omega_j) \qquad (A.4.8)$$

$$V_{j,max}(x) = \Gamma_j\,\omega_j\,S_v(\xi_j,\omega_j) \int_x^L m(x)\Phi_j(x)\,dx \qquad (A.4.9)$$

$$M_{j,max}(x) = \Gamma_j \, \omega_j \, S_v(\xi_j, \omega_j) \int_x^L x \, m(x) \, \Phi_j(x) \, dx \qquad (A.4.10)$$

A - 5 SUPERPOSITION OF RESPONSE MAXIMA

Several formulas are used in order to determine the maximum total response due to the modes considered among which one finds the Sum of Absolute Values (SAV) where one sums the absolute values of the modal maxima of the quantity to be determined, and the Square Root Sum of Squares (SRSS) where one sums the squares of the modal maxima and the takes the square root. The SAV is an upper envelop and in some cases overestimates the response since not all of the maxima occur at the same time. The SRSS on the other hand is not as severe and is currently widely used. As an example, the maximum shear force using SAV is given by

$$\begin{aligned} V_{max}(x) &= \sum_{j=1}^{r} \left| V_{j,max}(x) \right| \\ &= \left| V_{1,max}(x) \right| + \left| V_{2,max}(x) \right| + \cdots + \left| V_{r,max}(x) \right| \end{aligned} \qquad (A.5.1)$$

and using the SRSS

$$\begin{aligned} V_{max}(x) &= \sqrt{\sum_{j=1}^{r} \left(V_{j,max}(x) \right)^2} \\ &= \sqrt{\left(V_{1,max}(x) \right)^2 + \left(V_{2,max}(x) \right)^2 + \cdots + \left(V_{r,max}(x) \right)^2} \end{aligned} \qquad (A.5.2)$$

Another method of combining modal contributions is derived from the SRSS by noting that *(A.5.2)* can be written as

$$V_{max}(x) = V_{1,max}(x)\left\{1 + \frac{(V_{2,max}(x))^2}{(V_{1,max}(x))^2} + \cdots + \frac{(V_{r,max}(x))^2}{(V_{1,max}(x))^2}\right\}^{1/2} \qquad (A.5.3)$$

which can be approximated as

$$V_{max}(x) = V_{1,max}(x)\left\{1 + \frac{1}{2}\left(\frac{(V_{2,max}(x))^2}{(V_{1,max}(x))^2} + \ldots + \frac{(V_{r,max}(x))^2}{(V_{1,max}(x))^2}\right)\right\} \qquad (A.5.4)$$

One can transform the SRSS into a Modified Square Root Sum of Squares (MSRSS) by changing the half in *(A.5.4)* , and rewriting it in terms of a parameter α where for larger contributions of higher modes than would be obtained using an SRSS, α is taken to be larger than one half. Equation *(A.5.4)* in terms of α is given by

$$V_{max}(x) = V_{1,max}(x)\left\{1 + \alpha\left(\frac{(V_{2,max}(x))^2}{(V_{1,max}(x))^2} + \ldots + \frac{(V_{r,max}(x))^2}{(V_{1,max}(x))^2}\right)\right\} \qquad (A.5.5)$$

Similar equations can be written for superposing modal contributions of the other quantities that may be of interest. Several other techniques for superposing modal contributions of maxima can be applied, however, for the purpose of this work, only those are used. The values obtained by the superposition process, are the values for which the members of a structure have

to be designed. Chapters Four through Eight make extensive use of the formulation developed herein, in superposing modal rigidity contributions to determine the one that leads to the desired uniform deformation state.

APPENDIX B

ACCELEROGRAM DATABASE

This appendix shows the accelerograms used in this research. Table B.1 provides a listing of the different accelerograms used, their peak values (acceleration, velocity, displacement) and the times at which those peak values occur. The accelerogram values are given at equally-spaced intervals of 0.02s. Whenever smaller intervals are required, linear interpolation is used to obtain the additional acceleration values. Fig. B.1 to B.6 plot the acceleration of the different earthquakes used, plotted as a function of time and scaled to a peak acceleration of 1g.

EARTHQUAKE	DATE	COMP	PEAK ACC (CM/S^2)	@ TIME (S)	PEAK VEL (CM/S)	@ TIME (S)	PEAK DISP (CM)	@ TIME (S)
EL-CENTRO	MAY 18, 1940	S00E	341.69531	2.12000	33.44914	2.18000	10.86678	8.58000
		S90W	210.14227	11.44000	-36.92113	2.14000	-19.78262	3.00000
		VERT	-206.34700	0.98000	-10.83688	3.26000	-5.55814	3.42000
GOLDEN GATE	MAR 22, 1957	N10E	-81.79077	1.34000	-4.91696	1.40000	-2.25282	1.94000
		S80E	-102.80478	1.44000	-4.60863	1.50000	-0.82591	2.56000
		VERT	37.19843	1.18000	-1.21440	1.80000	-0.67964	18.24000
HELENA	OCT 31, 1935	S00W	143.46764	3.04000	7.34117	1.92000	1.42914	2.36000
		S90W	142.49608	2.42000	-13.32821	1.82000	-3.73656	2.32000
		VERT	-87.49394	2.32000	9.70312	2.26000	-2.82247	1.70000
OLYMPIA	APR 13, 1949	N04W	161.63023	10.94000	21.39984	11.04000	-8.57898	10.68000
		N86E	-274.62964	19.62000	-17.08972	8.46000	10.37631	7.30000
		VERT	-90.62807	0.14000	-7.02949	0.74000	-4.03140	2.58000
PARKFIELD	JUN 27, 1966	N05W	-347.81787	7.40000	-23.17166	7.50000	-5.30553	10.64000
		N85E	-425.68188	7.50000	-25.43748	7.60000	-7.11352	10.12000
		VERT	116.88695	6.20000	-7.28020	7.86000	3.44049	6.88000
TAFT	JUL 21, 1952	N21E	152.69830	9.10000	-15.71838	3.40000	-6.69654	44.14000
		S69E	175.94533	3.70000	-17.71347	3.56000	-9.15207	44.12000
		VERT	102.85297	9.76000	6.67392	7.80000	-5.03408	41.56000

TABLE B-1: ACCELEROGRAMS - PEAK VALUES

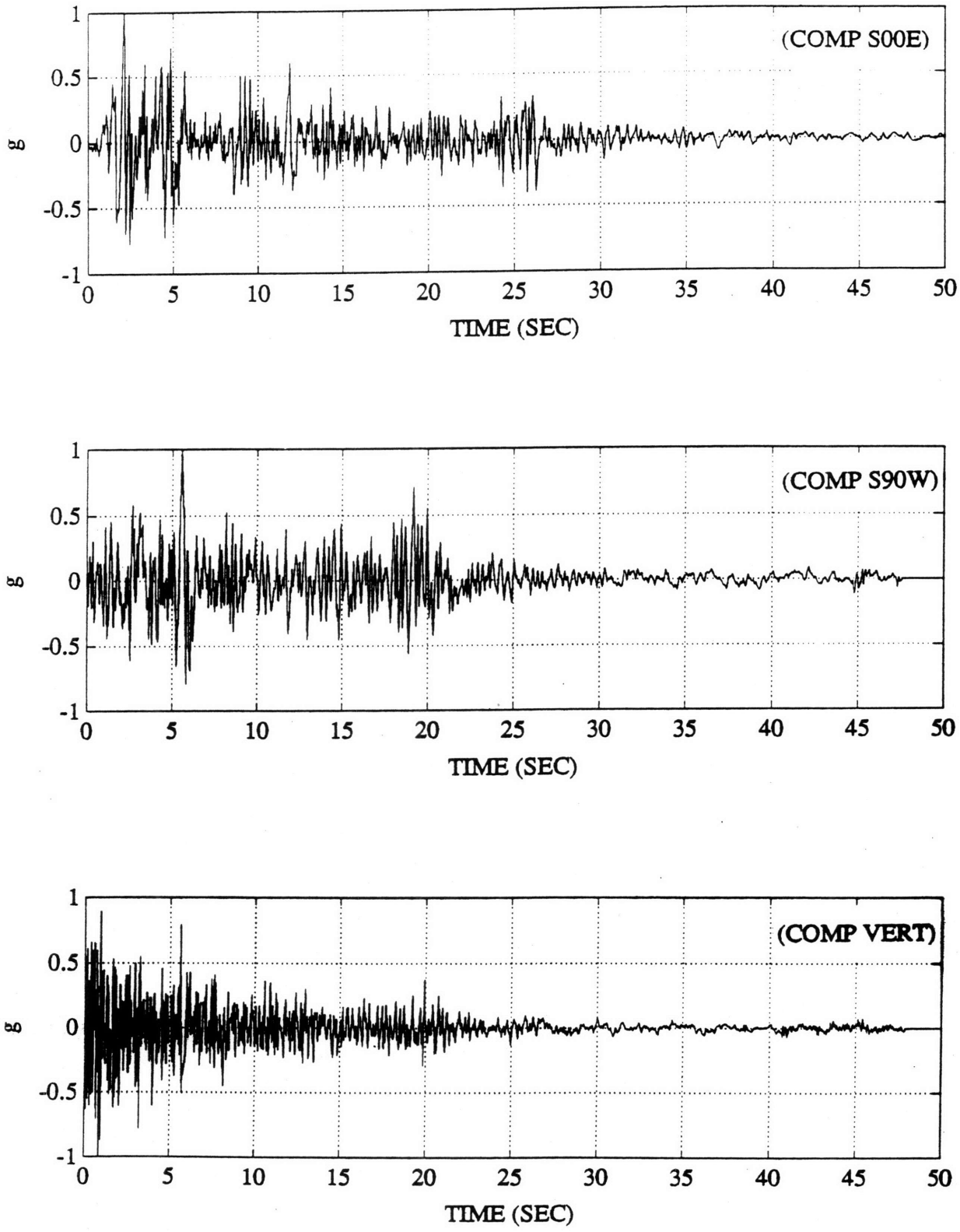

FIGURE B.1: EL-CENTRO

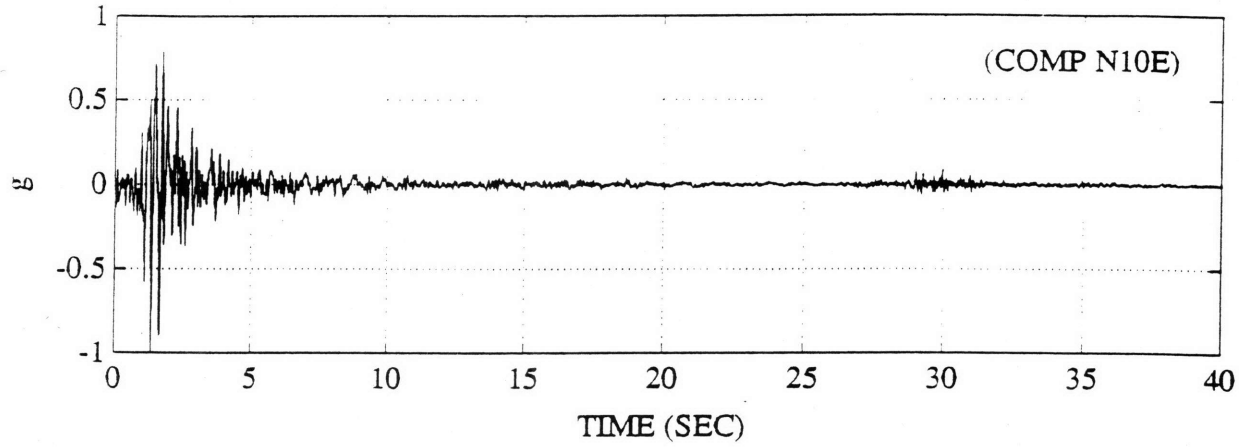

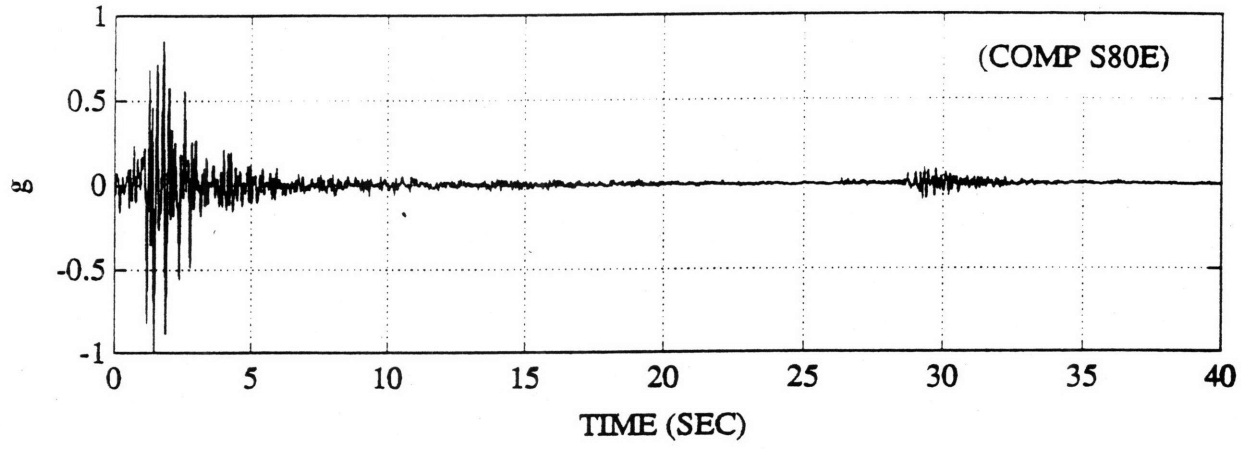

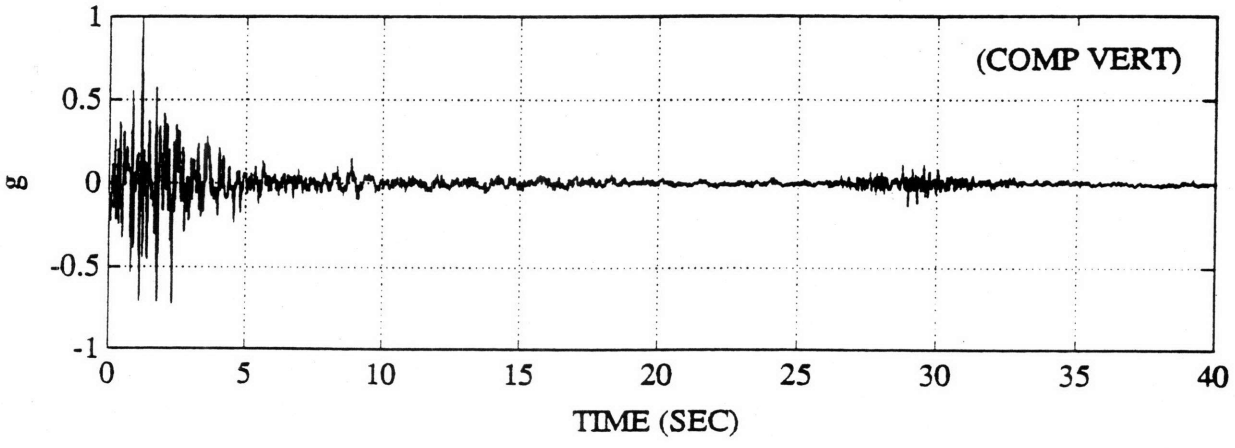

FIGURE B.2: GOLDEN GATE

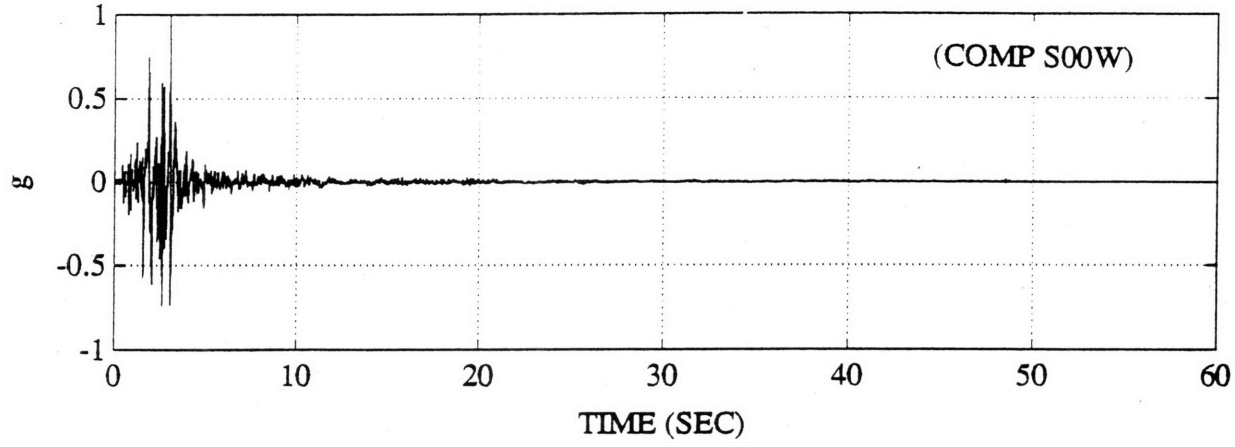

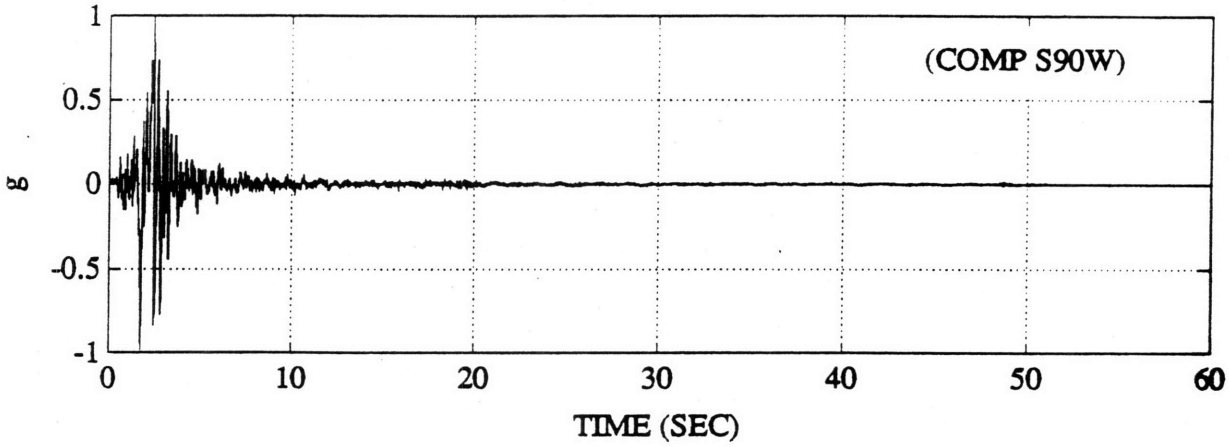

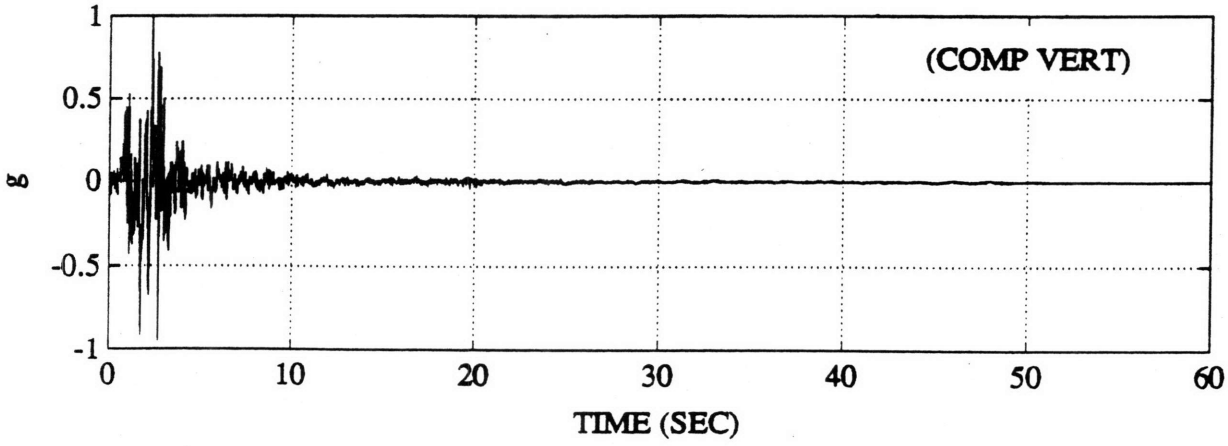

FIGURE B.3: HELENA

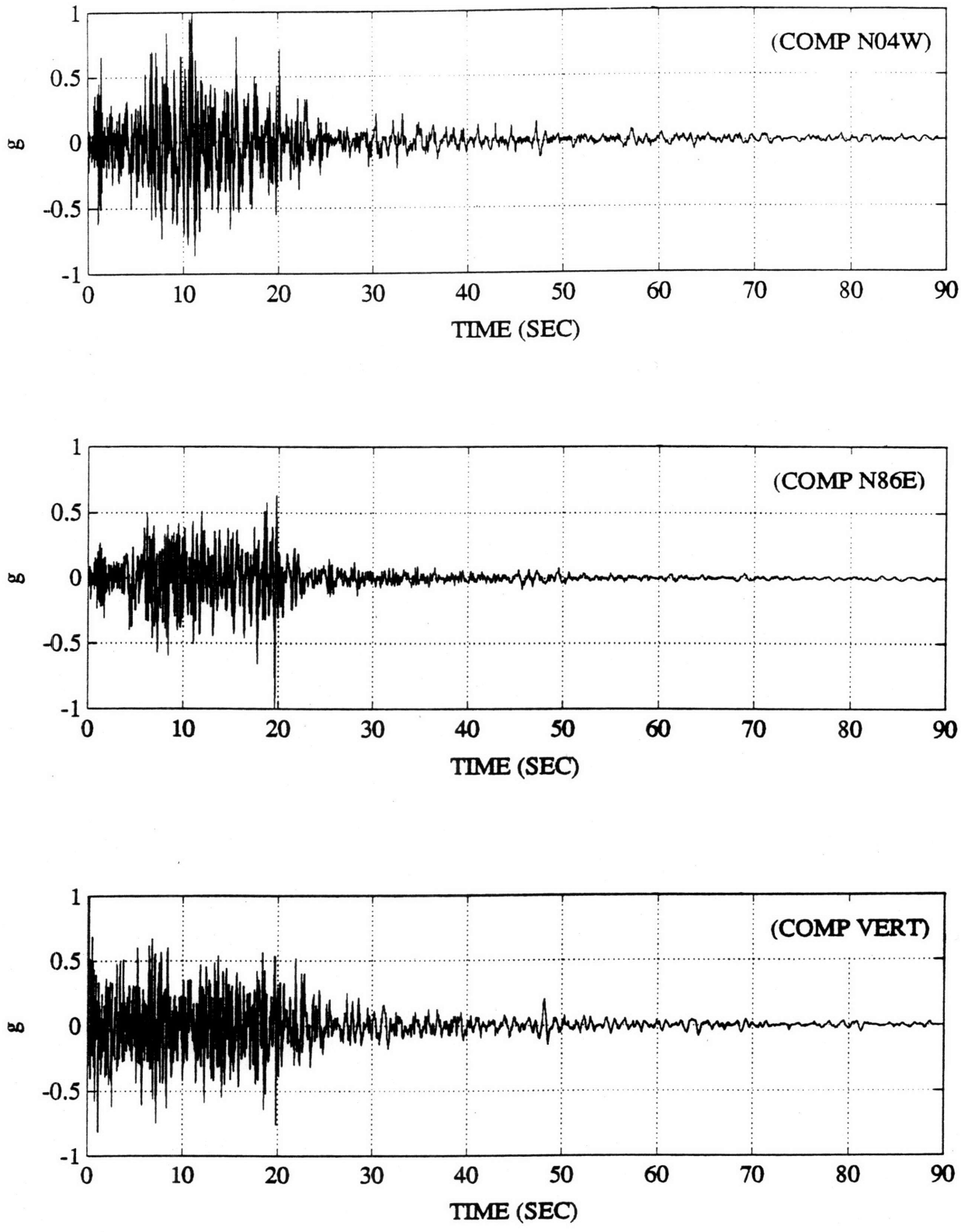

FIGURE B.4: OLYMPIA

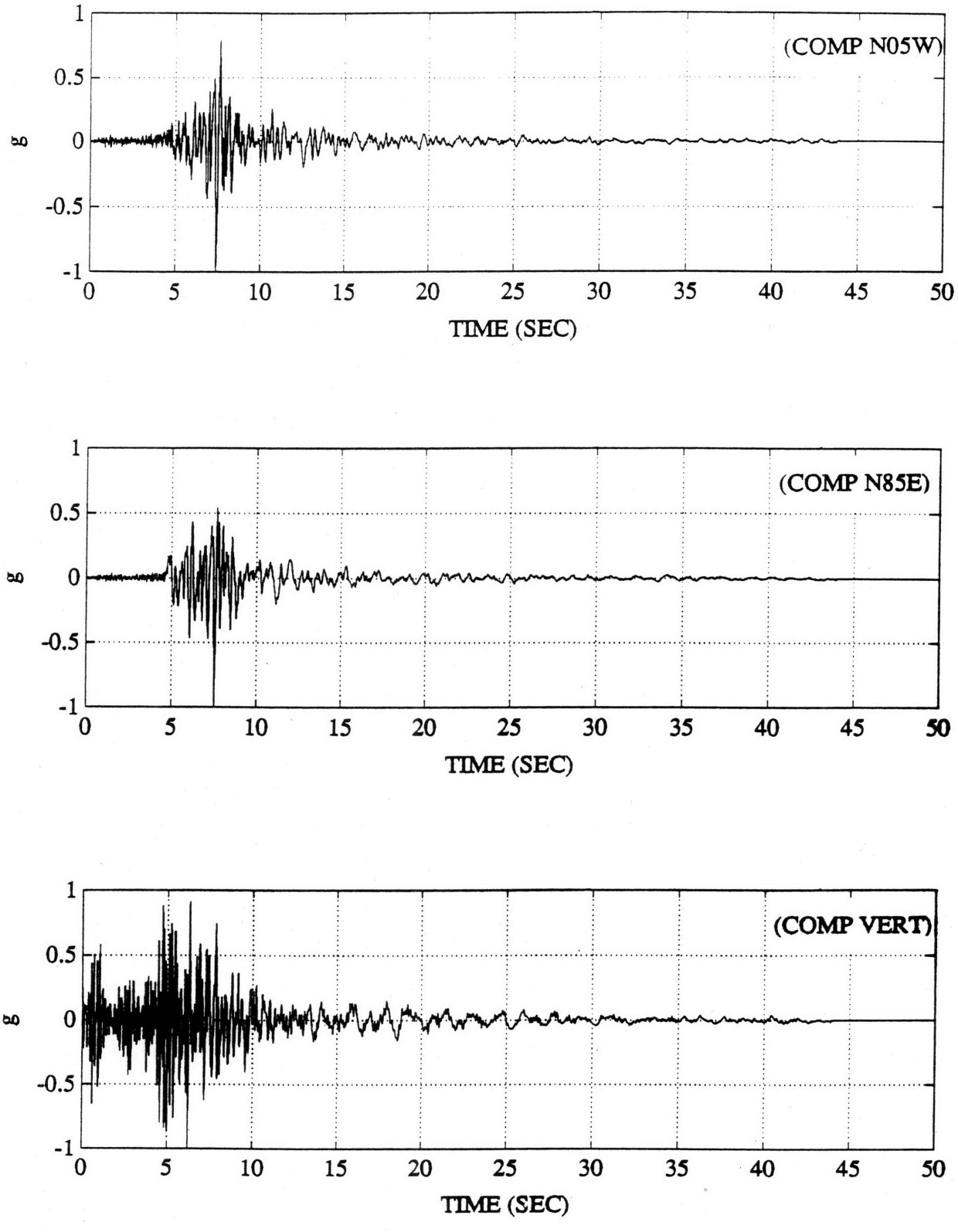

FIGURE B.5: PARKFIELD

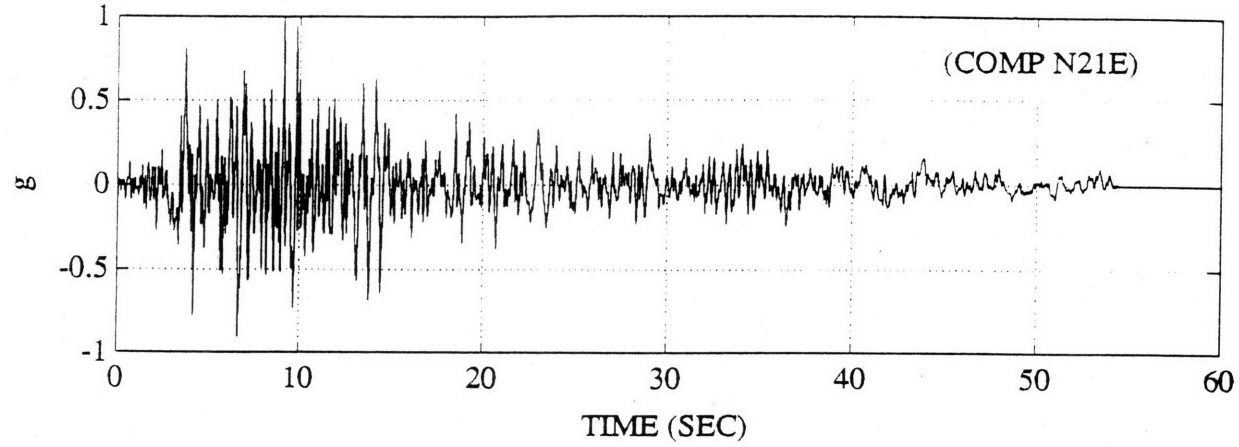

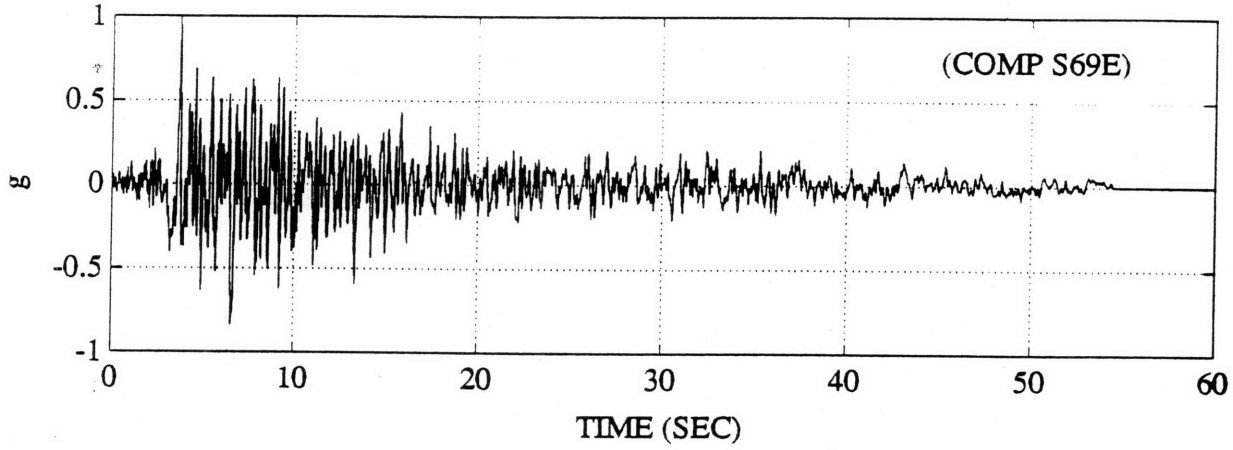

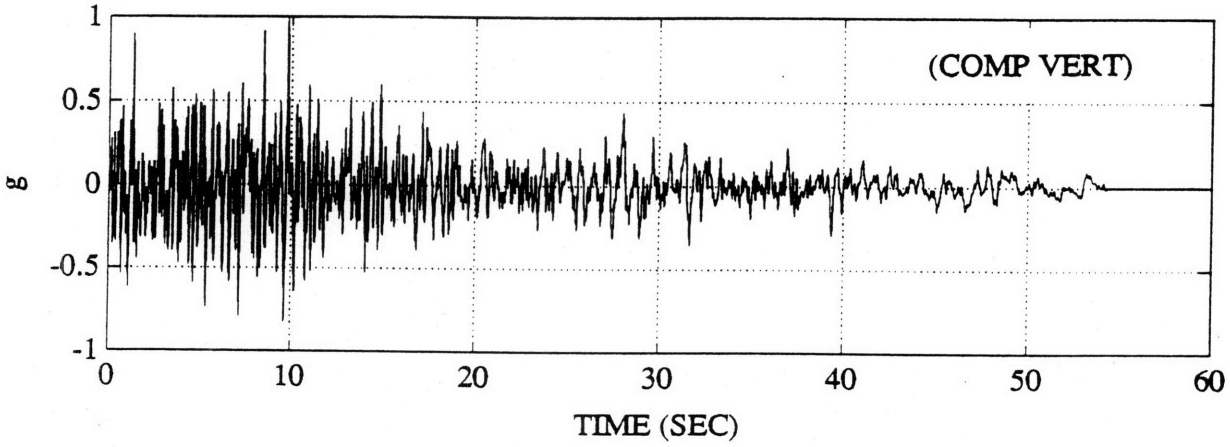

FIGURE B.6: TAFT

APPENDIX C

DISCRETIZATION

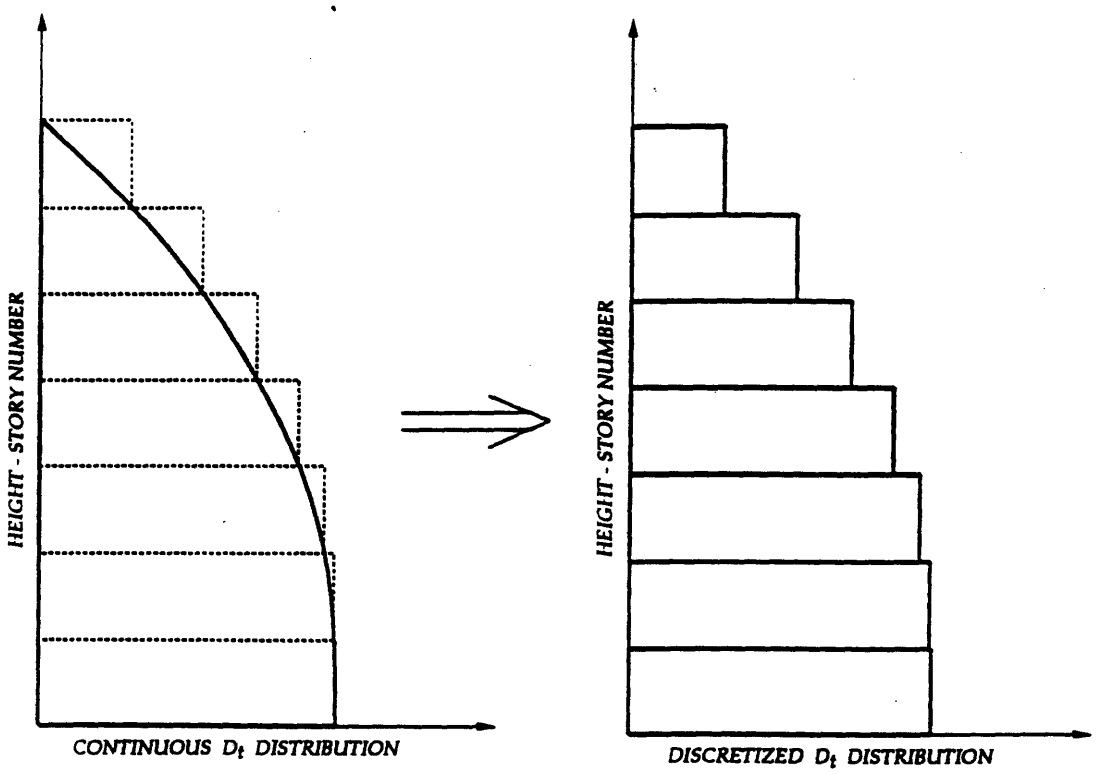

FIGURE C.1: DISCRETIZING CONTINUOUS STIFFNESS DISTRIBUTIONS

APPENDIX D
REFERENCES

Akiyama H., **Earthquake-Resistance Limit-State Design for Buildings**, University of Tokyo Press, 1985.

Albano L., **Axiomatic Approach for Performance Based Design**, Ph.D. Thesis, Department of Civil and Environmental Engineering at MIT, Jan. 1992.

Bathe K. J., **Finite Element Procedures in Engineering Analysis**, Prentice-Hall, 1982.

Clough R. W. and Penzien J., **Dynamics of Structures**, McGraw-Hill, 1975.

Connor J. J., **Analysis of Structural Member Systems**, Ronald Press, 1976.

Connor J. J. and Wada A., **Performance Based Design Methodology For Structures**, International Workshop on Recent Developments in Base-Isolation Techniques for Buildings, Tokyo, 1992.

Humar J. L., **Dynamics of Structures**, Prentice-Hall, 1990.

Iwata M., Wada A., Kawai H., and Watanabe A., **Study of Damage Tolerant Structures**, To be published.

Paz M., **Structural Dynamics (2nd Edition)**, Van Nostrand Reinhold, 1985.

Peetathawatchai C., **Preliminary Design Strategies for Tall Buildings**, S.M. Thesis submitted to the Department of Civil and Environmental Engineering at MIT, May 1992.

Suh N., **The Principles of Design**, Oxford University Press, 1990.

Wada A. and Huang Y., **Performance Based Design of Tall Buildings**, To be published.

Wada A. and Huang Y., **Optimum Stiffness Distribution for Building Structure Under Earthquake**, To be published.

Wada A., Connor J. J., Kawai H., Iwata M., and Watanabe A., **Damage Tolerant Structures**, To be published.